POLITECNICO DI TORINO

Department of Energy

Master of Science in Energetic and Nuclear Engineering

Master Degree Thesis

Tritium Purification Systems

Applications to Generation IV and Fusion Reactors

Thesis Advisors

prof. Massimo Zucchetti
ing. Raffaella Testoni

Candidate

Serena Crobu

Centro Ricerche ENEA Brasimone

ing. Marco Utili
ing. Dario Diamanti

APRIL 2018

Acknowledgements

Firstly, I would like to thank professor Massimo Zucchetti and engineers Marco Utili and Dario Diamanti for the help during this experience.

Thanks to Beatrice, Michele and Gianluca for support and company in the studies, because with them I managed to cope with all these stressful years.

Thanks to Riccardo and Dojo Fiorilli, for their valuable lessons.

Thanks to Marco, always by my side, because all that we built together is very important for me.

Last but not least, thanks to my parents, who gave this opportunity to me and always supported and encouraged me.

    Thanks to all of you, sincerely.

Innanzitutto vorrei ringraziare il professor Massimo Zucchetti e gli ingegneri Marco Utili e Dario Diamanti per tutto l'aiuto fornito durante questa esperienza.

Ringrazio Beatrice, Michele e Gianluca per il supporto e la compagnia nello studio, perché con loro sono riuscita a far fronte allo stress di tutti questi anni.

Ringrazio Riccardo e tutto il Dojo Fiorilli, per i loro preziosi insegnamenti.

Ringrazio Marco, che mi è sempre stato vicino, perché quello che abbiamo costruito insieme è per me molto importante.

Per ultimi, ma non meno importanti, ringrazio i miei genitori, che mi hanno dato questa opportunità e mi hanno sempre sostenuto e incoraggiato.

    A voi tutti, un sincero grazie.

Serena

Summary

The main purposes of this work are the analysis of the Coolant Purification System (CPS) to be used in the European Test Blanket Systems (TBS), that are supposed to be installed and tested in ITER, and the study of its application to Generation IV (Gen IV) fission reactors, in particular for the purification of the cover gas of the Sodium-cooled Fast Reactor (SFR) ASTRID.

The TBS under study are the HCLL (Helium-Cooled Lithium Lead) and the HCPB (Helium-Cooled Pebble Bed).

The CPS is one of the so-called "ancillary systems", whose main function is to purify the helium of the cooling systems, keeping under control the chemical compisition of the cooling gas. A further scope of the CPS is the extraction of tritium that, from the breeding zone, permeates into the cooling system; the recovery of tritium from the cooling systems is highly necessary because the fusion reactors must be able to guarantee the self-sufficiency in terms of tritium production and consumption. In fission reactors, the extraction of the tritium produced inside the core is important to reduce the release of the isotopes into the environment.

The work will include the design of a purification system to be applied to the cover gas of the ASTRID reactor, in terms of flow-rate and quantity of material to be used.

As validation of the design, an experimental activity on the HYDREX facility, built at the Research Centre ENEA Brasimone, will be performed: this work will present the very first step to be done in order to carry on the objective of this facility, which consists on the calibration of a quadrupole mass spectrometer and its interfacing with HYDREX.

Contents

List of Figures

List of Tables

13

Chapter 1

Nuclear reactors

1.1 Introduction

Nuclear power plays an important role in the world's energy context and major attention is given not only to fusion power, with ITER and DEMO projects, but also to Gen IV fission reactors, that constitute an element of the solution to global warming and a way of delivering power to emerging and developed countries [1]. The road to commercial fusion energy has to cope with many technological challenges and research is carried on all over the world, with the cooperation of industries, research laboratories and universities. For this purpose, the European Commission asked EFDA (European Fusion Development Agreement) to prepare a technical roadmap to fusion electricity that was published at the end of 2012 [2]. The roadmap is focused on three main projects:

- the ITER project, that represents the key step to fusion power;

- the DEMO project as intermediary step between ITER and the commercial fusion power plant;

- the IFMIF (International Fusion Materials Irradiation Facility) project, in parallel with ITER, focused on materials qualification under neutron irradiation.

This roadmap also defines three different periods with some main objectives:

- **Horizon 2020 (2014-2020)** that involves the construction of ITER together with the preparation of engineers, scientists and operators towards the fusion power plant technology;

- **Second period (2021-2030)** that will exploit ITER at its maximum performances and prepare DEMO construction;

- **Third period (2031-2050)**, focused in the completion of ITER exploitation, construction and operation of DEMO.

For what regards fission energy, a Technology Roadmap Update for Generation IV Nuclear Energy Systems was published in 2014, issued by the OECD (Organisation for Economic Co-operation and Development) Nuclear Energy Agency for the Generation IV International Forum (GIF) [1]. This document is an update of the original 2002 Technology Roadmap and its objective is to give attention on the six Gen IV systems originally selected and to provide a realistic technical progress report.
The Gen IV systems under study are: Gas-cooled Fast Reactor (GFR), Lead-cooled Fast Reactor (LFR), Molten Salt Reactor (MSR), Sodium-cooled Fast Reactor (SFR), Supercritical-water-cooled reactor (SCWR) and Very-high-temperature reactor (VHTR).

The main goals of GIF Technology Roadmap are summarised in four areas:

- **Sustainability**: the aim is to generate a sustainable energy minimising nuclear waste;

- **Safety and reliability**: it is of major importance to reach the maximum level of safety, especially after Fukushima Daiichi nuclear power plant accident, focusing on decrease the likelihood and degree of reactor core damage;

- **Economics**: nuclear power plants must have an advantage over other energy sources for what regards life cycle cost and financial risk;

- **Proliferation resistance and physical protection**: the risk of theft of weapon-usable material must be the lowest possible and physical protection against acts of terrorism has to be increased.

There are also additional issues for Generation IV systems to be considered, with respect to advanced light water reactors, that are related in particular to the use of non-water coolants in most of the designs, higher operational temperatures and power density [1].
The main purpose is to demonstrate that Gen IV systems are able to fulfil the requirements for safety and reliability goals. This condition can be reached also implementing the lessons learnt from the Fukushima accident.

1.2   Fusion reactors

The beginning of research on fusion energy can be traced back to the twenties but after the Second World War, the interest for thermonuclear fusion has become significant, particularly after 1958 with the "Atoms for Peace" conference in Geneva, during which American, British and Soviet fusion programs were made public [3]. Since that time, fusion research has been characterized by international collaboration [4] and today, several countries are involved: from European Union to USA, Russia and Japan, but also China, Canada and Korea.

So far, many fusion reactors have been constructed. Among tokamak[1] reactors there are JET (Joint European Torus), MAST (Mega Amp Spherical Tokamak) in the United Kingdom and the TFTR (Tokamak Fusion Test Reactor) in the USA. The most important international project is ITER, currently under construction in Cadarache, France. Meanwhile, China is working on a project that involves CFETR (Chinese Fusion Engineering Test Reactor) and is running the Experimental Advanced Superconducting Tokamak (EAST).

A tokamak is constituted by a toroidal vacuum chamber, which hosts the plasma, surrounded by several magnetic coils, as it can be seen in Figure 1.1.
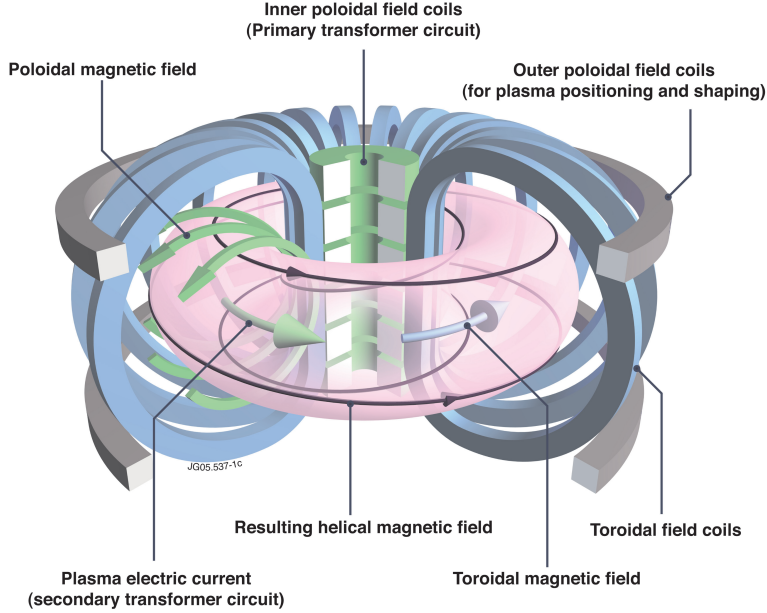
Figure 1.1: General structure of a tokamak [5]

---

[1]from Russian **to**(raidalnij) **ka**(mera) **mak**(ina), meaning 'toroidal chamber machine'.

Thermonuclear reactions take place in the plasma which must be maintained in a limited volume and kept away from any structural material, in order to preserve a sufficiently high temperature. In other words, it has to be confined.

Since the plasma is made of charged particles, it can be done by means of a magnetic field. The torus shape is created by the toroidal coils that surround the plasma. To minimize particle leakage, the field lines must be helicoidal and this is possible by adding another magnetic field to the toroidal one, which is perpendicular to it and called poloidal field. Plasma equilibrium, position and shape are controlled by a group of horizontal magnets called poloidal coils.

Fusion research also involves *stellarators*. For instance, there is the Large Helical Device (LHD) at Japan's National Institute of Fusion Research that is operating since 1998 and at the Max Planck Institute for Plasma Physics in Germany, the Wendelstein project is being progressed at the Wendelstein 7-X, that started at the end of 2015.
The main difference whit respect to a tokamak is that a stellarator relies on a very peculiar shape of the field coils that permit to have the toroidal twisted shape required to contain the plasma. Whit this design, the plasma current is not needed and this allows to avoid the difficult steady-state operation due to current-driven instabilities that affect tokamaks. In Figure 1.2 is possible to see the comparison between the two fusion reactor designs.
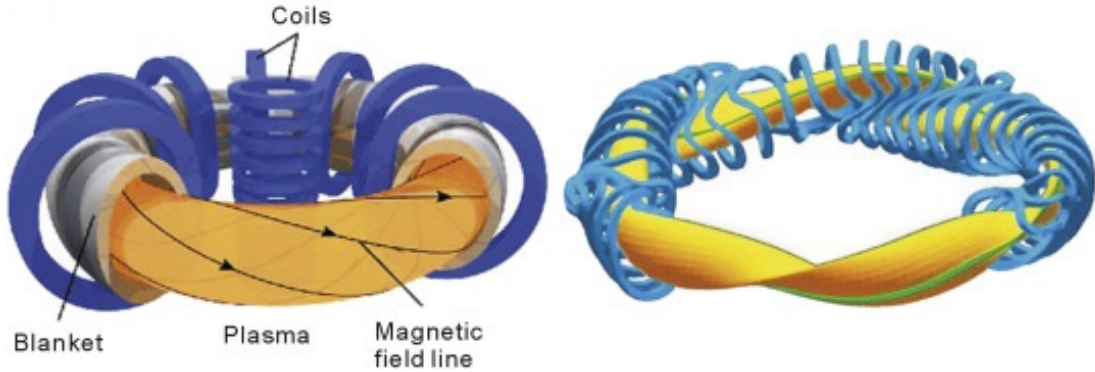
Figure 1.2: Comparison between a tokamak and a stellarator [6]

1.2.1 JET

Operating since 1983, the Joint European Torus (JET) is the largest tokamak in the world [7]. The project started in 1978 in the UK, launched by the European Community (Euratom with Sweden and Switzerland) and today, a lot of scientists and engineers are cooperating in this programme from all over the Europe.

JET is the key point for the design and construction of ITER since it is the current fusion device closest to it. In fact, all the experiments carried out on JET gave significant contribution for technologies and plasma operating scenarios.

In the last few years, JET became more similar to ITER so that it was possible to perform dedicated experiments and studies. For example, an important modification has been made on the JET vessel using the same First Wall materials planned for ITER (beryllium and tungsten) and this helped scientists to develop plasma scenarios as similar as possible to ITER's.
Another objective of JET is to demonstrate an acceptable tungsten and impurities concentration in the plasma core, coming from the wall, for the foreseen ITER regimes.

JET has some very important features. First of all, it is the only device among today's tokamaks capable of using deuterium-tritium fuel mix during its operation. It has also a powerful plasma heating system consisting of Neutral Beam Injection, Ion Cyclotron Resonance Heating and Lower Hybrid Current Drive. The beryllium handling facilities and the remote handling facilities allow the use of beryllium plasma-facing components (First Wall and divertor) and to work inside the vacuum vessel without the need for access. An inside view of JET can be seen in Figure 1.3.
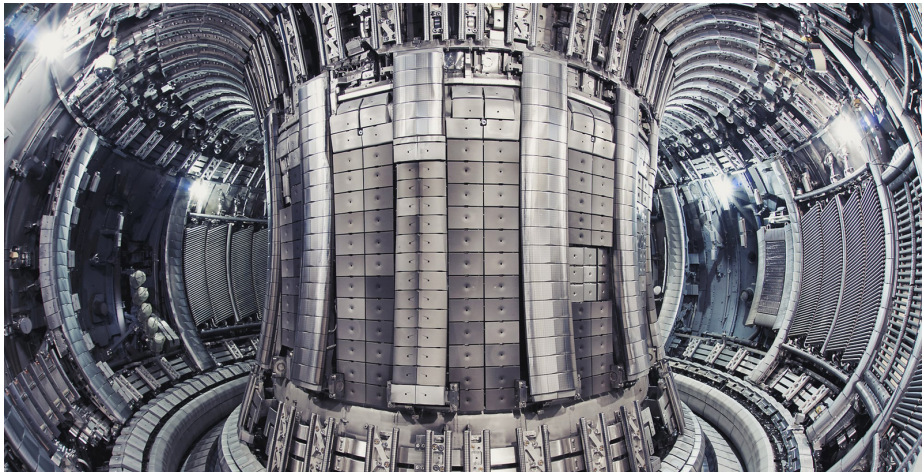
Figure 1.3: Inside view of the Joint European Torus [8]

1.2.2 ITER

The ITER project started in 1985 as a result of the cooperation among Soviet Union, Europe, Japan and USA. ITER stands for International Thermonuclear Experimental Reactor and its aim is to demonstrate that the production of energy from fusion is technically possible. The word "ITER" comes from the Latin "iter,-ineris", with the meaning of path towards the future. This reactor is currently under construction in Cadarache, in southern France, and the first D-T plasma is not expected until 2035 [9].

ITER's objective is to work at 500 MW continuously for a plasma discharge time of at least 400 seconds with an input power of 50 MW, having a gain factor of 10. It must be noticed that ITER will not produce electricity: this task is assigned to a Demonstration Power Plant, also known as DEMO, which is foreseen to begin operating in the early 2050s.

1.2.3 DEMO

DEMO (DEMOnstration Power Station) has the role of next step towards a commercial Fusion Power Plant: it is intended to produce a few hundreds of MW of electricity and to integrate the results obtained with the previous projects, including JET and ITER. Figure 1.4 shows an overview of the three reactors.

So, DEMO must demonstrate and validate all technologies involved in mechanical and structural materials, plasma facing materials, component resistance against 14 MeV neutron damage, tritium self-sufficiency and tritium extraction cycles.
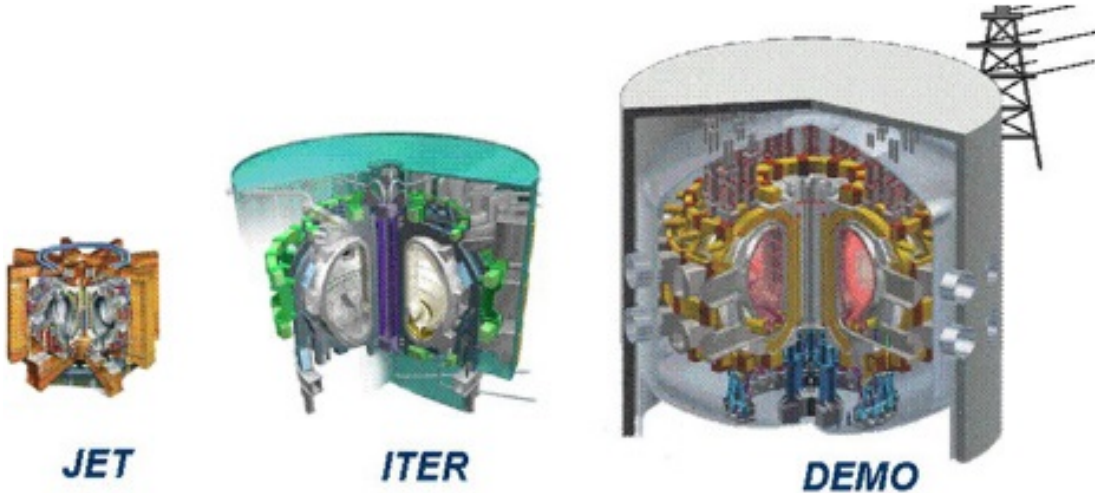
Figure 1.4: Overview of JET, ITER and DEMO [10]

1.3   Generation IV fission reactors

The GIF roadmap underlined six systems, summarizing the research progresses in the last decade and listing the challenges to be taken for the design of these nuclear reactors [1]. The Generation IV systems under study are:

- Sodium-cooled Fast Reactor (SFR);

- Lead-cooled Fast Reactor (LFR);

- Gas-cooled Fast Reactor (GFR);

- Molten Salt Reactor (MSR);

- Supercritical-water-cooled reactor (SCWR);

- Very-high-temperature reactor (VHTR).

A higher attention is given to SFR and LFR since France, the most important Country in Europe for what concerns nuclear energy, is working on a Sodium-cooled Fast Reactor called ASTRID (Advanced Sodium Technological Reactor for Industrial Demonstration) and the ENEA Research Centre in Brasimone is involved in the LEADER (Lead-cooled European Advanced Demonstration Reactor) project for the design of ALFRED (Advanced Lead-cooled Fast Reactor European Demostrator).

1.3.1   Characteristics of fast reactors

The main characteristic of a fast reactor is the absence of neutron moderator so the chain reaction is sustained only by fast neutrons [11].
In a thermal reactor, fuel is slightly enriched in fissile material ($<5\%$ in U^{235}) and the moderator slows down neutrons coming fission reactions: U^{235} is directly burned while U^{238} can capture a neutron and transmute into Pu^{239}, that has a neutron cross section similar to that of U^{235}.

Even if U^{235} and Pu^{239} are more sensitive to thermal neutrons, with a sufficiently enriched ($>20\%$ in U^{235}) or plutonium-based fuel it is possible to achieve a threshold quantity of fissile atoms to maintain a chain reaction also with fast neutrons [11]. Furthermore, fission reactions from Pu^{239} generate more neutrons with respect to uranium reactions, so this is possible not only to maintain the chain reaction but also to convert U^{238} into Pu^{239}.

So, in general, the main advantages of fast reactors are the improved neutron economy due to a greater number of neutrons per fission at high energies and the possibility to use fast neutron spectrum for breeding or transmutation of transuranic waste products. But, a drawback of fast reactors is the necessity of high fuel enrichment that is an expensive process.

1.3.2   Sodium-cooled Fast Reactors

In a Sodium-cooled Fast Reactor (SFR), the coolant is constituted by liquid sodium that has advantageous thermo-physical properties such as high boiling point, heat capacity and heat conductivity, leading to a high thermal inertia. These characteristics allow a low-pressure coolant system and high-power-density operation. In Table 1.1 the main thermo-physical properties of sodium are summarised.

Table 1.1: Thermo-physical properties of Na [12]

Boiling point	883 °C
Heat capacity (at 500 °C)	29.17 J/mol/K
Thermal conductivity (at 500 °C)	139.5 W/m/K

The plant size can range from 50 to 150 MW_e for small modular reactors and from 300 to 1500 MW_e for pool-type and loop-type reactors. Figure 1.5 shows the two possible configurations for a SFR.
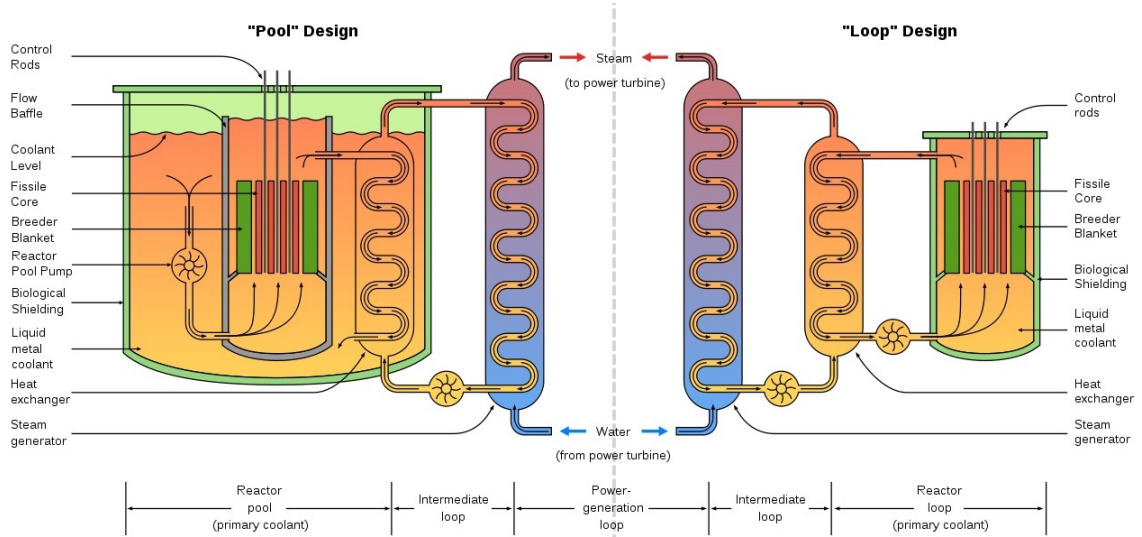
Figure 1.5: Possible configurations of a SFR [13]

In a "pool" design the primary coolant remains inside the reactor vessel that also contains the Intermediate Heat Exchanger (IHX). This configuration implies a large reactor vessel but reduces the risks of a primary pipe break or leak.

In a "loop" design the primary coolant leaves the reactor vessel and goes to the IHX which is located in the containment building, outside the reactor vessel. In this way, it is easier to isolate the loop for emergency or maintenance.

SFR in general have three heat transport systems:

- Primary Heat Transfer System (PHTS) that cools the core (with sodium);

- Intermediate Heat Transfer System (IHTS) that transports heat from the primary loop to the steam generator (with sodium);

- Energy Conversion System (Balance of Plant) that generates electricity through a turbine.

Both PHTS and IHTS operate at low pressure thanks to the high boiling point of sodium, while the BOP area is similar to a PWR but it runs at higher temperatures, leading to a higher energy conversion efficiency. Also, the presence of a secondary sodium loop avoids that activated primary sodium coolant reacts with water because of a steam generator tube break.

SFR designs typically have a containment structure that acts as last barrier against uncontrolled release of radioactive products both in operation and accident conditions. Figure 1.6 illustrates the path of the various substances inside the reactor.

The reactor vessel covers the core and most of primary heat transport system (PHTS) components and provides mechanical support for core and internals. Furthermore, it acts as barrier against the release of radioactive material.

There is also a guard vessel that protects the reactor vessel in case of failure caused by natural events or thermal creep induced rupture.

Other safety features are the presence of various reactivity control systems, passive or self-actuated shutdown systems and several decay heat removal systems, as shown in Figure 1.7.
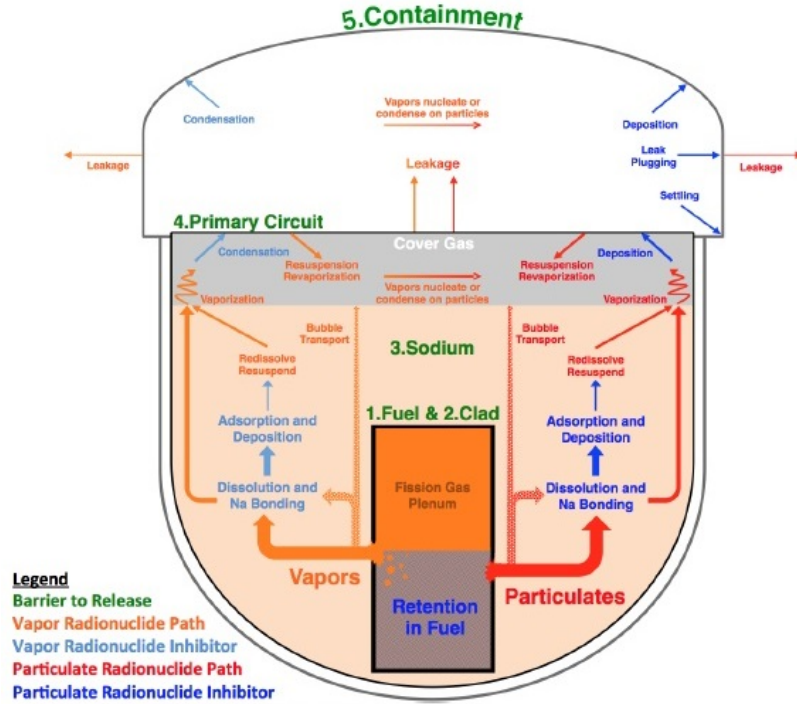
Figure 1.6: Barriers in a SFR [14]
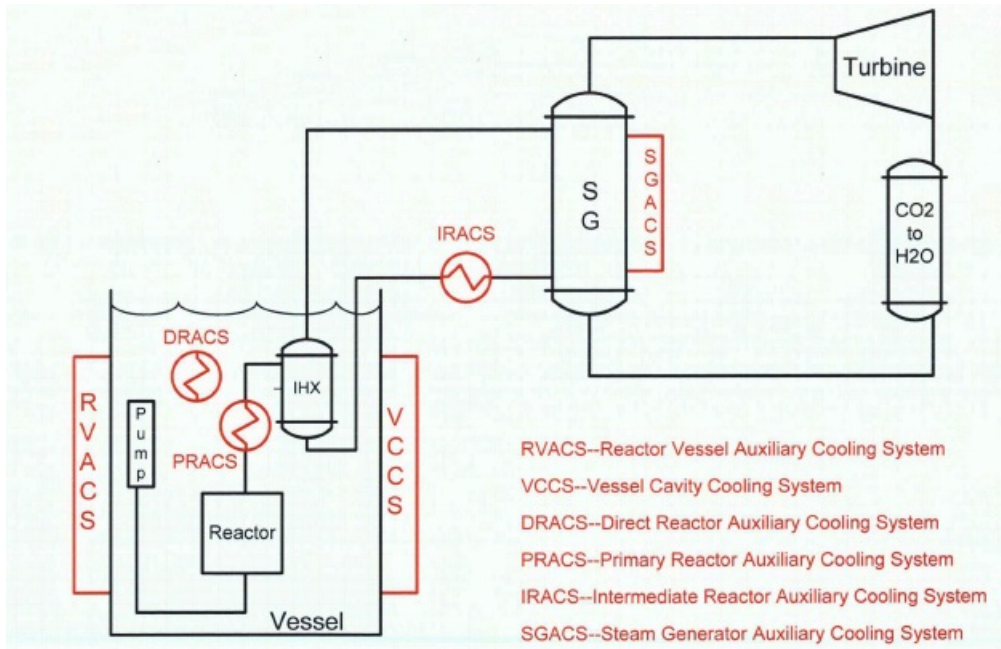
Figure 1.7: SFR Auxiliary Cooling Systems [13]

1.3.3 Lead-cooled Fast Reactors

Lead-cooled fast reactors use Pb or Pb-Bi alloy as coolant and operates at atmospheric pressure and at high temperature thanks to the boiling point of the coolant that is very high. In Table 1.2 it is possible to see the main properties of lead and lead-bismuth.

Table 1.2: Thermo-physical properties of Pb and Pb-Bi [12]

	Pb	Pb-Bi
Boiling point	1737 ℃	1670 ℃
Melting point	327.4 ℃	125 ℃
Specific heat (at 500 ℃)	145.3 J/kg/K	141.4 J/kg/K
Thermal conductivity (at 500 ℃)	17.67 W/m/K	14.48 W/m/K

Usually, the configuration of LFRs is "pool-type" but there is no need for the intermediate heat exchanger, thanks to the inertness of the coolant: the secondary loop, with high pressure superheated water, can interface directly the primary side with a steam generator inside the pool.

Another feature of LFRs is the closed fuel cycle that allows an efficient conversion of fertile uranium and management of actinides.

Figure 1.8 shows the typical scheme of a LFR:
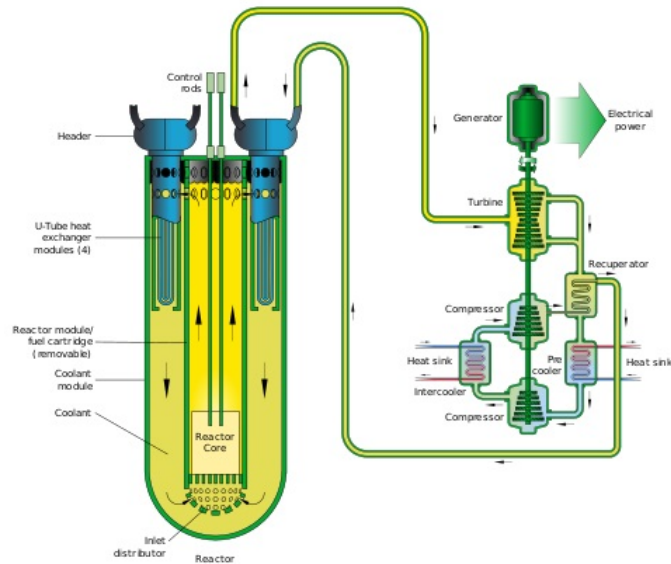
Figure 1.8: General design of a LFR [15]

Several LFR concepts are under study all around the world.

In Japan have been developed two basic concepts: a small LFR and a PBWFR (Pb-Bi cooled direct contact boiling Water Fast Reactor).

The Russian Federation is carrying out design activities for the BREST-300, expected to be in operation after 2020.

In Europe, there is a number of activities, starting from the conceptual design of a 300 MW$_{th}$ demonstrator called ALFRED (Advanced Lead Fast Reactor European Demonstrator) to the activities on MYRRHA (an acceleration driven lead-bismuth cooled system).

There are some advantages in using Pb and Pb-Bi because:

- they are chemically inert;

- there is no exothermic reaction between lead and water or air;

- in case of loss-of-heat-sink there is a significant thermal inertia thanks to the high heat of vaporization and high thermal capacity of lead;

- lead is a low neutron moderator, and this allows greater spacing between fuel pins so that there is a low core pressure drop and a lower risk of flow blockage;

- the coolant flow path together with the low core pressure drop allow natural convection cooling in the primary system for shutdown heat removal.

But there are also several drawbacks to face such as the need for coolant control to avoid corrosion effects on structural material and seismic/structural issues caused by the high weight of the coolant.

It is also difficult the inspection and monitoring of core components and fuel handling because of the opacity of lead and its high melting temperature (327 ℃) forces to maintain the temperature of the primary system at the right value to prevent the coolant from solidification.

In fact, the main efforts in the next decade will be focused on material research, lead corrosion, innovative systems, components and fuel developments.

1.3.4 Gas-cooled Fast Reactors

The GFR is a system which is cooled by helium and works at high temperature with a fast spectrum in a closed fuel cycle.

The use of helium as coolant has some advantages such as the fact that it is chemically inert, so corrosion and coolant radiotoxicity are avoided at high temperature operation, it is a single-phase fluid and it has low neutron moderation.
But helium has a low thermal inertia and this could cause problems since the core will rapidly heat-up if there is the loss of forced cooling and the gas density is too low to reach natural convection. System pressurization is also required, to allow natural convection in the circuit.

Figure 1.9 shows a typical GFR system scheme:
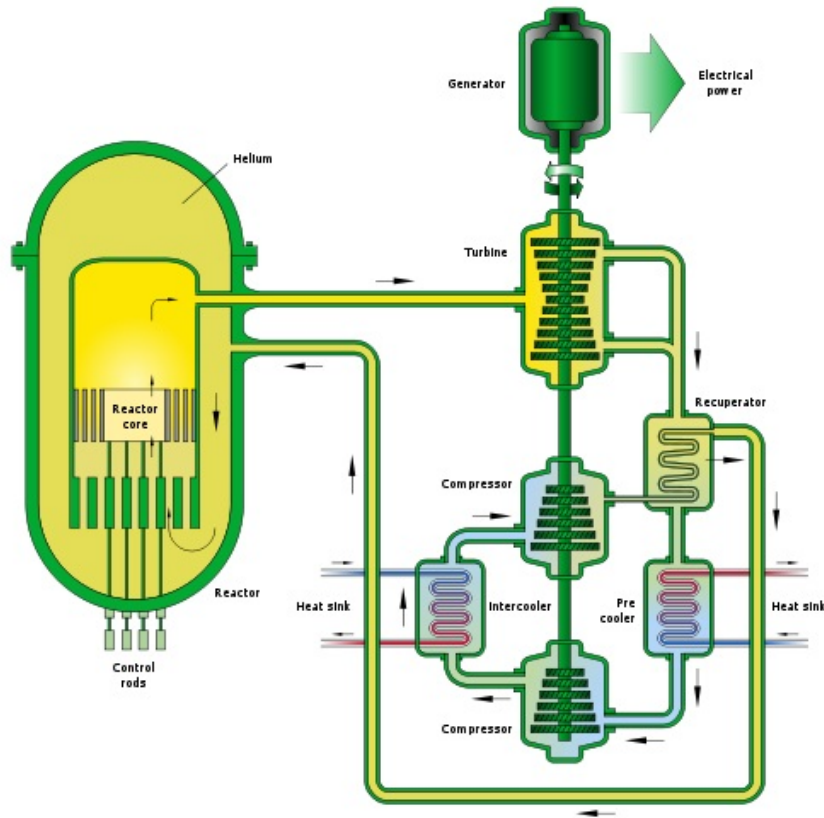
Figure 1.9: General design of a GFR [16]

At the moment, a consortium of four countries (Czech Republic, Hungary, Poland and Slovak Republic) is working on a project of an experimental reactor called ALLEGRO.

1.3.5 Molten Salt Reactors

In MSRs, the coolant is constituted by molten fluoride salts, in particular it is a lithium fluoride (LiF) and beryllium fluoride (BeF_2) mixture (FLiBe), and the operation is kept at low pressure. In Table 1.3 the main characteristics of the coolant are shown.

Table 1.3: Thermo-physical properties of FLiBe [17]

Melting point	460 ℃
Heat capacity (at 700 ℃)	2415.78 J/kg/K
Thermal conductivity (at 700 ℃)	1.0 W/m/K

Molten salt reactors can operate with thermal or fast neutron spectrum but their main characteristic is that the fuels (thorium, uranium and plutonium) are dissolved in the coolant in the form of fluoride salts. The moderator, in the case of thermal reactor, is constituted by graphite that is chemically compatible with the fluorides [18]. Figure 1.10 illustrates a molten salt reactor scheme:
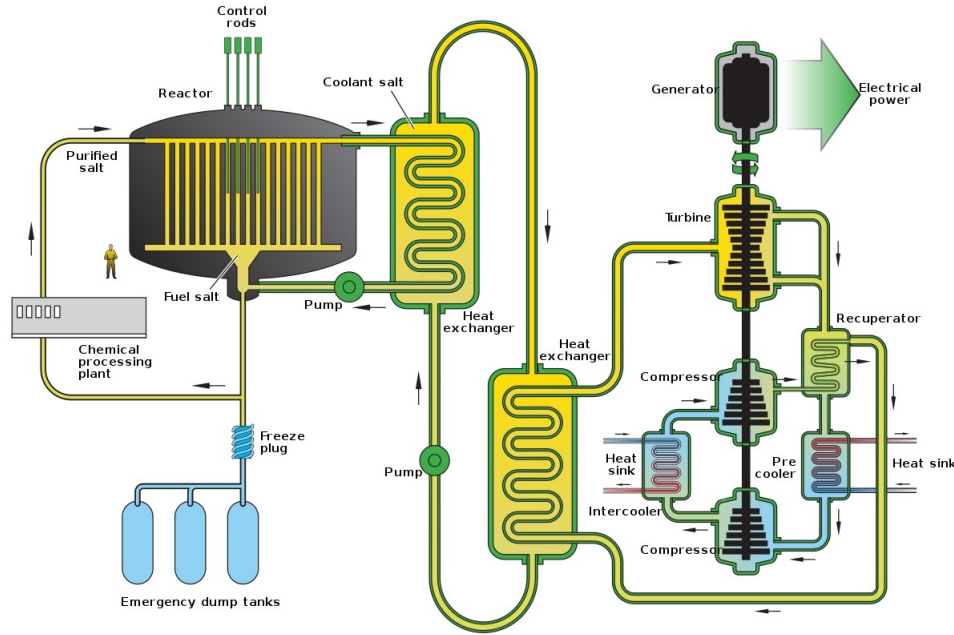
Figure 1.10: General design of a MSR [19]

The heat is transferred first to a secondary salt loop and then to a tertiary circuit with steam. According to the liquid-fuel design, fission products are removed in a purification loop and replaced with fresh fuel.

About safety, the plant is provided with freeze plugs which have the function of draining the molten salt away from the moderator if excessive temperatures are reached.

There are some drawbacks as the primary coolant is concerned. First of all, having the fuel in solution leads to a radioactive primary coolant and this can complicate maintenance chemistry control procedures. Furthermore, beryllium is toxic so it is better to foresee a design without it, even if to maintain LiF in liquid form requires higher temperatures. Also, the lithium used is as purer as possible Li^7, since Li^6 produces tritium when hit by neutrons. So, lithium must be enriched beyond its natural level of Li^7 to minimise tritium production.

For now, research is focused on solid fuel MSR technology because it is difficult to use molten salt with very high activity levels associated with dissolved fuels and fission products. When there will be enough experience in component design, operation and maintenance using clean salts, it will be much easier to consider the use of liquid fuels.

1.3.6 Supercritical-water-cooled Reactors

SCWRs are systems that work at high temperature and pressure, operating above the critical point of water (374 ℃ and 221 bar), and are cooled by light water. According to the core design, the neutron spectrum can be thermal or fast and the moderator can be light or heavy water.

With respect to traditional water-cooled reactors, SCWRs have some advantages:

- since the coolant experiences a higher enthalpy rise in the core, the efficiency can reach 44% or more, compared to 34-36% or current reactors [20];

- the coolant is in superheated conditions, so steam generators used in PWRs and steam separators and dryers can be omitted, as can be seen in Figure 1.11;

- it is possible to decrease the capital cost of the conventional island since a smaller size of the turbine system is required for a steam with a higher enthalpy.

However, research is still in progress since there are many challenges to be taken into account, starting from the validation of the transient heat transfer models, in case of depressurization from supercritical to sub-critical conditions, the qualification of materials, since they experience a higher temperature compared to current LWRs, the control of the density inside the core, since it significantly changes and this can lead to instability, demonstration of passive safety systems and so on.
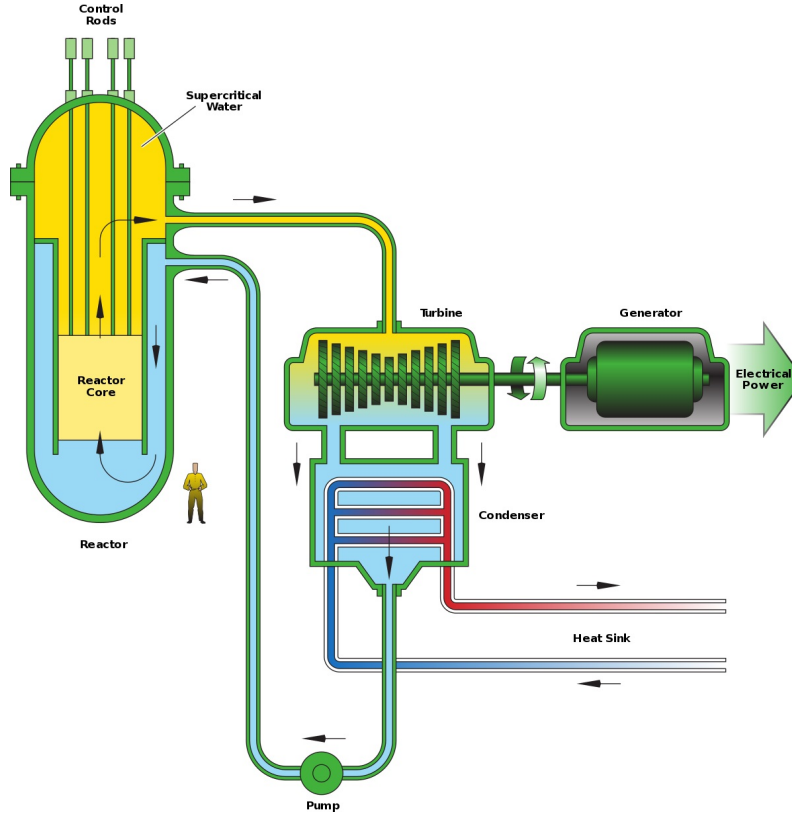
Figure 1.11: General design of a SCWR [21]

1.3.7 Very-High-Temperature Reactors

In the history of HTGRs (High Temperature Gas-cooled Reactors), VHTR represents an important step since it is dedicated not only to the generation of electricity but also to the production of hydrogen via thermochemical, electrochemical or hybrid processes.

VHTR has a thermal neutron spectrum, it is cooled by helium, uses graphite as moderator and works in a range of temperatures between 700 and 950 ℃, but it will potentially go beyond 1000 ℃ in the future.

There are two typical reactor configurations for a VHTR, that are the pebble bed type and the prismatic block type. Even if the two layouts have a different shape, both configurations use TRISO (TRIstructural ISOtropic) coated particle fuel in the graphite matrix, have the core structure entirely constituted by graphite and have a low power density: this allows to achieve high outlet temperatures avoiding the release of fission products from the coated particle under both normal and accident conditions.

The heat transfer process is very simple: there can be a direct cycle with a gas turbine system directly placed in the primary loop or a Rankine cycle with the use of a conventional steam generator.

As can be seen in Figure 1.12, the heat application process, which can be process heat for refineries or metallurgy or hydrogen production, is joined to the reactor with an intermediate heat exchanger (IHX).
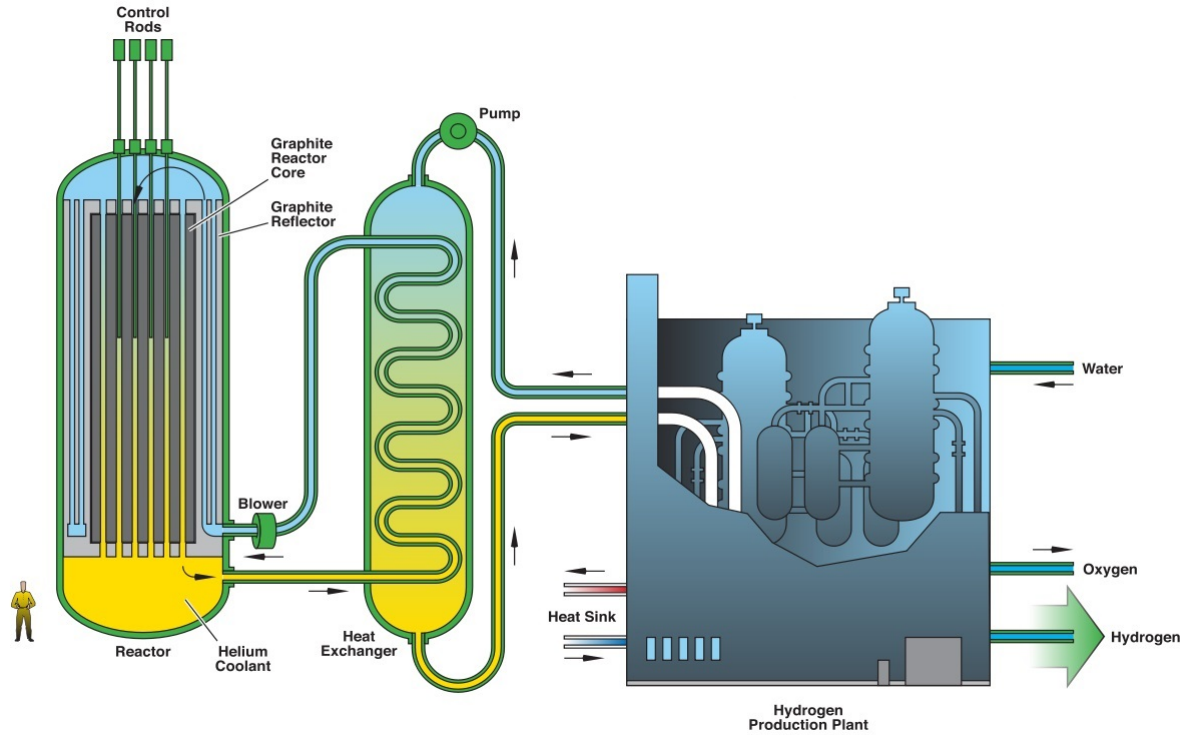
Figure 1.12: General design of a VHTR [22]

Chapter 2

Purification from tritium

2.1 Introduction

The presence of tritium is a relevant issue for both fusion reactors and fission reactors. For what concerns fusion reactors, tritium is needed as fuel in plasma D-T reactions, as explained with the following equation:

$$D^2 + T^3 \longrightarrow He^4 + n \tag{2.1}$$

Since the required quantity of tritium cannot be found in nature, these reactors must self-produce it to feed the fusion reactions. So, the neutron coming from the fusion reaction is used to produce tritium according to the following equation, which takes place in the blanket:

$$Li^7 + n \longrightarrow T^3 + He^4 + n \tag{2.2}$$
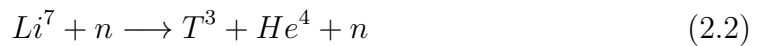
Considering that some neutrons are lost and the reactor must produce slightly more tritium than it burns to take into account tritium losses, there is the need for neutron multipliers, such as beryllium or lead, which react with neutrons to produce a second neutron. The ratio between the amount of generated and burnt tritium is called *tritium breeding ratio* and it is a fundamental parameter for the self-sufficiency of the fusion reactor.

In fission reactors, tritium is produced by:

- ternary fissions (in which there are three fission products instead of two and the third is a nucleus of tritium);

- neutron capture reactions involving the boron inside the control rods, according to the following equations:

$$B^{10} + n \longrightarrow T^3 + 2\ He^4 \tag{2.3a}$$

$$B^{10} + n \longrightarrow He^4 + Li^7 \tag{2.3b}$$

$$Li^7 + n \longrightarrow T^3 + He^4 + n \tag{2.3c}$$
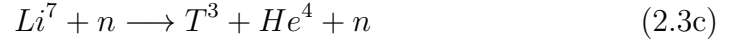
- activation of impurities contained in the coolant and structural materials, for which the major reaction is the following:

$$Li^6 + n \longrightarrow T^3 + He^4 \tag{2.4}$$

For both types of reactors, it is necessary to keep the release of this isotope under a specific threshold value since it is very penetrating and can permeate through plant's components and escape into the environment, representing a risk for human health.

This chapter will explain how a purification system works and what are the main technologies used in nuclear reactors, from the CPS of fusion systems to the cold traps employed in fission systems.

2.2   Fusion systems

Fusion power plants are provided of some ancillary systems that have the function of manage the tritium present in the blanket; in particular, these systems are supposed to extract the tritium from the breeding zone and from the cooling system.

Europe is working on two types of Test Blanket Modules (TBMs) to be tested in ITER, based on HCLL (Helium Cooled Lithium Lead) and HCPB (Helium Cooled Pebble Bed) breeding blanket (BB) concepts.
The ancillary systems foreseen for these TBMs are:

- the PbLi circuit (only for the HCLL-TBM);

- the Helium Cooling System (HCS);

- the Coolant Purification System (CPS);

- the Tritium Extraction System (TES).

Figure 2.1 shows the schematic location of the ancillary systems: TBMs are inside the vacuum vessel (VV), the tritium extraction system and the PbLi loop are arranged in a port cell (Port Cell #16) while HCSs and CPSs are in a chemical and volume control system (CVCS) area. The tritium building hosts the Tritium Recovery System (TRS) and the Tritium Exhaust Processing system (TEP).
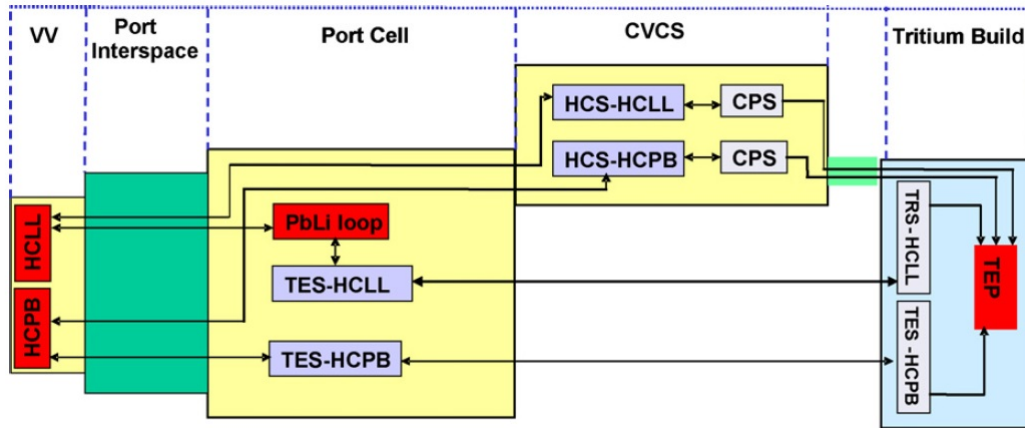
Figure 2.1: Schematic location of the ancillary systems [23]

In this work, attention is given to HCS, which will be briefly described in this section, and CPS, which will be analysed in detail.

The Helium Cooling System has the primary function of extracting the thermal power from the TBM due to plasma radiation and neutron interaction. The used coolant is helium working at 80 bar and 1.3 kg/s, while inlet and outlet temperatures are 300 and 500 ℃. Figure 2.2 shows the process flow diagram of the HCS.
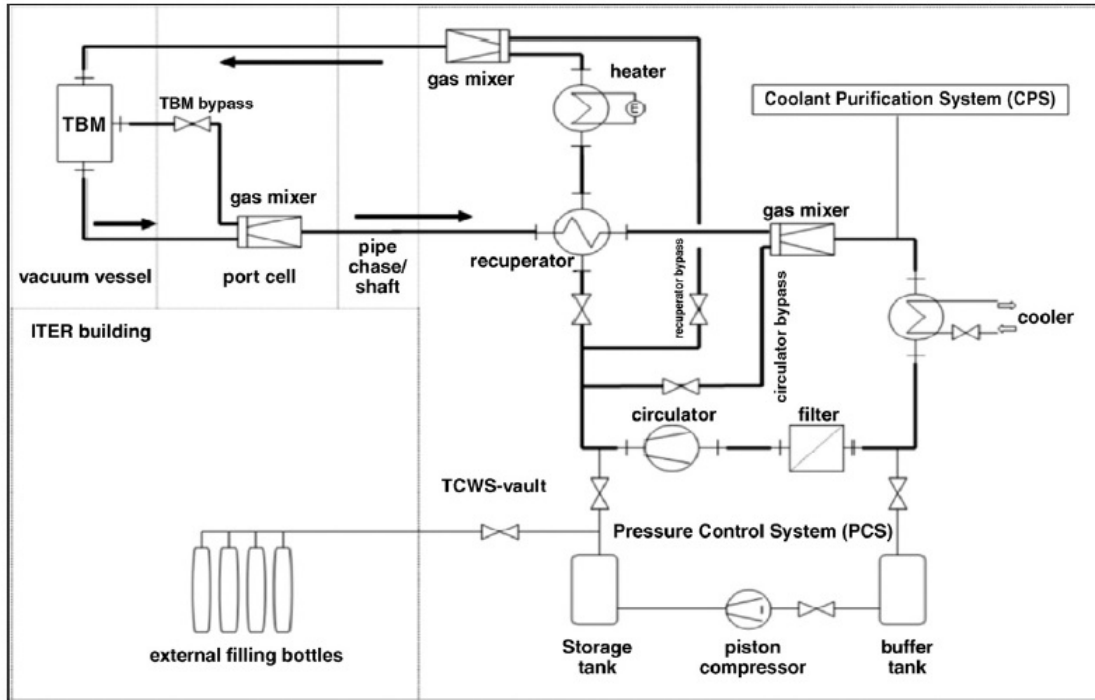
Figure 2.2: HCS Process Flow Diagram [23]

The loop has an "eight" shape where the TBM is installed on the hot leg and the circulator on the cold leg. Before the circulator there is a cooler that brings the temperature to a value suitable for its proper operation (below 50 ℃). Then, an electrical heater increases helium temperature to the inlet value for the TBM operation.

In the middle of the loop there is a heat recovery unit with a high heat exchange efficiency that minimizes the power to be added by the heater.

2.2.1 CPS

The Coolant Purification System is a very important auxiliary circuit whose main function is to extract the tritium permeated from the primary circuit, keeping under control the chemistry of the coolant in the HCS [24].

The removal of tritium is necessary since it is required to keep at low value the tritium partial pressure inside the HCS. In fact, the driving force of permeation is characterised by the tritium partial pressure which is related to tritium concentration through the Sievert's law [25]:

$$C_{eq} = K \cdot p^{1/2} \tag{2.5}$$

Where C_{eq} [mol/m^3] is the concentration of the gas dissolved at chemical equilibrium, p [Pa] is the partial pressure and K is called Sievert's constant.
So, the release into the environment through permeation or leakage has to be controlled.

In order to clearly understand the function of the CPS, Figure 2.3 illustrates a simple flow diagram of HCS and CPS:
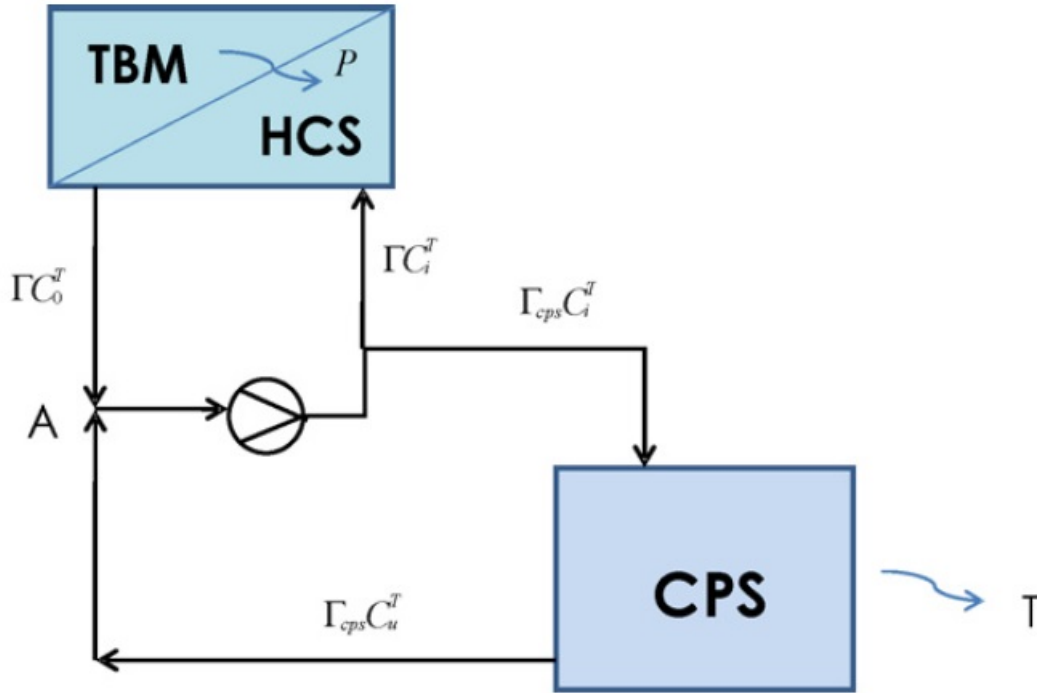
Figure 2.3: CPS Flow Diagram [24]

In the diagram, Γ_{cps} [kg/s] is the gas mass flow rate entering the CPS, $C_i{}^T$ and $C_o{}^T$ are the tritium concentrations at HCS inlet and outlet, $C_u{}^T$ is the tritium concentration at the CPS outlet, P [kg/s] is the tritium permeation rate from the blanket and Γ [kg/s] is the total helium flow rate in the HCS.

The process of the CPS is constituted by three steps:

- oxidation of Q_2 (H_2 and T_2) into Q_2O in a metal oxide bed;

- adsorption of Q_2O using a PTSA (Pressure Temperature Swing Adsorption);

- adsorption of other impurities using a heated getter.

Figure 2.4 shows the process flow diagram of the CPS for HCLL and HCPB modules:
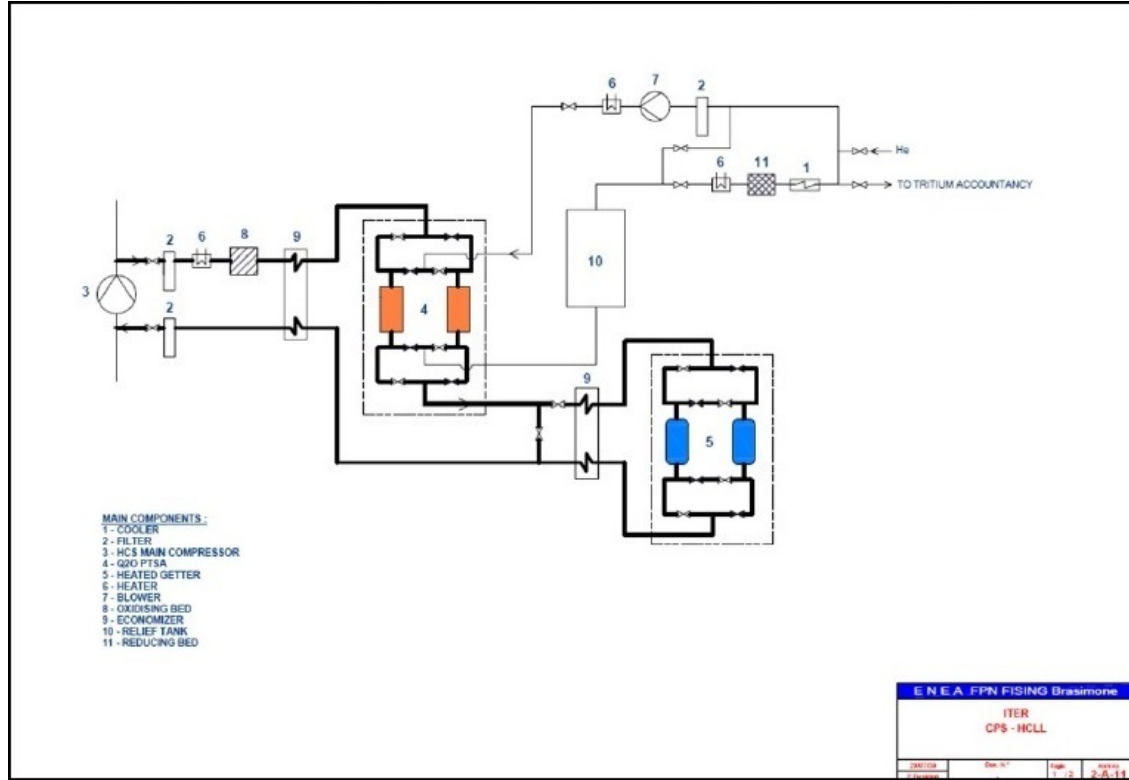
Figure 2.4: CPS Process Flow Diagram [24]

As can be seen from this diagram, the streaming gas is taken downstream the HCS compressor and sent to the first part of the CPS.

For what regards this first phase, it is convenient to use oxidizing particles, made of CuO which is reduced to Cu, according to the following equation:

$$Q_2 + CuO \longrightarrow Q_2O + Cu \qquad (2.6)$$

The temperature of the streaming gas is 250-300 °C.

The regeneration of the bed with addition of O_2 is quite difficult: a first flux of pure helium (or using vacuum) is necessary in order to remove H_2 that is explosive with O_2, and then another flux of helium is required to eliminate residual O_2. So, the best solution would be to overestimate the oxidizing bed so that when the reduction of CuO is complete, only a change of the bed is required.

In the second part of the system, the streaming gas is required to be at room temperature, so a helium-helium economizer is installed.
The flow is then sent to a system consisting of two columns in parallel (PTSA Columns), one operating in adsorption mode at room temperature and the other one operating in regeneration mode, using a flow of helium at high temperature; when a column is saturated, it is switched in regeneration mode and the regenerated column is placed in adsorption mode.
This type of technology is widely used in industrial applications (process industry, insulating glass industry, for refrigerant drying, packaging desiccants...), but the process used in the CPS is quite different, since between the two modes of operation there is not only a considerable difference of temperature, but also a strong difference of pressure for the gas to be purified (about 80 bars in adsorption mode and some bars in regeneration mode).

The two columns are filled with Zeolite Molecular Sieves (zeolites are highly porous materials which are produced synthetically and which belong to the class of alluminosilicates) for the adsorption of CO_2 and Q_2O. The candidate materials are two types of molecular sieves: Type X and Type A. The most suitable material to contemporarily remove H_2O and CO_2 is the 13X molecular sieve, while the zeolites 3A and 4A are the most used in case of H_2O adsorption only.

After the adsorption phase in the PTSA, a portion of the CPS flow rate is sent to a heated getter based on a zirconium alloy. Some experimental data show that with this component, the quantity of impurities (O_2, CH_4, H_2, CO, N_2...) can be reduced to less than 1 ppbv, also with a concentration of 5-10 ppmv for each impurity species [26]. This getter cannot be regenerated, so it must be replaced.
The streaming gas is then sent to the HCS upstream the compressor, so that a dedicated compressor for the CPS is not necessary.

2.3   Fission systems

Tritium production is actually a relevant issue for fast reactors. The most interesting cases for this work are the High Temperature Reactors (HTRs), since they are usually cooled by helium, and fast reactors cooled by liquid metals, that are Sodium-cooled Fast Reactors (SFRs) and Lead-cooled Fast Reactors (LFRs). There are three main tritium sources in fission reactors:

- ternary fissions in the fuel;

- boron activation in control and shielding rods (made of B_4C);

- activation of impurities in the coolant, such as lithium.

The importance of tritium removal relies in the fact that this hydrogen isotope is very penetrating and has a high mobility, so it can be dangerous since it can easily reach the environment.

For what regards HTRs, the CPS was employed to avoid the oxidation of graphite (used as moderator) by impurities and corrosion of the materials exposed to high temperatures, in particular the steam generator [24]. The proposed solution for the CPS in ITER is a process that is very similar to that adopted for HTRs.

As liquid metal-cooled reactors are concerned, the technology that is commonly used is based on cold traps. This method has been developed to remove tritium and other impurities from sodium, used as coolant in LMFBRs (Liquid Metal Fast Breeder Reactors) [27]. Several experiments have been done and was found that the most effective mechanism of tritium removal is the co-precipitation (simultaneous precipitation of hydrogen and tritium).

The principle of operation of a cold trap is quite simple: in this device, the crystallization of sodium oxides and hydrides (Na_2O and NaH) is forced by cooling and this causes a decrease of the solubility in liquid sodium of hydrogen and oxygen that precipitate. A reference design of a
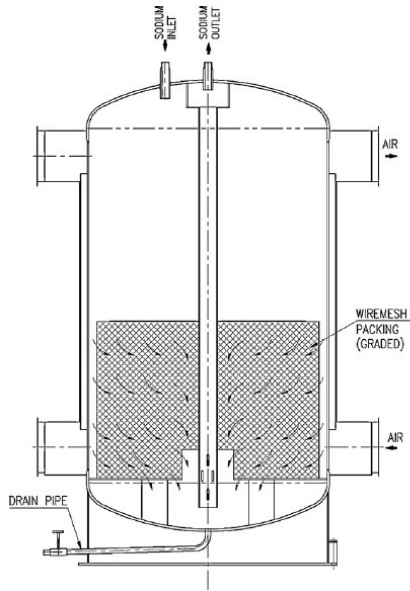
Figure 2.5: Scheme of a cold trap [28]

cold trap is shown in Figure 2.5. Air, used as cooling medium, enters at the bottom and exits from the top of the cold trap. Sodium passes through the wired mesh and gets purified, since oxygen and hydrogen precipitate as sodium reaches the lower part of the cold trap.

An example of a sodium purification loop using a cold trap is shown in Figure 2.6.
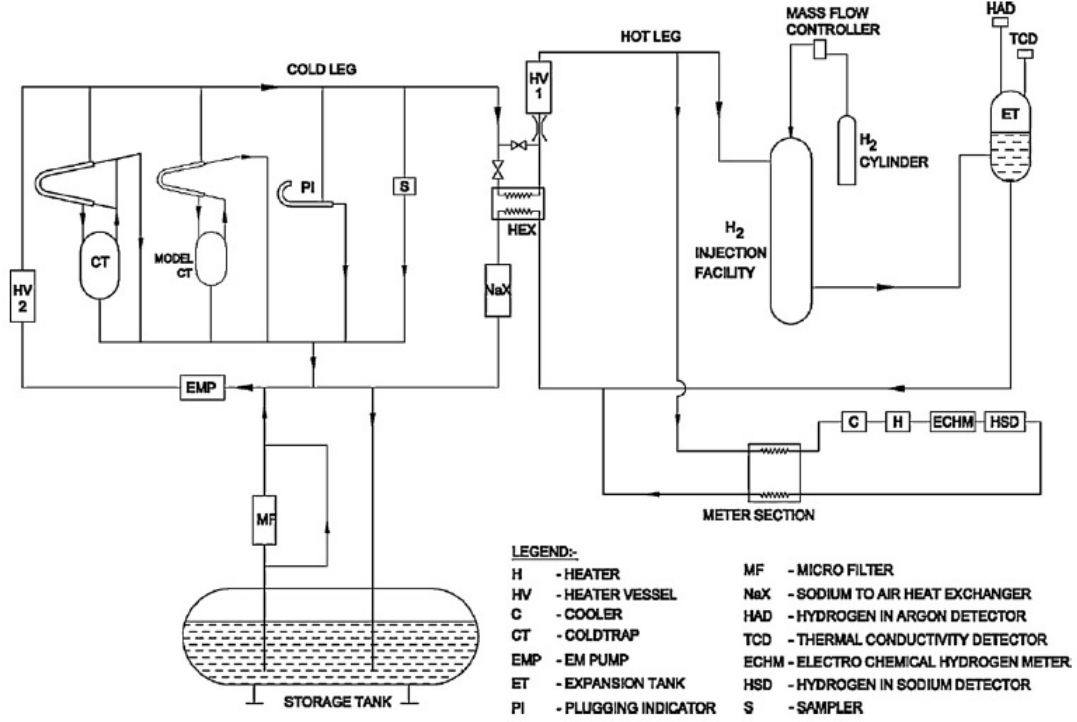
Figure 2.6: Example of a sodium purification circuit [28]

The presence of tritium involves not only the coolant, but also the cover gas of pool-type reactors. The technologies developed for fusion reactors could find an application also in fission reactors, in order to purify the cover gas of LMFR and to perform the chemistry control of GFRs and VHTRs.

Some international projects are in progress with the aim of studying the applicability of fusion technologies to Generation IV reactors, such as the project HORIZON 2020 – TRANSAT – TRANSversal Actions for Tritium.

This work will present a preliminary study of the applicability of the CPS technology to a purification system for the cover gas of the ASTRID reactor.

Chapter 3

Application of fusion systems to Gen IV reactors

3.1 Introduction

One of the purposes of this work is to study the application of the technologies used in fusion systems for the purification of the cover gas of the ASTRID reactor.

ASTRID (Advanced Sodium Technological Reactor for Industrial Demonstration) is a pool-type Sodium-cooled Fast Reactor, with an electrical capacity of 600 MW_e (1500 MW_{th}), that will be designed in order to achieve the requirements given from the Generation IV International Forum on sodium fast reactors, in particular for what regards safety and operability.

In this section, input data and preliminary calculations for a tritium purification system of the cover gas will be presented. Two types of solution will be adopted: the first one foresees a circuit with a single adsorption column designed for the whole life of the plant; the second one involves an additional circuit that allows the regeneration of the adsorption column.
A short description of candidate materials necessary to carry out the analysis will be provided.

3.2 ASTRID purification system

The main purpose of the purification system for the cover gas of ASTRID reactor is to remove the tritium that permeates from the liquid sodium.

Even though there is not a great amount of tritium in the cover gas, since most of it permeates into the steel of the IHX and goes into secondary and third cooling systems, it is very important to remove it to avoid an excessive release into the environment. The limit of release has been set equal to the dose that is received from the water consumption during a year, since it is naturally tritiated. In particular, the tritium limit is 0.04 mSv (4% of the annual dose limit, which is 1 mSv for the public) [29].

Figure 3.1 and Figure 3.2 illustrate the preliminary schemes of the two purification system solutions.
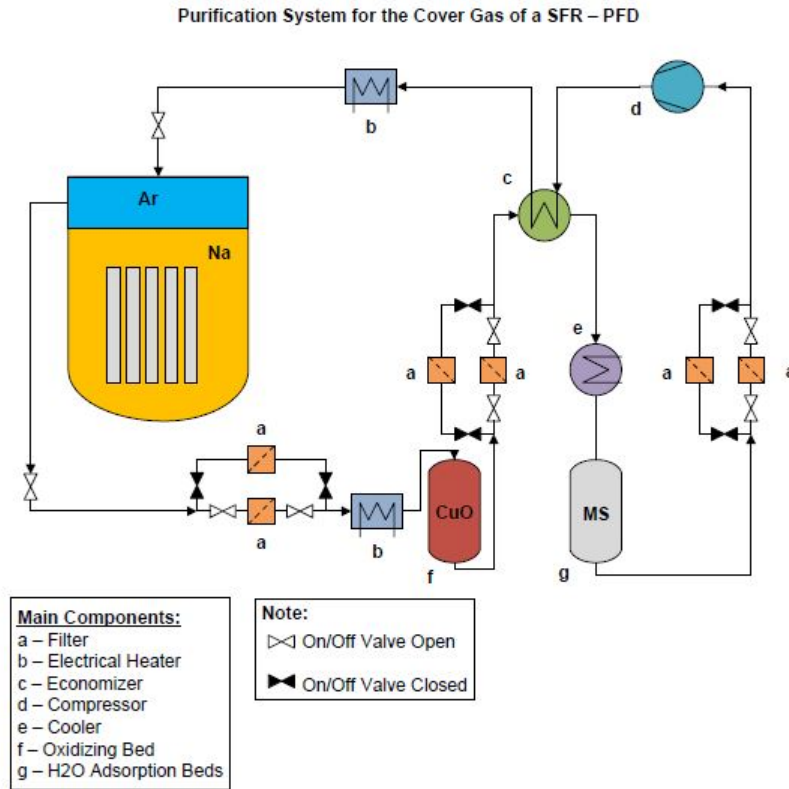
Figure 3.1: Purification System solution without regeneration of the molecular sieves
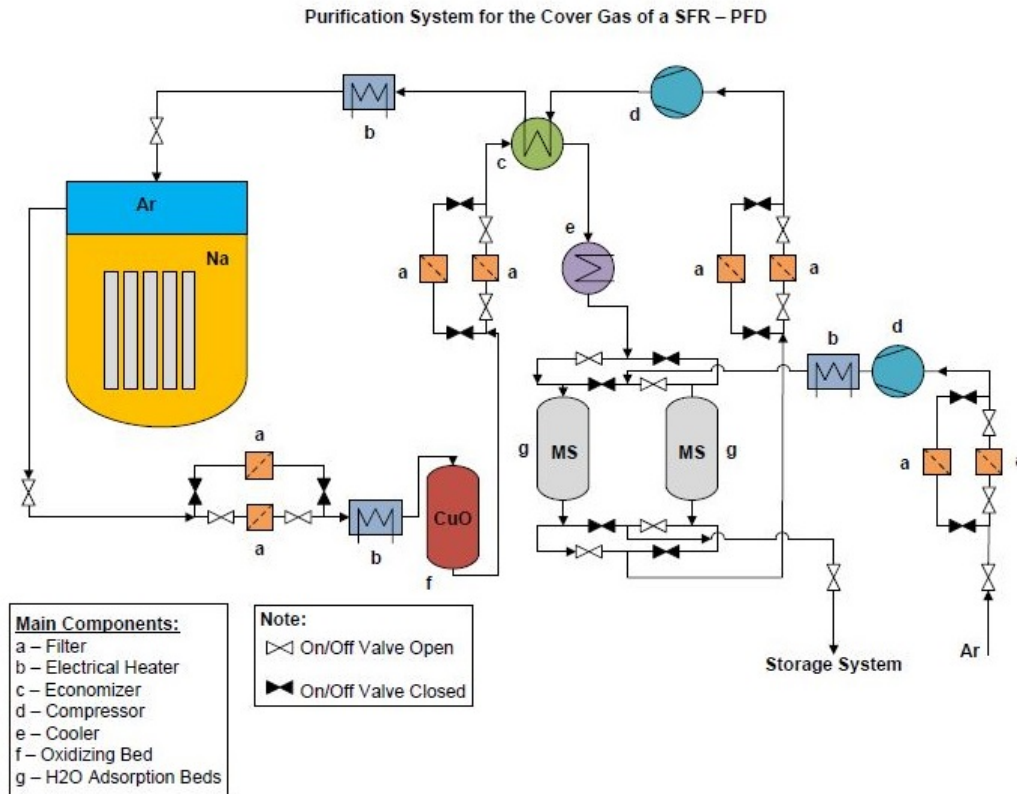
Figure 3.2: Purification System solution with regeneration of the molecular sieves

The two Process Flow Diagrams show the flow of the gas that has to be purified and the main components of the system.

Argon is withdrawn from the cover gas and sent to the Purification System (PS), passing through a filter to eliminate solid or aerosol impurities. The presence of two filters allows the operation to continue in case one of them is obstructed.

Inside the Oxidizing Bed, the tritiated gas (H_2 + HT) is transformed in tritiated water (H_2O + HTO), since the extraction of water from argon is easier and more efficient with respect to hydrogen. The catalytic reaction needs high temperatures to occur (about 250 °C) so, an Electrical Heater is placed at the inlet of the Oxidizing Bed.

The mixture of Ar and Q_2O (where Q = H, D, T) coming from the Oxidizing Bed goes through a filter, to keep the powders generated by the friction between the gas and the solid catalyst.

After the filter, the gas enters an Economizer: in fact, the gas entering the molecular sieve bed needs to be cooled, while the purified gas must be heated

before coming back in the cover gas. In this way the heat exchanger recovers part of the heat, allowing an energy saving.

The molecular sieves considered for the adsorption of tritiated water are the zeolites, which have the highest performances at low water pressure, in comparison with others commercial sorbents (activated carbon, alumina, silica gel) [30]. To be effective, zeolites must work at low temperature (room temperature or lower) so, the gas needs to be cooled using a water cooler.

In the first solution, all the tritiated water is trapped in one fixed bed. In the second solution, two fixed beds are present: the first one works in purification phase at room temperature and the second one works in regeneration phase at high temperature (250-300 ℃). When a fixed bed is saturated, it is placed in regeneration phase and the regenerated one is instead placed in adsorption phase. The regeneration loop foresees the presence of filters, a gas circulator and an electric heater.

The purified gas coming from the molecular sieve bed goes through a filter to eliminate the powders generated by the friction between gas and zeolites, to protect the compressor. The gas, driven by the compressor, is finally reintroduced into the cover gas, after having passed through the Economizer and the Electrical Heater.

These two solutions are very similar to the first part of the Cooling Purification System (CPS) proposed by ENEA for the Helium-Cooled Pebble-Bed (HCPB) and Helium-Cooled Lithium-Lead (HCLL) Blankets of ITER Reactor [24].
As indicated in the previous chapter, the proposed solution for the CPS of ITER is a three-stage process:

- oxidation of Q_2 and CO to Q_2O and CO_2 by means of a mix of Cu_2O-CuO or CuO only;

- adsorption of Q_2O and CO_2 on molecular sieves (zeolites) at room temperature;

- removal of residual impurities using a heated getter component.

The solutions proposed for the purification of the ASTRID cover gas take into account only the first two steps, because there is interest in the removal of tritium only.
In Figure 3.3 the part of the ITER CPS considered in these evaluations has been highlighted.
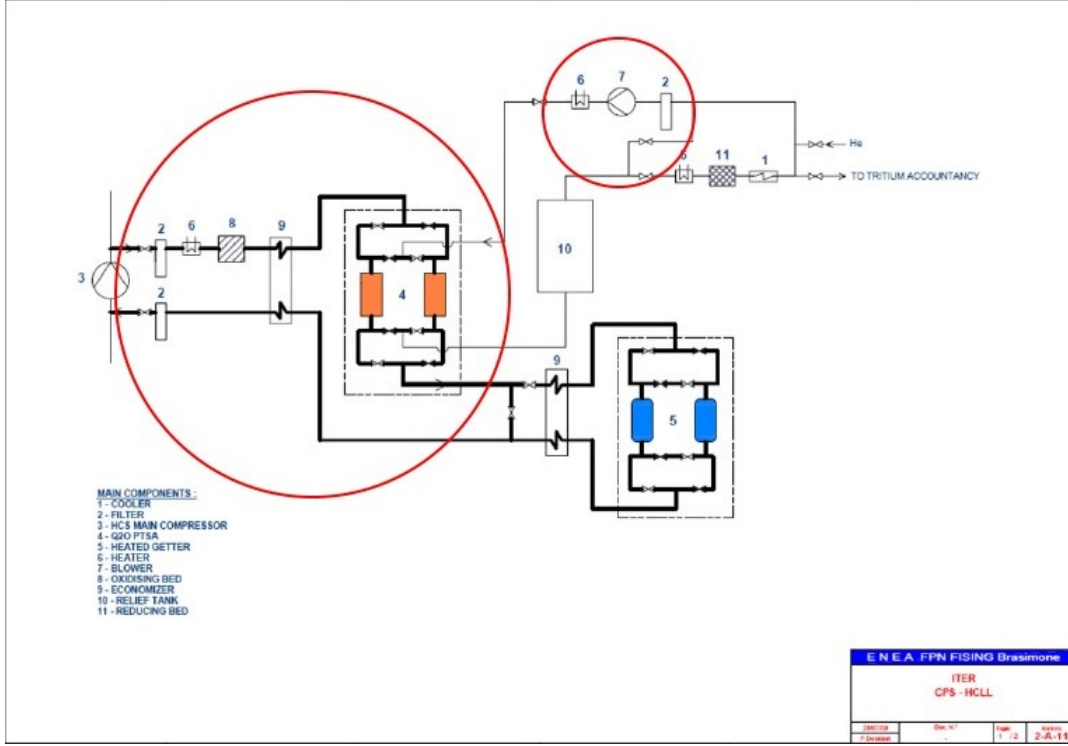
Figure 3.3: PFD of the CPS relevant to the HCLL Blanket of ITER [24]

3.2.1 Theoretical aspects of fixed beds

For the oxidation of hydrogen isotopes and the adsorption of tritiated water, fixed beds will be used. These vessels are very used in the process industries as catalyst reactors and adsorption/desorption beds. They contain granular material, typically in the form of pellets or beads, packed in a bed. The catalytic reaction occurs when the process gas enters in the bed, coming in contact with the solid material. The fixed bed geometry is usually cylindrical and the direction of the gas flow is parallel to the cylinder axis.

One of the most important parameters for the design of a fixed bed is the pressure drop. In fact, insufficient or excessive pressure drop is one of the most important factors responsible of a poor performance of the fixed bed [30]. The pressure drop across a fixed bed is usually evaluated considering empirical correlations and one of the most used has been proposed by S. Ergun [31].

Ergun equation for pressure drop in a fixed bed

The Ergun correlation expresses the relation between the friction factor in packed columns and the modified Reynolds number:

$$f_p = \frac{150}{Re_p} + 1.75 \tag{3.1}$$

Where f_p and Re_p are the friction factor of the fixed bed and the modified Reynolds number, respectively. These quantities are defined as:

$$f_p = \frac{\Delta p}{L} \frac{D_p}{\rho {v_s}^2} \left(\frac{\varepsilon^2}{1 - \varepsilon} \right) \tag{3.2}$$

$$Re_p = \frac{\rho v_s D_p}{(1 - \varepsilon)\mu} \tag{3.3}$$

Where

- Δp is the pressure drop across the bed, in [Pa];

- L is the length of the bed, in [m];

- D_p is the equivalent spherical diameter of the particles of the bed, in [m];

- ρ is the fluid density, in [kg/m^3];

- v_s is the superficial velocity of the fluid (considering the empty bed and the same volumetric flow rate), in [m/s];

- ε is the void fraction of the bed;

- μ is the dynamic viscosity of the fluid, in [Pa·s].

Substituting into Eq. (3.1) it is possible to put in evidence the pressure drops per unit length for a fixed bed, obtaining:

$$\frac{\Delta p}{L} = \frac{G}{\rho D_p} \left(\frac{1 - \varepsilon}{\varepsilon^3} \right) \left[\frac{150(1 - \varepsilon)\mu}{D_p} + 1.75G \right] \tag{3.4}$$

Where $G = \rho \cdot v_s$ is the mass flux, expressed in [kg/m^2/s].

Eq. (3.4) depends on the streaming gas through the fixed bed (density, mass flux and viscosity) and on the characteristics of the bed (void fraction and mean diameter of the particles) and it has been applied to evaluate pressure drops.

3.2.2 Materials

Piping material

The material considered for the manufacturing of pipes and fixed bed vessels is the austenitic stainless-steel ASTM A312 Type 316L. The ASTM A312 is the standard specification dedicated to the seamless and welded stainless-steel pipes. This is the type of material selected by most of the producers of pipes and adsorption columns, as it can be seen in [32].

Catalyst for the oxidizing bed

The selected type of catalyst is the Puristar® R3-11G by BASF [33] whose main characteristics are listed in Table 3.1. The BASF Puristar® R3-11G is a robust copper catalyst used for the purification of gases and liquids and can be used especially for the oxidation of hydrogen and CO in gases.

Table 3.1: BASF Puristar® R3-11G characteristics

Parameter	Value
Composition	45wt% CuO on a Mg-silicate carrier
Bulk density	830 [kg/m³]
Form	Tablets, 5x3 [mm]
Operating temperature	From 0 to 275 [℃]

Molecular sieves for the adsorption column

There are several types of adsorbent materials that can be used for the purpose, for example zeolites, silica gel or alumina (Al_2O_3).

Some experimental activities [34] [35] showed that zeolites have a better water adsorption capacity with respect to alumina and silica gel at low values of humidity as can be seen in Figure 3.4, so this type of material has been selected for the calculations.

Zeolites molecular sieves are crystalline aluminosilicates produced to have a highly porous structure. Zeolites have precisely uniform pore sizes and their structure is composed of tetrahedras of AlO_4 and SiO_4, giving different types of molecular sieves such as type A or X (see Figure 3.5), which are the most common. This results in a peculiar sieve-like selectivity which, combined with a wide range of operating conditions, gives zeolites a high level of adsorption efficacy [36].

49
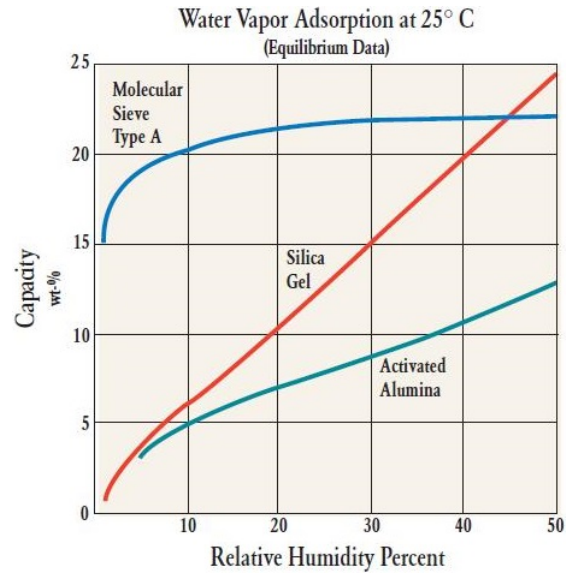
Figure 3.4: Adsorption on zeolite molecular sieves [36]
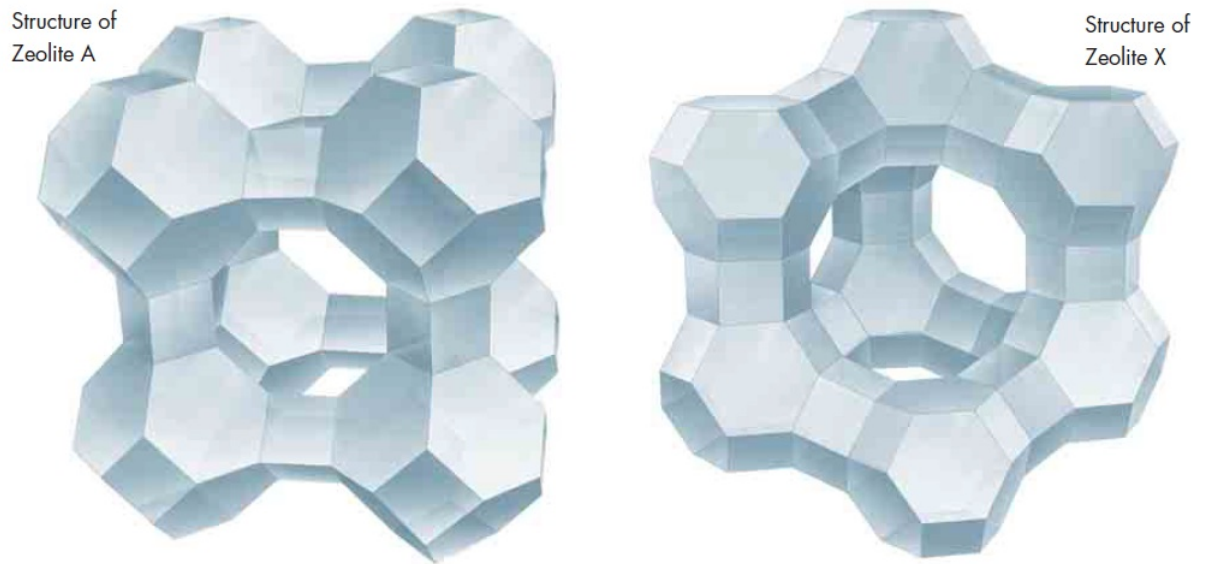
Figure 3.5: Structure of the zeolites types A and X [37]

Adsorption is a physical process in which atoms, ions or molecules interact with an adsorbent material and adhere to its surface. Zeolites have the capability to adsorb some types of molecules on the internal surfaces of the pores. The interaction mechanism between the molecules (adsorbates) and the zeolites (adsorbents) is the physisorption [37] and the main interacting force is the van der Waals force.

Zeolites present a negatively charged framework, due to the presence of alumina, balanced by the positive charge of cations, and this causes a strong electrostatic field on the internal surface. The cations act as sites of strong localized positive charges that attract the negative end of polar molecules. Moreover, the cations can induce polarity in the molecules which are adsorbed due to the electrostatic attraction of cations [36].

Depending on the type of cation in the structure, the adsorption characteristics change: for instance, the zeolite A with sodium as cation has a pore opening of about 4 Ångstrom ($4 \cdot 10^{-10}$ m) and it is called 4A molecular sieve; if instead there is potassium, which is a larger ion, the pore opening is approximately 3 Ångstrom.

The pore size is very important because it allows or not the entrance of the molecules inside the zeolites. Adsorption depends on the following molecular properties [37]:

- size and shape: molecules larger than the pore opening cannot be adsorbed;

- molecular polarity: molecules with large polarity or polarizability can be adsorbed preferentially.

The adsorption process is completely reversible: adsorbed molecules can be released at high temperature and/or reduced pressure or concentrations.

When zeolites interact with an adsorbate, they remove the molecules until an equilibrium is reached. The amount of adsorbate removed under constant environmental conditions is known as equilibrium capacity. This characteristic is affected by the type of adsorbent/adsorbate, concentration of adsorbate, pressure, temperature, co-adsorption effects (simultaneous adsorption of other molecules), aging of the adsorbent. Figures 3.6, 3.7 and 3.8 show the isotherms for the water adsorption capacity of different types of zeolites. It is possible to see that the capacity increases at lower temperatures.

The zeolite molecular sieve type 4A will be used in the present design because it is the suggested adsorbent for water removal from noble gas mixtures [38].
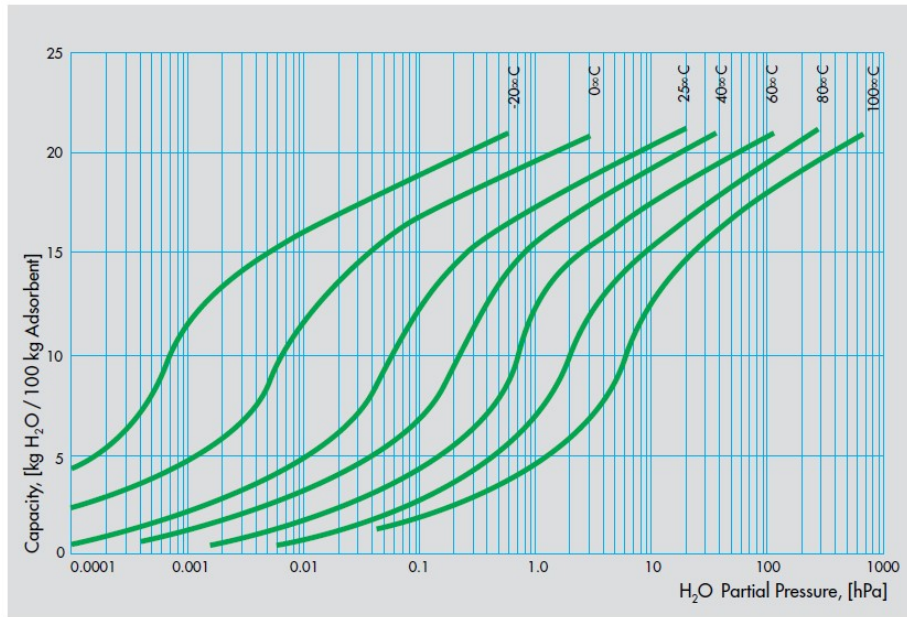
Figure 3.6: Isotherms for Water Adsorption Capacity of SYLOBEAD 3A Molecular Sieve [37]
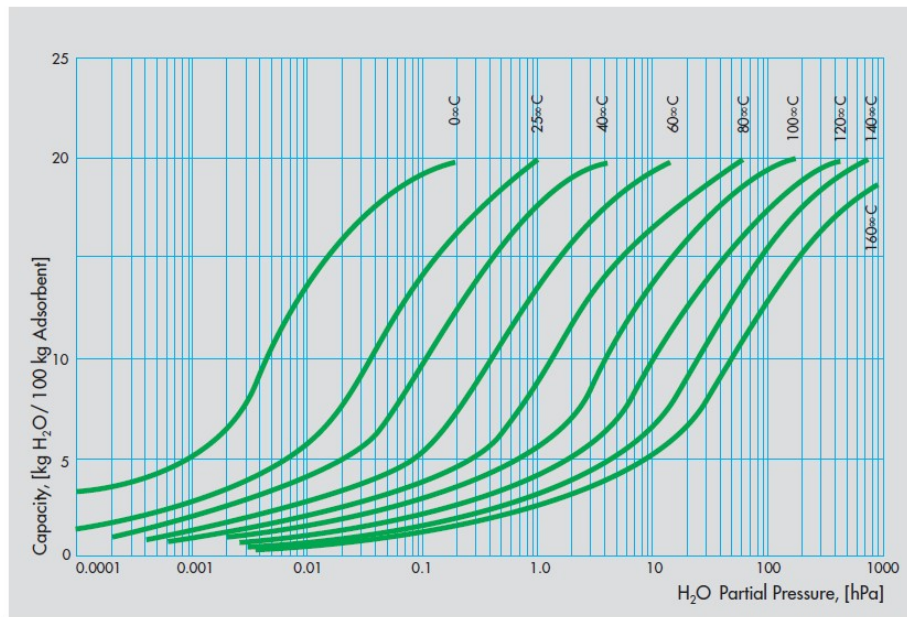
Figure 3.7: Isotherms for Water Adsorption Capacity of SYLOBEAD 4A Molecular Sieve [37]
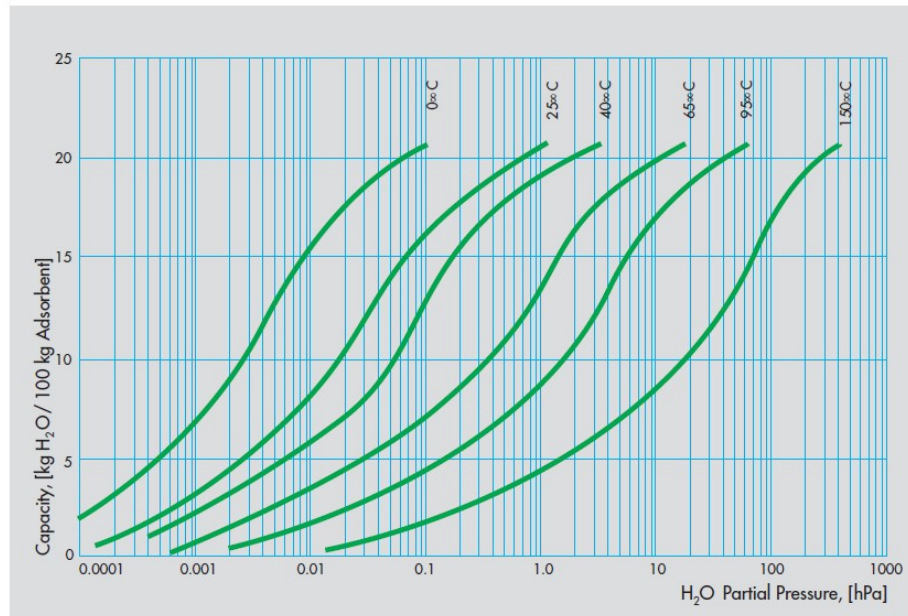
Figure 3.8: Isotherms for Water Adsorption Capacity of SYLOBEAD 13X Molecular Sieve [37]

3.3   Preliminary calculations

The design of the purification system is focused on the oxidizing beds and the adsorption columns. Therefore, it is necessary to evaluate the quantity of oxidizing material and of molecular sieves material and to estimate the pressure drops along the beds.

3.3.1   Input data

The starting point of the analysis consists of the determination of the main input data necessary for the design of the purification system, that are:

- the partial pressures of H_2 and HT in the cover gas;

- the amount of gas to be extracted, purified and reintroduced in the cover gas to keep under control the release of tritium;

- the thermodynamic conditions of the cover gas (temperature and pressure).

Preliminary data have been supplied by CEA researchers who used the KUTIM code to make a preliminary evaluation of the quantity of tritium in the various parts of ASTRID [39]. In particular, hydrogen and tritium partial pressures are originated from the permeation of these gases from the liquid sodium to the argon cover gas. The flow rate has been calculated in order to have a release of tritium that is below the imposed limit.

These preliminary data have been summarised in Table 3.2 [39] [40]:

Table 3.2: Input data for the Purification System sizing

Quantity of impurities in Argon cover gas		
	H_2	HT
Partial pressure	$8.0 \cdot 10^{-3}$ [Pa]	$1.4 \cdot 10^{-5}$ [Pa]
Cover gas conditions		
Temperature, T_{Ar}		723.15 [°C]
Pressure, P_{Ar}		112500 [Pa]
Volumetric flow rate, $\dot{V}_{Ar}$		20 [Nm^3/h]

3.3.2 Oxidizing bed

Firstly, it is necessary to estimate the quantity of oxidizing material necessary to convert H_2 and HT into H_2O and HTO.

The operating temperature of the bed is $T_{bed} = 250$ ℃. This is an important parameter because the efficiency of the conversion is a function of the temperature of the fixed bed. With a temperature of 250 ℃, it is expected an efficiency higher than 90%, as can be seen in Figure 3.9, which shows the relation between the percentage of combustion of hydrogen and the temperature of the catalyst bed.
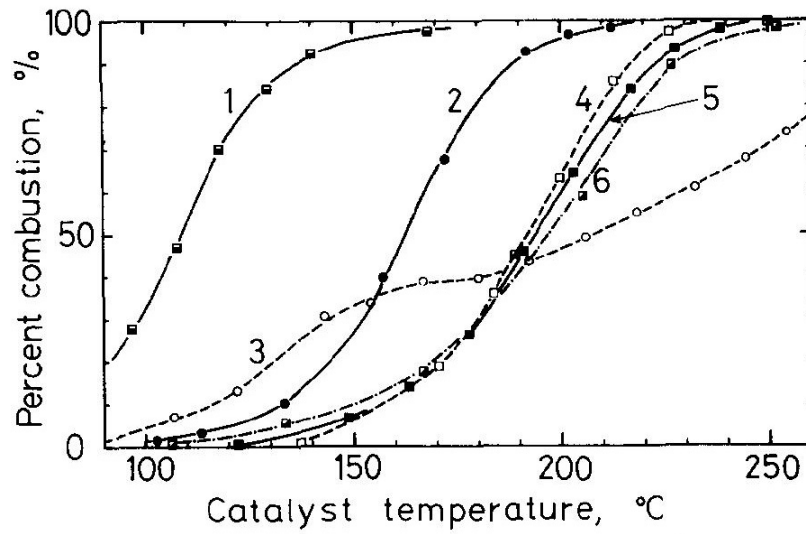
Figure 3.9: Relation between percent combustion of hydrogen and temperature of catalyst bed: 1-Hopcalite I (commercial); 2-Co$_3$O$_4$; 3-MnO$_2$; 4-NiO; 5-CuO; 6- Hopcalite II (commercial). [41]

The selected type of material is a metal oxide, CuO which is reduced to Cu, according to the reactions:

$$CuO + H_2 \longrightarrow Cu + H_2O \tag{3.5a}$$

$$CuO + HT \longrightarrow Cu + HTO \tag{3.5b}$$
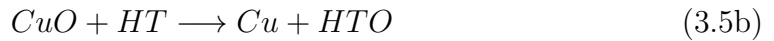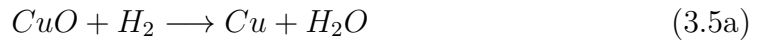
So, each mole of H_2 needs a mole of CuO and the same is for HT. Knowing the partial pressure of these gases in the argon flow rate, the value of the purification flow rate and the duration of the process, it is possible to obtain the total amount (moles) of Q_2 to be transformed into Q_2O ($Q_2O = H_2O + HTO$) and, consequently, the total amount of the catalyst.

As a consequence of the Dalton's law of partial pressures, the mole fraction of Q_2 in the cover gas is:

$$X_{Q_2} = \frac{moles \ of \ Q_2}{total \ moles \ of \ gas} = \frac{P_{Q_2}}{P_{Ar}} \tag{3.6a}$$

$$X_{Q_2} = \frac{8.0 \cdot 10^{-3} + 1.4 \cdot 10^{-5}}{112500} = 7.12 \cdot 10^{-8} = 7.12 \cdot 10^{-2} \ [ppmv] \tag{3.6b}$$

Considering a purification flow rate $\dot{V}_{Ar}$ of 20 [Nm^3/h], the rate of Q_2 moles to be oxidized is:

$$\dot{n}_{Q_2} = \dot{n}_{tot} \cdot X_{Q_2} = \frac{P_n \dot{V}_n}{R T_n} \cdot X_{Q_2} \tag{3.7a}$$

$$\dot{n}_{Q_2} = \frac{101325 \cdot 20}{8.314 \cdot 273.15} \cdot 7.12 \cdot 10^{-8} = 6.35 \cdot 10^{-5} \ \left[\frac{moles \ of \ Q_2}{h}\right] \tag{3.7b}$$

Where P_n = 101325 [Pa], R = 8.314 [J/mol/K] and T_n = 273.15 [K].

In order to determine the total amount of moles of H_2 and HT, some aspects about ASTRID fuel cycle must be considered. From the results of neutronic and physic of fuel cycle calculations, the fuel residence time is supposed to be 1080 Effective Full Power Days (EFPD)[1] and the load factor is considered to be 86% [42]. So, the total fuel residence time is:

$$t_{fuel} = \frac{1080}{0.86} \ [d] \cdot 24 \ \left[\frac{h}{d}\right] = 30140 \ [h] \tag{3.8}$$

It is supposed that the change of the oxidizing bed can take place concurrently with the fuel replacement.

The total moles of Q_2 can be now evaluated:

$$Q_2 = \dot{n}_{Q_2} \cdot t_{fuel} = 6.35 \cdot 10^{-5} \cdot 30140 = 1.91 \ [mol] \tag{3.9}$$

The molecular weight of CuO is 79.54 [g/mol]. So, the masses of CuO and of the catalyst are:

$$m_{CuO} = 152 \ [g] \tag{3.10a}$$

---

[1]It specifies the burnup of a given fuel assembly by the number of days it has resided in the core while the core was operated at full power.

$$m_{R3-11G} = 338 \ [g] \tag{3.10b}$$

Considering an Extent of Reduction (EOR) of 75% (maximum reduction of the catalyst), the total mass and volume of catalyst required are:

$$m_{R3-11G}(req.) = 451 \ [g] \tag{3.11a}$$

$$V_{R3-11G}(req.) = 0.54 \ [l] \tag{3.11b}$$

For what regards the size of the vessel that will host the catalyst, SAES vessels will be taken into account to have some reference dimensions. In particular, SAES MicroTorr® MC700 will be considered (see Figure 3.10), since it has an internal capacity of approximately 0.7 litres.
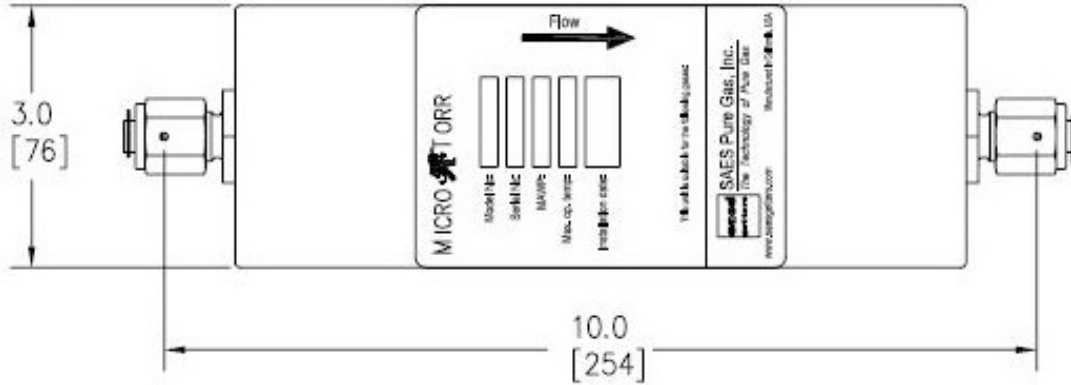
Figure 3.10: SAES MicroTorr® MC700 – Overall dimensions [43]

Therefore, a simple pipe with a similar diameter was foreseen for the analysis. Table 3.3 shows the numerical values used in the calculations:

Table 3.3: Pipe characteristics

Parameter	Value
Material	AISI 316L
Nominal pipe size	2-1/2"
External diameter	73.03 [mm]
Schedule	10 (3.05 [mm])

With these values of external diameter and thickness, the internal diameter and transversal section are:

$$\Phi_{int\_ox} = 66.93 \ [mm] \tag{3.12a}$$

$$A_{ox} = 3518 \ mm^2 = 3.518 \cdot 10^{-3} \ [m^2] \tag{3.12b}$$

The height of the bed is:

$$H_{ox} = \frac{V}{A_{ox}} = \frac{0.54 \cdot 10^{-3}}{3.518 \cdot 10^{-3}} = 0.153 \ [m] \tag{3.13}$$

Now it is possible to evaluate the pressure drop, using the Ergun equation. The mass flux is:

$$G_{ox} = \frac{\dot{V}_{Ar} \cdot PM_{Ar}}{3600 \cdot 22.414 \cdot 10^{-3} \cdot A_{ox}} = 2.81 \ \left[\frac{kg}{m^2 \ s}\right] \tag{3.14}$$

Where $PM_{Ar} = 0.03995$ [kg/mol] is the molecular weight of Argon and 0.022414 [Nm^3/mol] is the molar volume in normal conditions ($T_n = 273.15$ [K] and $P_n = 101325$ [Pa]).

For what regards the density of the process gas at the inlet of the bed, the ideal gas law has been used:

$$\rho_{Ar\_ox} = \frac{P_{Ar} \cdot PM_{Ar}}{R \cdot T_{bed}} = \frac{112500 \cdot 0.03995}{8.314 \cdot 523.15} = 1.033 \ \left[\frac{kg}{m^3}\right] \tag{3.15}$$

The dynamic viscosity of Argon has been computed using a diagram reported by Hougen & Watson [44], shown in Figure 3.11. From this diagram, knowing the values of critical viscosity, critical pressure and critical temperature (listed in Table 3.4), it is possible to evaluate the viscosity at any pressure and temperature.

Table 3.4: Critical constants of Argon [44]

Parameter	Value
Critical temperature, T_C	-122 [°C]
Critical pressure, P_C	4.87 [MPa]
Critical viscosity, μ_C	2.64$\cdot$ 10^{-5} [Pa·s]

With a value of reduced pressure $P_r = P_{Ar}/P_C = 0.023$ and reduced temperature $T_r = T_{Ar}/T_C = 3.46$, the reduced viscosity results $\mu_r = \mu_{Ar\_ox}/\mu_C = 1.3$.
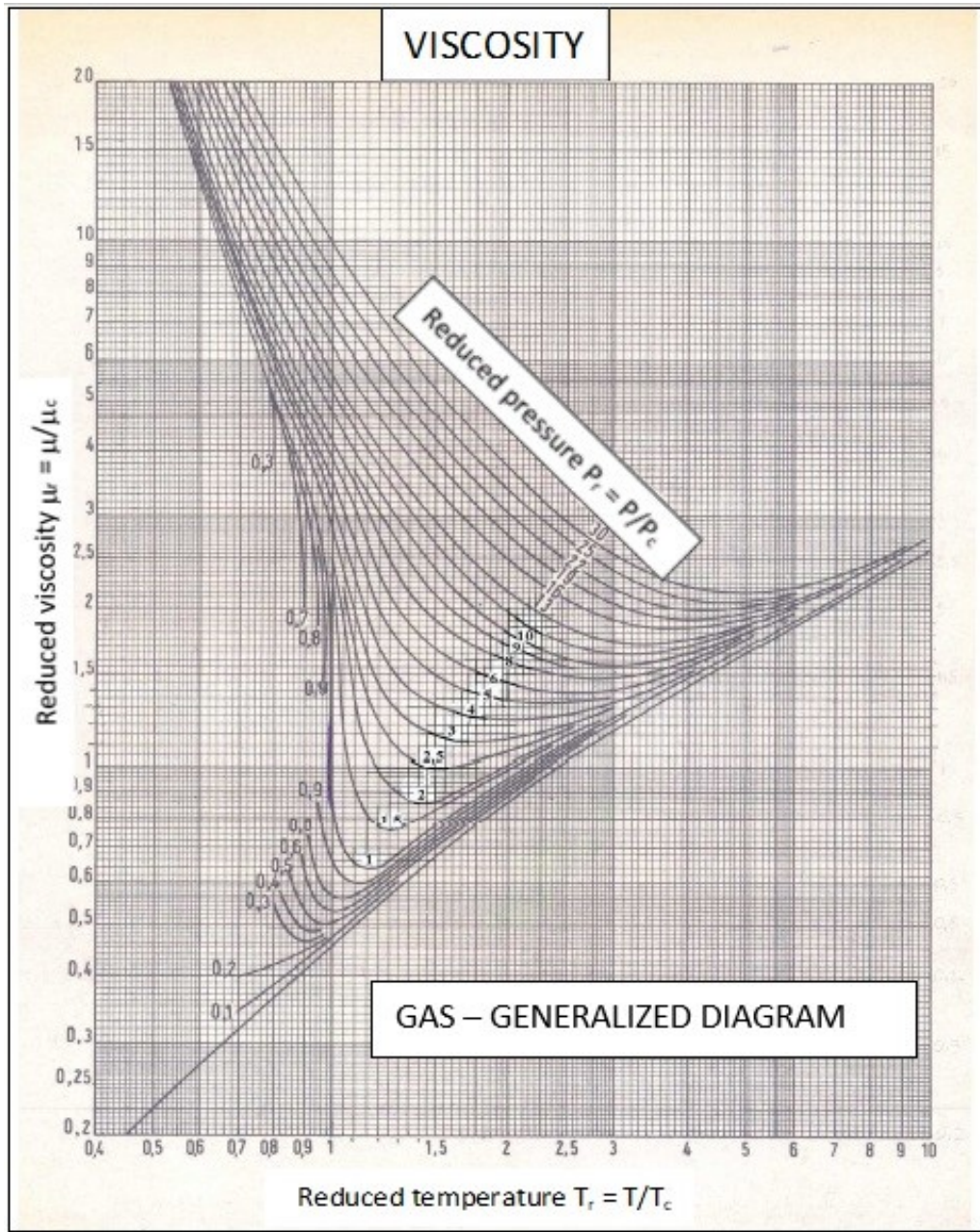
Figure 3.11: Argon reduced viscosity as a function of reduced temperature/pressure

So, the dynamic viscosity is $\mu_{Ar\_ox} = \mu_r \cdot \mu_C = 3.432 \cdot 10^{-5}$ [Pa·s].

The bed characteristics that are needed for Eq. (3.4) are the void fraction and the equivalent spherical diameter of the particles of the bed.

According to [45], the void fraction ε can be approximated to 0.37 for most particle shapes (spherical, extruded or granular), so this value has been considered in the calculations.

The equivalent spherical diameter for extruded media can be approximated by the following formula [45]:

$$D_{p\_ox} = \frac{D_c}{\frac{2}{3} + \frac{1}{3}\frac{D_c}{L_c}} \tag{3.16}$$

Where

- D_c is the average particle diameter (in this case, 5 mm);

- L_c is the average particle length (in this case, 3 mm).

The result gives a D_p of 4.09 [mm], that is the same value given from a formula developed by J. Sauter, which is usually used in fluid dynamics:

$$D_{p\_ox} = 6 \cdot \frac{V_p}{S_p} = 4.09 \ [mm] \tag{3.17}$$

where

- V_p is the volume of the particle;

- S_p is the surface of the particle.

Now, it is possible to calculate the pressure drops per unit length along the oxidizing bed. All necessary data are summarized in Table 3.5.

Table 3.5: Design parameters for the oxidizing bed

Parameter	Value
Mass flux, G_{ox}	2.81 [kg/m^2/s]
Gas density, ρ_{Ar_ox}	1.033 [kg/m^3]
Equivalent particle diameter, D_{p_ox}	4.09·10^{-3} [m]
Void fraction, ε	0.37 [-]
Gas dynamic viscosity, μ_{Ar_ox}	3.4·10^{-5} [Pa·s]

From Eq. (3.4) results:

$$\left(\frac{\Delta P}{L}\right)_{ox} = 47.2 \ \left[\frac{kPa}{m}\right] \tag{3.18}$$

In [45] some information about pressure drop limitations for the correct operation of a fixed bed can be found. In fact, insufficient pressure drop will cause an uneven distribution of the flow and channelling of the fluid, while an excessive pressure drop will result in bed compaction or lifting. Table 3.6 shows the reference values for the pressure drop in fixed beds:

Table 3.6: Pressure drop guidelines [45]

Vapor Phase Service	
< 0.23 [kPa/m]	Uneven distribution and channeling
0.23 – 4.5 [kPa/m]	Upflow or downflow operation
4.5 – 2260 [kPa/m]	Downflow operation only (upflow will result in bed lifting)
> 2260 [kPa/m]	Bed compaction

In this case, the result of pressure drop calculations falls in the third range. This means that only down-flow operation is admitted otherwise bed lifting will occur.

3.3.3 Adsorption column

The procedure for the sizing of an adsorption column can be divided into the following steps [46]:

a. determination of the bed diameter and the corresponding ΔP/L and superficial velocity;

b. estimation of the amount of tritiated water to be removed;

c. determination of the required amount of zeolites and of the bed height;

d. check of the bed design and of the total pressure drop.

In case it is foreseen the regeneration of the zeolites, the procedure continues with the following steps:

   e. calculation of the total heat required to desorb the water;

   f. calculatation of the regeneration gas flow rate;

   g. check of the $\Delta P/L$ value, corresponding to the regeneration gas flow rate.

Solution without regeneration

In adsorption phase, the conditions of the gas at the inlet of the adsorption column are shown in Table 3.7:

Table 3.7: Gas conditions at the inlet of the adsorption column

Parameter	Value
Temperature, T_{Ar_ads}	25 [°C]
Pressure, P_{Ar}	112500 [Pa]
Flow rate, $\dot{V}_{Ar}$	20 [Nm^3/h]
Density, ρ_{Ar_ads}	1.813 [kg/m^3]
Viscosity, μ_{Ar_ads}	2.2704·10^{-5} [Pa·s]

Regarding the density of the process gas at the inlet of the bed, the ideal gas law has been used:

$$\rho_{Ar\_ads} = \frac{P_{Ar} \cdot PM_{Ar}}{R \cdot T_{Ar\_ads}} = \frac{112500 \cdot 0.03995}{8.314 \cdot 298.15} = 1.813 \left[\frac{kg}{m^3}\right] \qquad (3.19)$$

The gas viscosity has been evaluated considering a value of reduced pressure $P_r = P_{Ar}/P_C = 0.023$ and reduced temperature $T_r = T_{Ar}/T_C = 1.97$; using Figure 3.11, the reduced viscosity results $\mu_r = \mu_{Ar\_ads}/\mu_C = 0.86$.
So, the dynamic viscosity is $\mu_{Ar\_ads} = \mu_r \cdot \mu_C = 2.2704 \cdot 10^{-5}$ [Pa·s].

The adsorbent material considered is a highly porous crystalline aluminosilicate zeolite in beaded form, type 4A (the pore openings have diameter of approximately 4 Ångstrom). The Grace Davison® SYLOBEAD® MS 514 product [47], which is a type 4A adsorbent, has been considered as reference and its main characteristics are listed in Table 3.8:

Table 3.8: Grace Davison® SYLOBEAD® MS 514 characteristics

Parameter	Value
Molecular sieve type	4A
Bulk density	720 g/l
Form	Beads, 1.6-2.5 mm (8x12 mesh)

a. Determination of the bed diameter and the corresponding ΔP/L and superficial velocity

The procedure starts with the determination of the bed diameter, which is function of the superficial velocity. For the calculation of the superficial velocity, the modified Ergun correlation will be considered: this equation puts in relation the pressure drop through the bed with the superficial velocity [46].

$$\frac{\Delta P}{L} = B\mu V + C\rho V^2 \quad \left[\frac{kPa}{m}\right] \tag{3.20}$$

Where μ is in [mPa·s], ρ is in [kg/m³] and V is in [m/h].

The constants B and C are listed in Table 3.9:

Table 3.9: Constants for the modified Ergun Equation

Partycle type	B	C
1/8" bead (4x8 mesh)	0.0693	$3.75 \cdot 10^{-7}$
1/8" extrudate	0.0893	$5.23 \cdot 10^{-7}$
1/16" bead (8x12 mesh)	0.1881	$5.74 \cdot 10^{-7}$
1/16" extrudate	0.2945	$8.86 \cdot 10^{-7}$

As shown in [46], a typical value of $(\Delta P/L)_{max}$ to be considered for a fixed bed design is 7.5 [kPa/m]. Starting from the modified Ergun correlation, the maximum superficial velocity can be obtained analytically through the following equation, whose values are shown in Table 3.10:

$$V_{max} = \left\{\frac{(\Delta P/L)_{max}}{C \cdot \rho} + \left[\frac{(B/C)(\mu/\rho)}{2}\right]^2\right\}^{\frac{1}{2}} - \left[\frac{(B/C)(\mu/\rho)}{2}\right] \tag{3.21}$$

Table 3.10: Parameters included in the modified Ergun Equation

Parameter	Value
$(\Delta P/L)_{max}$	7.5 [kPa/m]
B	0.1881 [-]
C	$5.74 \cdot 10^{-7}$ [-]
ρ	1.813 [kg/m^3]
μ	$2.2704 \cdot 10^{-5}$ [Pa·s]

By solving Eq. (3.21), the maximum superficial velocity results:

$$V_{max} = 1327 \left[\frac{m}{h}\right] \tag{3.22}$$

The minimum diameter for the design is given by the following formula:

$$D_{minimum} = \left(\frac{4 \cdot q}{\pi \cdot V_{max}}\right)^{0.5} = \left(\frac{4 \cdot 19.66}{\pi \cdot 1327}\right)^{0.5} = 0.137 \ [m] \tag{3.23}$$

For the calculation of the actual flow rate q, the following equation has been used:

$$q = \frac{\dot{m}}{\rho_a} = \frac{\rho_n \cdot \dot{V}_n}{\rho_a} = \frac{1.7825 \cdot 20}{1.813} = 19.66 \ \left[\frac{m^3}{h}\right] \tag{3.24}$$

Where

- $\dot{m}$ is the mass flow rate, in [kg/h];

- ρ_a is the actual gas density, in [kg/m^3];

- ρ_n is the gas density in normal conditions, in [kg/m^3];

- $\dot{V}_n$ is the flow rate in normal conditions, in [Nm^3/h].

Since the minimum diameter is 0.137 m, it will be selected the nearest internal diameter for commercial pipes, which is 0.1615 m, corresponding to a 6" pipe, sch 10. The main data relevant for the selected pipe are summarized in Table 3.11.

Table 3.11: Parameters included in the modified Ergun Equation

Parameter	Value
Material	AISI 316L
External diameter	6" (168.3 mm)
Schedule	10
Thickness	3.4 mm
Internal diameter ($D_{selected}$)	161.5 mm

Consequently, the value of the superficial velocity must be corrected using the following formula:

$$V_{adjusted} = V_{max} \left(\frac{D_{minimum}}{D_{selected}} \right)^2 = 955 \ \left[\frac{m}{h} \right] \tag{3.25}$$

With the corrected value $V_{adjusted}$ for the velocity, the resulting pressure drop across the bed, calculated using the modified Ergun correlation, is:

$$\frac{\Delta P}{L} = 5.03 \ \left[\frac{kPa}{m} \right] \tag{3.26}$$

At the end of the calculation, a verification of the pressure drop just calculated will be carried out considering the Eq. (3.4) already used for the oxidizing bed. The values used in the equation are listed in Table 3.12:

Table 3.12: Parameters included in the Ergun Equation

Parameter	Value
Superficial velocity, V	0.265 [m/s]
Gas density, ρ	1.813 [kg/m^3]
Mass flux, G = ρ·V	0.482 [kg/(m^2/s)]
Void fraction, ε	0.37 [-]
Gas viscosity, μ	2.2704·10^{-5} [Pa·s]
Equivalent particle diameter, D_p	0.0016 [m]

where, according to [45], D_p = D_m· 0.8 = 0.002·0.8 = 0.0016 [m], with D_m equal to the mean diameter of the particle. The coefficient 0.8 is to take into account the increased packing density, typically afforded by granular media.

Considering the above values in Eq. (3.4), the result is:

$$\frac{\Delta P}{L} = 4.51 \left[\frac{kPa}{m}\right] \tag{3.27}$$

It is clear that, taking into account the various assumptions included in the two methods, the results are not so different.

b. Estimation of the amount of tritiated water to be removed

The procedure for the design of the adsorption column is quite similar to the one for the oxidizing bed, but in this case, the adsorption capacity of the adsorber will be considered.
First of all, the partial pressures of H_2O and HTO are equal to the partial pressures of H_2 and HT, having conservatively considered an efficiency of 100% for the transformation of tritiated gas in tritiated water:

$$CuO + Q_2 \longrightarrow Cu + Q_2O \tag{3.28}$$

So, the number of moles of Q_2O is:

$$n_{Q_2O} = n_{Q_2} = 1.91 \ [mol] \tag{3.29}$$

And the mass of Q_2O is:

$$m_{Q_2O} = PM_{H_2O} \cdot n_{Q_2} = 34.4 \ [g] \tag{3.30}$$

with $PM_{H_2O} = 18$ [g/mol] (the contribution of HTO is negligible if compared to H_2O).

c. Determination of the required amount of zeolites and of the bed height

During the adsorption phase, the bed can be considered divided in three zones (see Figure 3.12):

- equilibrium (saturation) zone;

- mass transfer zone;

- active (safety) zone.

The equilibrium zone is at the inlet end of the bed and defines how much adsorbate the zeolites can hold under the process conditions (temperature, pressure and adsorbate concentration in the feed) [48]. The adsorbate loading limit is also called Equilibrium Capacity, reported in the isotherms as a weight percentage [$kg_{adsorbate}$/ 100 $kg_{adsorbent}$]. This capacity is the theoretical maximum value since drop of performances, such as co-adsorption effects, aging, etc, are not considered.

The Mass Transfer Zone (MTZ) is the part of the bed where the adsorption takes place. It defines the adsorbent volume that is required to reduce adsorbate inlet concentration to that required by effluent specifications in the portion of the bed where active adsorption is taking place.

The bottom zone contains the unused adsorbent, that can be considered as a safety zone.

During the adsorption bed operation, the MTZ begins to move from top to the bottom of the bed, causing the so-called "breakthrough". At breakthrough, the water content of the outlet gas begins to increase, reaching the water content of the feed gas when the MTZ is completed displaced [46], as can be seen in Figure 3.13.

Figure 3.12: Adsorption Bed Profile
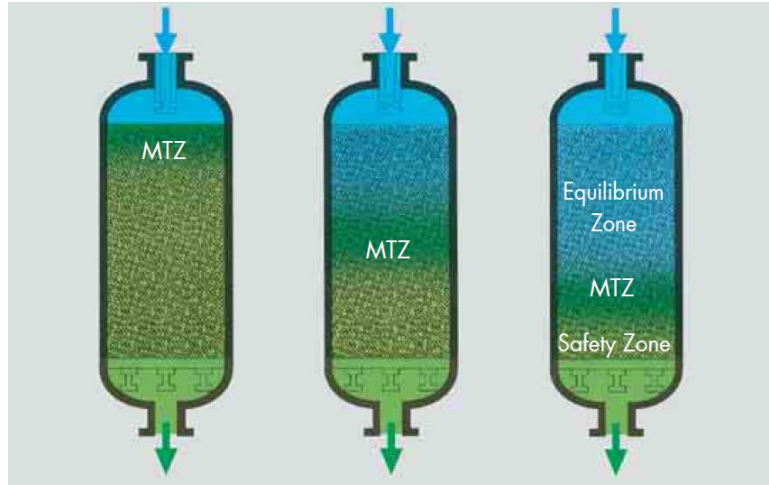
Figure 3.13: Progress of MTZ through the bed during the adsorption period (Beginning, middle and end of cycle) [37]

The total bed height is the summation of saturation zone and MTZ heights (the safety zone will not be considered) [46].

For the theoretical adsorption capacity of a zeolite type 4A, parameter necessary to evaluate the volume of the equilibrium zone, the isotherm corresponding to the temperature of 25 °C will be used, as shown in Figure 3.14.
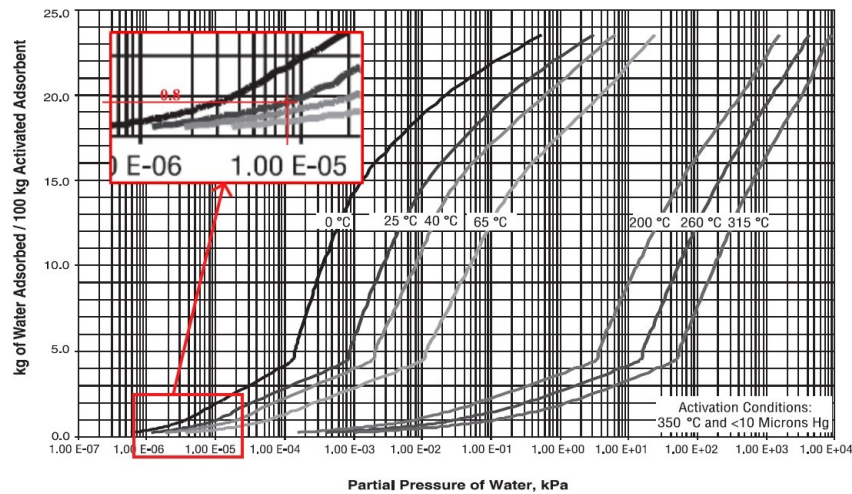
Figure 3.14: UOP^{TM} adsorbents - 4A-DG MOLSIV^{TM} pellets – Water adsorption isotherms [46]

The graph reported in Figure 3.14 shows the water adsorption isotherms for zeolite 4A-DG MOLSIV^{TM} by UOP^{TM} Adsorbents.

With $P_{Q_2O} = 8.01 \cdot 10^{-3}$ [Pa] $= 8.01 \cdot 10^{-6}$ [kPa], the theoretical adsorption capacity is approximately 0.8% in weight. For a proper overdesign of the adsorption column, a reduction of the capacity of 20% is considered to take into account adsorbent decay (crystal loss), fouling, aging and safety margin. So, the actual capacity is 0.64%. With this information, the amount of molecular sieve that is needed is:

$$m_{mol\ sieve}(req.) = \frac{m_{Q_2O}}{capacity} = \frac{34.4}{0.0064} = 5375\ [g] \tag{3.31}$$

Since the density of this material is $\rho_{mol\_sieve} = 720$ [g/l], the required volume results:

$$V_{mol\ sieve} = \frac{m_{mol\ sieve}(req.)}{\rho_{mol\ sieve}} = 7.47\ l \simeq 7.5\ [l] \tag{3.32}$$

Now, the length of the bed must be determined. The length of the equilibrium zone is obtained by simply dividing the required volume of adsorbent by the section of the vessel A_{ads}.

$$L_{EZ} = \frac{V_{mol\ sieve}}{A_{ads}} = 3.66\ dm = 0.366\ [m] \tag{3.33}$$

where $A_{ads} = \pi/4 \cdot (D_{selected})^2 = 2.0485$ [dm²].

Even though the MTZ contains a certain amount of water (approx. 50% of the equilibrium capacity), the equilibrium zone is evaluated assuming that it will contain all the water to be removed [46]. For what regards the length of the mass transfer zone, it can be determined by using the following equation [46]:

$$L_{MTZ} = \left(\frac{V_{adjusted}}{640}\right)^{0.3} \cdot Z = \left(\frac{955}{640}\right)^{0.3} \cdot 0.26 = 0.293\ [m] \tag{3.34}$$

Where Z is an empirical value equal to 0.26 m, since the bead size is 1/16", and $V_{adjusted} = 955$ [m/h].

So, the total length of the bed is:

$$L_{bed} = L_{EZ} + L_{MTZ} = 0.66\ [m] \tag{3.35}$$

Consequently, the total quantity of adsorbent material is:

$$m_{molsieve} = 10.08\ [kg] \tag{3.36}$$

d. Check of the bed design and of the total pressure drop

The total bed height should not be less than the internal diameter [46]. In this case:

$$L_{bed} = 0.7 \ m \ > \ D_{selected} = 0.1615 \ [m] \tag{3.37}$$

The total pressure drop should not exceed 55 [kPa] [46] because the zeolites are fragile and could be crashed by the total weight of the adsorbent material and pressure drop forces. In this case:

$$\Delta P = \frac{\Delta P}{L} \cdot L_{bed} = 5.03 \cdot 0.7 = 3.5 \ [kPa] \tag{3.38}$$

Solution with regeneration

This design option foresees the use of a smaller vessel which can be regenerated with, for instance, a 1-month (30 days) regeneration cycle.

The PFD relevant for this option is shown in Figure 3.2 and foresees the use of two vessels: one working in adsorption mode and the other one in regeneration mode. This design option could be selected in case it is requested to avoid tritium accumulation inside the vessels.

In Table 3.13 the gas conditions in regeneration phase are summarized:

Table 3.13: Regeneration gas conditions at the inlet of the adsorption column

Parameter	Value
Temperature, T_{hot}	288 [°C]
Gas pressure, P_{Ar}	112500 [Pa]
Gas density, $\rho_{Ar \ rg}$	0.963 [kg/m^3]
Gas viscosity, $\mu_{Ar \ rg}$	3.564·10^{-5} [Pa · s]

Where the temperature T_{hot} of the regeneration gas is 28 °C above the temperature $T_{rg} = 260°C$ to which the bed must be heated [46].

The gas density has been evaluated as following:

$$\rho_{Ar\ rg} = \frac{P_{Ar} \cdot PM_{Ar}}{R \cdot T_{hot}} = \frac{112500 \cdot 0.03995}{8.314 \cdot 561.15} = 0.963 \left[\frac{kg}{m^3}\right] \tag{3.39}$$

The gas viscosity has been evaluated considering a value of reduced pressure $P_r = P_{Ar}/P_C = 0.023$ and reduced temperature $T_r = T_{hot}/T_C = 3.71$; using Figure 3.11, the reduced viscosity results $\mu_r = \mu_{Ar\_rg}/\mu_C = 1.35$.
So, the dynamic viscosity is $\mu_{Ar\_rg} = \mu_r \cdot \mu_C = 3.564 \cdot 10^{-5}$ [Pa·s].

In adsorption phase the conditions of the inlet gas are those shown in Table 3.7 and the design procedure is the same as before but, in this case, the height of the equilibrium zone will be much lower: in fact, the diameter is kept equal as the previous case to maintain the same pressure drop, but there is less water to be adsorbed.
Considering Eq. (3.7a) and the assumption that all Q_2 is transformed in Q_2O, the total number of Q_2O moles to be adsorbed is:

$$n_{Q_2O} = 6.35 \cdot 10^{-5} \cdot 30 \cdot 24 = 0.04572 \ [mol] \tag{3.40}$$

corresponding to a water mass of:

$$m_{water} = 0.82 \ [g] \tag{3.41}$$

Considering Eq. (3.31):

$$m_{mol\ sieve} = 128.1 \ [g] \tag{3.42}$$

The volume of the zeolites molecular sieves is:

$$V_{mol\ sieve} = \frac{m_{water}}{\rho_{mol\ sieve}} = 0.18 \ [l] \tag{3.43}$$

Finally:

$$L_{EZ} = \frac{V_{mol\ sieve}}{A_{ads}} = 0.09 \ [dm] = 0.009 \ [m] \tag{3.44}$$

The mass transfer zone does not change, since it depends, according to Eq. (3.34), on the superficial velocity, so the total height of the bed is:

$$L_{bed} = L_{EZ} + L_{MTZ} \simeq 0.009 + 0.293 = 0.302 \ [m] \tag{3.45}$$

The total bed height should be not less than the internal diameter [46]. In this case:

$$L_{bed} = 0.302 \ m \ > \ D_{selected} = 0.1615 [m] \tag{3.46}$$

The total pressure drop is obviously less than 55 [kPa] because the length of the bed is reduced compared to the case without regeneration.
With the value of the height of the bed it is possible to calculate the total quantity of sieve:

$$m_{si \ tot} = 4.45 \ [kg] \tag{3.47}$$

e. Calculation of the total heat required to desorb the water

For the regeneration phase, the first step is to determine the total heat required to desorb the water and heat the desiccant. The following equations will be considered:

$$Q_w = \left[4200 \ \frac{kJ}{kg}\right] \cdot m_{water} \tag{3.48a}$$

$$Q_{si} = \left[1.0 \ \frac{kJ}{kg \ K}\right] \cdot m_{si \ tot} \cdot (T_{rg} - T_i) \tag{3.48b}$$

Where Q_w and Q_{si} are the heat duties required to desorb the water and to heat the sieve, expressed in [kJ]; T_{rg} (260°C) and T_i (25 °C) are the regeneration temperature and the initial temperature of the bed, respectively.
Using these equations, the heat duties result:

$$Q_w = 3.44 \ [kJ] \tag{3.49a}$$

$$Q_{si} = 1045.8 \ [kJ] \tag{3.49b}$$

The next step is to calculate the heat required for the vessel, so it is necessary to know the total weight of the steel.

The height of the vessel must include, in addition to the space for the molecular sieve, the necessary space for filters and supports, which is taken into account adding the 20% of the height of the bed. Furthermore, it is necessary to take into account the weight of the two heads; the weight of a stainless-steel end cap NPS 6", Sch 10 is approximately 1.4 kg [49].

The weight of the vessel results:

$$W_{steel} = \pi \cdot D_m \cdot t \cdot 1.2 \cdot L_{bed} \cdot \rho_{steel} + 2 \cdot W_{head} \tag{3.50a}$$

$$W_{steel} = \pi \cdot 1.649 \cdot 0.034 \cdot 1.2 \cdot 3.02 \cdot 7.88 + 2 \cdot 1.4 = 7.83 \; [kg] \tag{3.50b}$$

Where D_m is the mean diameter of the vessel, t the thickness, 1.2 is a coefficient to increase the bed height of 20%, ρ_{steel} is the stainless-steel density (7.88 [kg/dm³]) and W_{head} the weight of each head.

The duty required to heat the steel is given by the following formula:

$$Q_{st} = \left[0.5 \; \frac{kJ}{kg \; K} \right] \cdot W_{steel} \cdot (T_{rg} - T_i) \tag{3.51}$$

and the result is: Q_{st} = 920.0 [kJ].
A 10% heat loss is assumed [46]:

$$Q_{hl} = 0.1 \cdot (Q_w + Q_{si} + Q_{st}) = 196.9 \; [kJ] \tag{3.52}$$

Finally, the total regeneration load is given by:

$$Q_{tr} = 2.5 \cdot (Q_w + Q_{si} + Q_{st} + Q_{hl}) \simeq 5415 \; [kJ] \tag{3.53}$$

Usually, it is assumed that only 40% of the heat in the regeneration gas transfers to the bed, vessel steel and heat loss to atmosphere. The remaining part goes away with the hot gas [46]. The 2.5 factor is present to take into account this fact.

f. Calculatation of the regeneration gas flow rate

In the next step, the regeneration gas mass flow-rate must be evaluated, using the following equation:

$$\dot{m}_{rg} = \frac{Q_{tr}}{C_p \cdot (T_{hot} - T_i) \cdot (heating\ time)} = 0.1 \left[\frac{kg}{h} \right] \qquad (3.54)$$

where C_p=0.52 [kJ/kg/K] is the heat capacity of Argon [50] and T_{hot} is 28 ℃ above the temperature to which the bed must be heated.

The heating time is usually 50% to 60% [46] of the total regeneration (adsorption) time which must include a cooling period. For the calculations, 55% is considered, which means about 396 hours.

The actual regeneration-gas flow-rate is:

$$q_{rg} = \frac{\dot{m}_{rg}}{\rho_{Ar\ rg}} = 0.104 \left[\frac{m^3}{h} \right] \qquad (3.55)$$

The corresponding superficial velocity of the regeneration gas results:

$$V_{rg} = \frac{4 \cdot q_{rg}}{\pi \cdot D_{int}^2} = 5.08 \left[\frac{m}{h} \right] \qquad (3.56)$$

g. Check of the ΔP/L value, corresponding to the regeneration gas flow rate

As last step, it is necessary to check that the pressure drop during the regeneration period are above 0.23 [kPa/m] to prevent channeling.

Channeling is a phenomenon for which the streaming gas does not reach all the particles of the bed but passes through preferential channels, so the bed is not regenerated in the correct way. It can be avoided by increasing the regeneration flow rate.

To do this verification, it will be considered the modified Ergun correlation (Eq. (3.20)):

$$\frac{\Delta P}{L} = 0.034 \left[\frac{kPa}{m} \right] \tag{3.57}$$

Since the resulting pressure drops are too low, the minimum velocity has been calculated, using the Eq. (3.21), setting the minimum allowable $\Delta P/L = 0.23$ [kPa/m] and, consequently, the minimum regeneration flow-rate has been determined. The results are:

$$V_{min} = 34.21 \left[\frac{m}{h} \right] \tag{3.58a}$$

$$q_{min} = 0.7 \left[\frac{m^3}{h} \right] \tag{3.58b}$$

With the above value of q_{min}, it is possible to calculate the corresponding value of $\dot{m}_{rg}$ and to evaluate how much the heating time should be reduced.
Considering Eq. (3.55) and Eq. (3.54), it is possible to calculate:

$$\dot{m}_{rg} = 0.67 \left[\frac{kg}{h} \right] \tag{3.59a}$$

$$heating\ time = 59\ [h] \tag{3.59b}$$

3.4 Comments and discussion

The calculations carried out in this chapter, demonstrate that the purification technologies foreseen in fusion applications can be used also in fission systems. Table 3.14 summarizes the results achieved for the oxidizing bed:

Table 3.14: Oxidizing bed design

Parameter	Value
Quantity of oxidizing material	451 [g]
Vessel internal diameter	$66.93 \cdot 10^{-3}$ [m]
Vessel height	0.153 [m]
Pressure drops per unit length	47.2 [kPa/m]

In Table 3.15 it is possible to visualize the results for the adsorption column:

Table 3.15: Adsorption column design

Solution without regeneration	
Parameter	Value
Quantity of adsorbent material	10.08 [kg]
Vessel internal diameter	0.1615 [m]
Vessel height	0.660 [m]
Pressure drops per unit length	5.03 [kPa/m]

Solution with regeneration	
Parameter	Value
Quantity of adsorbent material	4.45 [kg]
Vessel internal diameter	0.1615 [m]
Vessel height	0.302 [m]
Pressure drops per unit length	5.03 [kPa/m]
Total heat to desorb water	5415 [kJ]
Regeneration flow rate	0.7 [m^3/h]
Regeneration time	59 [h]

It is clear that the dimensions of the vessels and the overall design are acceptable.

Chapter 4

HYDREX Facility

4.1 Introduction

HYDREX (HYDRogen EXtraction) is a facility built by ENEA to support the experimental activities for the design of the Test Blanket Systems destined to ITER reactor, in particular for what concerns the Coolant Purification System.
The main objectives of the facility are:

- to compare the performances of different adsorbent materials in adsorption phase, analysing the breakthrough curves;

- to analyse the efficiency of the regeneration phase as function of flow rate and temperature;

- evaluate the influence of the presence of CO_2 on the adsorption process.

The main scope of HYDREX facility is to experimental validate the design of the Coolant Purification System, which is conceptually similar to that considered in Chapter 3, clearing some aspects that are still uncertain.

For what regards the first objective, the selected materials are listed in Table 4.1.

Table 4.1: Candidate materials for the adsorption column

Name	Description	Producer
SYLOBEAD®MS 564 C	Molecular sieve Type 3A	Grace Davison
SYLOBEAD®MS C 544 C	Molecular sieve Type X	Grace Davison
MOLSIV™TE 143R	Molecular sieve Type 4A	UOP
MOLSIV™PSA O_2 HP	Molecular sieve Type X	UOP

As the regeneration phase is concerned, since its efficiency depends on several factors, in particular temperature and flow rate, it is very important to assess its operating conditions.

About the last point, it is relevant to consider the presence of CO_2, in the gas to be purified. In particular at the inlet of the CPS it is foreseen the presence of CO, which will be transformed in CO_2 in the oxidizing beds, and CO_2. Generally, the isotherms describing the water adsorption capacity of the zeolites are referred to the maximum adsorption capacity, which can be lowered in presence of concurrent species, such as carbon dioxide. The objective is to perform a parametric study in order to understand how the presence of CO_2 influences the adsorption process and how much the adsorption capacity is reduced.

Another foreseen scope for HYDREX facility, but that is not part if this work, is the qualification of the reducing bed, based on the use of metallic alloys, having the scope to convert tritiated water in tritiated gas. The employed material for the experiments is the SAES St909/Al alloy, made of Zr-Mn-Fe using aluminium as binder for the pellet formation.
The main scopes of the experiments involving the reducing bed are:

- to determine breakthrough curves as a function of the experimental conditions;

- to determine the variations of efficiency depending on repeated cycles;

- to investigate the influence of the presence of H_2 on the reduction process.

The first part of experimental activities is dedicated to verify if the facility is able to perform the foreseen experiments. In particular it is important to understand if the interfacing between facility and quadrupole mass spectrometer is correct.
At this scope it is very important the calibration of the quadrupole, which requires the writing of an accurate procedure, being this operation very delicate for this type of instrument.

This chapter begins with the illustration of the plant and its components and the description of the operating modes. Then, a brief introduction on mass spectrometry is inserted before the description of the calibration procedure of the quadrupole.

The chapter concludes with the verification of the correct interfacing of the quadrupole to the plant. This work has not the scope to extract significant experimental data: it focuses on the qualitative analysis of the plant's functioning, including the quadrupole.

4.2   Facility layout

HYDREX is a facility whose scope is to support the experimental activities for the design of the Coolant Purification System destined to ITER reactor. In Table 4.2 can be seen a brief comparison between the same operating conditions for the two plants, in purification mode:

Table 4.2: Comparison of the operating condisstions between the CPS of ITER and HYDREX [51] [52]

Name	Oxidizing Bed		PTSA		Reducing Bed	
	CPS	HYDREX	CPS	HYDREX	CPS	HYDREX
He Flow Rate [Nm^3/h]	75	$1.5 \div 7$	75	$1.5 \div 7$	2	$0.1 \div 2.5$
Pressure [bar]	82	$9 \div 16$	82	$9 \div 16$	1.1	$1.5 \div 4.5$
Temperature [°C]	250	$250 \div 275$	RT	RT	400	$350 \div 450$

HYDREX is characterized by a semi-closed loop and uses helium as process gas. A layout of the plant is shown in Figure 4.1:
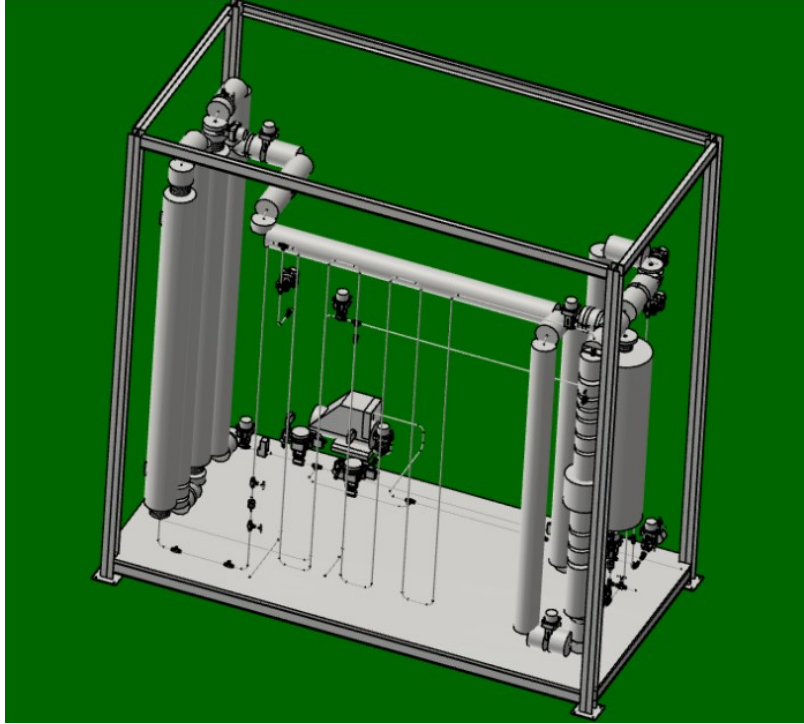

Figure 4.1: HYDREX layout

A more detailed overview of the facility is shown in Figure 4.2. It illustrates the synoptic of the plant on which the data coming from the sensors are displayed.
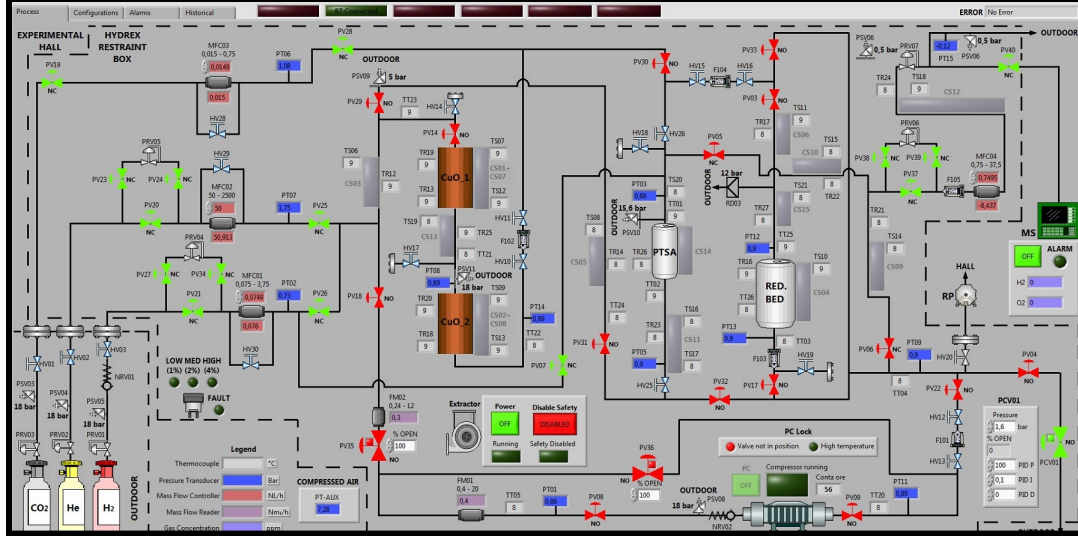

Figure 4.2: Synoptic of HYDREX

The main components of the plant that can be seen on the synoptic are listed below:

- Oxidizer columns (CuO_1 and CuO_2), PTSA column (PTSA) and Reducing bed (RED. BED);

- Quadrupole Mass Spectrometer (MS);

- Compressor (PC) and Mechanical Vacuum Pump (RP);

- Mass Flow Controllers (MFC) and Flow Meters (FM);

- Pressure Reducing Valves (PRV), Pneumatic Valves (PV), Manual Valves (HV), Non-return Valves (NRV), Pressure Control Valve (PCV) and Safety Valves (PSV);

- Pressure Transducers (PT) and Thermocouples (TT/TR/TS);

- Heating Cables (CS) and Filters (FI);

- Rupture Disk (RD) and Hydrogen Concentration Detector (H_2);

- Cylinders for He, H_2 and CO_2;

- Stainless Steel Piping.

The facility is arranged in a box, having the scope to contain and convey outside the experimental hall, by means of an aspirator, accidental leakages of hydrogen. Figures 4.3 and 4.4 illustrate an overall view and a detail of the plant, respectively.

Figure 4.3: Overall view of the facility

Figure 4.4: Details of the facility

4.3   Description of the main components

4.3.1   Pipes

The piping of the plant is made of stainless steel ASTM A213 – A269 type 316/316L (EN 1.4435). The main pipes have dimensions 12.7 x 1.24 mm (1/2" Swagelok), while the pipes regarding the quadrupole have dimensions 6.35 x 1.65 mm (1/4" Swagelok).

Some pipes, in general including heating cables, have an external insulation to decrease the thermal dissipation. On the external surface of the insulation material there must be a temperature less than 50 ℃, due to safety reasons.

4.3.2   Oxidizing columns

These columns are made for containing the oxidizing material, having the scope to transform H_2 into H_2O, and their main characteristics are listed in Table 4.3:

Table 4.3: Oxidizing columns characteristics

Component	Oxidizing column
Type	Vertical axis cylinder
Material	ASTM A 182 F 316L – A312 Type 316L
Volume	3.3 [l]
External diameter	48.3 [mm] (1-1/2")
Thickness	5.08 [mm] (sch 80)
Height	3156 [mm]
Weight (empty)	38 [kg]
Design temperature	+300 / -10 [℃]
Max operating temperature	272 [℃]
Design pressure	20 [barg]
Test pressure	39.5 [barg]

The columns are equipped with heating cables and have an external thickness of 80 mm of insulating material, so that the thermal dissipation is limited.

4.3.3   PTSA column

In order to contain the molecular sieves, the SAES MC700 column has been selected, for which the maximum allowable flow rate is 7.2 [Nm^3/h]. The maximum operating temperature is given by the zeolites contained in the column, so they are generally regenerated at temperatures between 250 and 300 ℃. The zeolite contained inside the column at the moment installed on the facility is the type 3A Grace Davison SYLOBEAD® MS 564 C. The main characteristics of the column are listed in Table 4.4:

Table 4.4: PTSA columns characteristics

Component	PTSA column
Type	Vertical axis cylinder
Material	ASTM Type 316L
Volume	0.7 [l]
External diameter	76 [mm]
Height	254 [mm]
Weight	3.4 [kg]
Min/max operating temperature	-20 / 300 [℃]
Max operating pressure	17.3 [barg] at 40 [℃] (4.5 [barg] at 300 [℃])
Test pressure	19 [barg]

The column is equipped with heating cables and has a thickness of 90 mm of external insulation to limit thermal dissipations.

4.3.4   Quadrupole mass spectrometer

The gas chemical composition is analysed using the quadrupole mass spectrometer Hiden Analytical HPR 20 QIC, of which main parameters are shown in Table 4.5.

The gas to be sent to the quadrupole is taken from the main loop using lines LP18 and LP 19. Looking at the synoptic of the plant, opening and closing alternatively PV05 and PV06 valves, it is possible to send the gas to the quadrupole from different points of the circuit. In adsorption phase, the opening of PV05 valve allows to analyse the gas that enters the PTSA, while the opening of PV06 valve allows to analyse the gas that exits the PTSA. In regeneration phase, the PV05 valve will be used to analyse the gas that exits the PTSA.

84

The reference software for data acquisition is Hiden QGA Professional: it is a specific application for quantitative gas and vapor analysis which provides real time continuous analysis of up to 32 species with concentrations that vary in the range 0.1 ppmv to 100%.

Table 4.5: Quadrupole Mass Spectrometer characteristics

Component	HIDEN Quadrupole Mass Spectrometer
Mass range	1 - 100 a.m.u.
Faraday cup detection limit	10^{-11} [Torr]
SEM detection limit	$10^{-13} - 10^{-14}$ [Torr]
Inlet pressure	200 [mbar] - 2 [bar]
Max inlet temperature	350 [℃]
Capillary heating	up to 200 [℃]

4.3.5 Compressor

The compressor selected for the facility is an air-cooled HAUG compressor, type SOGX 30 D4 and it is a high performance, oil-free device for gas compression. Environment or process gas contamination is almost impossible, using this type of compressor. The characteristics of the machine are listed in Table 4.6:

Table 4.6: Compressor characteristics

Component	Compressor
Type	SOGX 30 D4
Max suction pressure	20 [bar]
Max discharge pressure	55 [bar]
Flow rate at max motor speed	17.5 [Nm^3/h]
Motor power	1.5 [kW]

4.4 HYDREX operating modes

HYDREX facility can work in two different ways: in adsorption mode or in regeneration mode.

The main operative conditions in the two modes of functioning of the plant are shown in Table 4.7:

Table 4.7: Operative conditions relevant to HYDREX facility

	Adsorption	**Regeneration**
He Pressure	Max 15 [barg]	Max 4.5 [barg]
He Temperature	RT[1]	Max 450 ℃[2]
He Flow Rate	1.5 ÷ 7 [Nm^3/h]	75 ÷ 350 [Nl/h]
H_2O Concentration	15/300 [ppmv]	[-][3]
H_2 Concentration	[-][4]	Max 300 [ppmv][5]
CO_2 Concentration	10 [ppmv]	[-][6]

The notes in the previous table are listed below and specify the different modes of operation or experimental activities:

1. The gas is in general at room temperature, except for the inlet/outlet of the oxidizers.

2. The temperature of 450 °C refers to the maximum operating temperature of the reducing bed.

3. In regeneration phase, the gas entering the PTSA column does not contain water. The outlet gas will contain the water coming from the PTSA with variable concentration depending on the operating conditions and the type of material.

4. In adsorption phase, the presence of hydrogen has the scope of generating the required concentration of water by means of the oxidizers.

5. The use of hydrogen is foreseen only in some tests.

6. In regeneration phase, the gas entering the PTSA column does not contain CO_2. The outlet gas will contain the CO_2 coming from the PTSA with variable concentration depending on the operating conditions and the type of material.

4.4.1 Operation in adsorption mode

In adsorption mode, the facility works as a closed circuit, in which the compressor keeps the helium circulating inside the plant. The helium is pure at 99.999% (grade 5.0). During this phase, the oxidizer columns CuO_1 and CuO_2 and the other components provided of heating cables are heated and the pressure control valve PCV01 is supposed to maintain the pressure increase under control (max 15 barg).

In Figure 4.5 there is the part of the circuit that is involved in the adsorption phase:
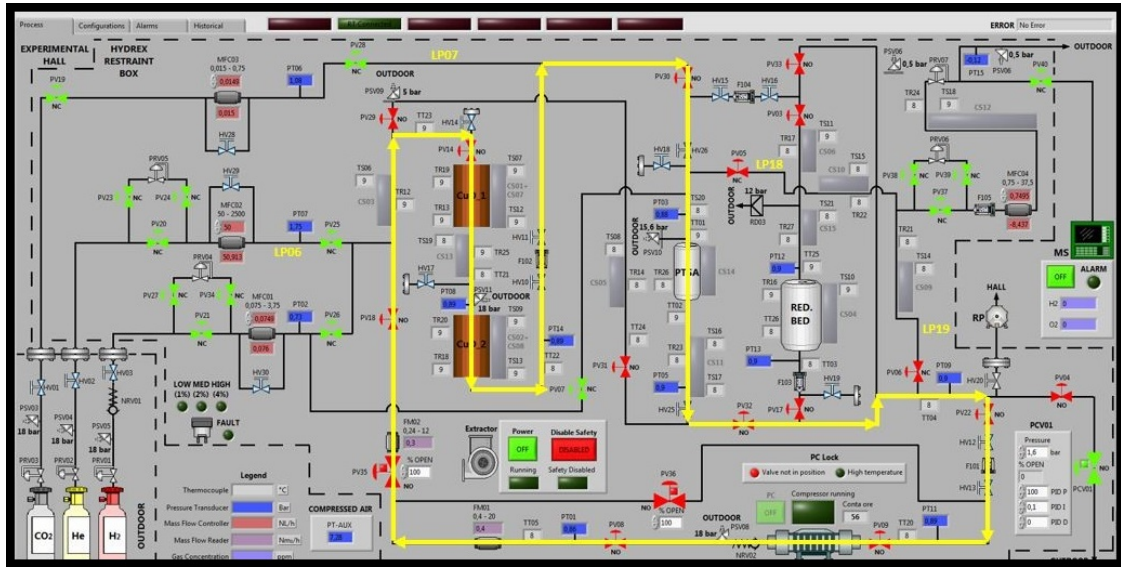
Figure 4.5: Flow path in adsorption mode

The picture shows that the helium, containing a certain amount of water, flows through the PTSA column, where it is purified from water thanks to the molecular sieves. The process continues until the PTSA column is saturated.

In order to produce water, a hydrogen flow is introduced inside the helium flow by means of the Mass Flow Controller MFC01 and, coming in contact with the oxidizing material, it generates water according to the reaction:

$$CuO + H_2 \longrightarrow Cu + H_2O$$

87

The selected oxidizing material is: BASF Puristar® R3-11G T5x3 [33]. The oxidizing material must be heated so that the reaction can take place. So, the gas is pre-heated, using heating cables CS03 and CS13, and also the columns are equipped with heating cables (CS01, CS02, CS07, CS08) that allow the material to work at the correct temperature (max 275 ℃). In order to avoid excessive stress in the oxidizing material, it is necessary to heat at a rate less than 50 [℃/h]. Inside the oxidizers there is a filter which withholds the bigger powders (max 1 µm) while the filter FI02 is placed outside to block the finest ones.

Since the molecular sieves need to work at room temperature to efficiently adsorb the water molecules contained in the helium flow, the gas must be cooled down and this is done using a sufficiently long not insulated pipe: the hot gas exchanges heat with the external environment flowing through this pipe. The purified helium comes back to the compressor, passing through the filter FI01.

For what regards the tests that foresee the analysis of the influence of CO_2 on adsorption capacity, the CO_2 injection is done using the line LP07.

4.4.2 Operation in regeneration mode

In regeneration mode, the facility works as an open circuit, in which the valve PCV01 guarantees the correct value of the pressure (few bars) while the mass flow controller MFC02 ensures the required value of the flow rate. Figure 4.6 shows the part of the circuit involved during regeneration phase:
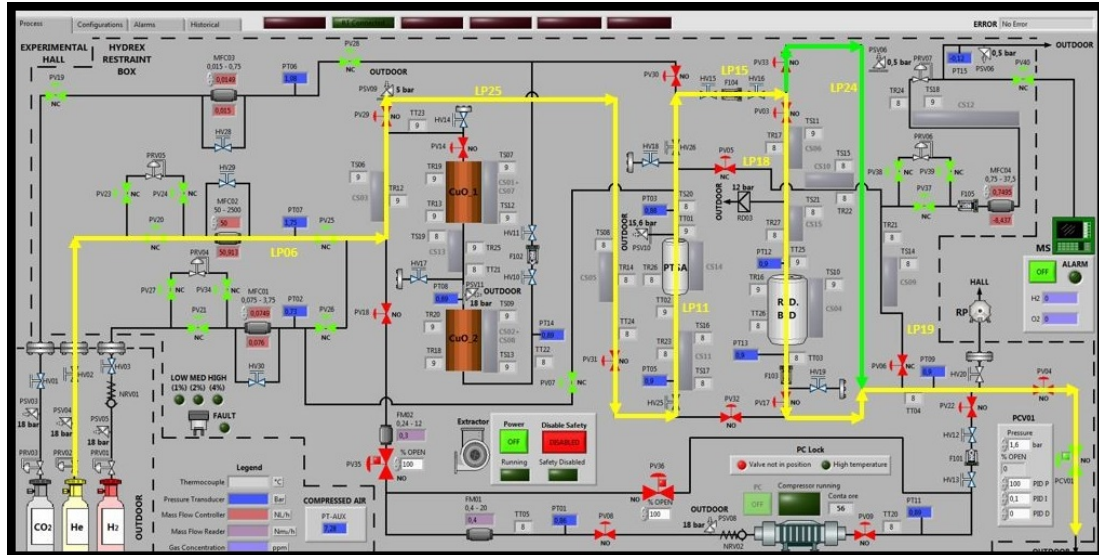

Figure 4.6: Flow path in regeneration mode

88

The pressure of the helium coming from the cylinder is reduced by using the regulation valves PRV02a, PRV02b and PRV05. The gas flows through the line LP25, bypassing the oxidizing columns, and through the line LP11, entering the PTSA column from below. Before entering, the gas is heated up by the heating cables CS05, CS11a and CS11b, while CS14 heats directly the column.

The regeneration mode can involve or bypass the reducing bed. If the RB is bypassed, the gas exiting the PTSA flows through the lines LP15 and LP24 (green line) and it is discharged into the atmosphere through the valve PCV01.

4.5 Activity on the mass spectrometer

4.5.1 Mass spectrometry concepts

The principle of mass spectrometry is based on the fact that ionized atoms or molecules can be distinguished thanks to their mass-to-charge ratio (m/z) [53].
The mass spectrometer generates ions from the gas under investigation by electron ionization. Then these ions are separated and a mass spectrum of the molecules is produced.
Generally, a mass spectrometer consists of three components [54]:

- **Ionizer**: the conversion of gas molecules into charged particles is achieved by electron impact through thermionic emission from a hot filament, in which flows a current of typically $1 \cdot 10^{-4}$ Amps. Then the extracted ions go into the mass filter.

  Figure 4.7 shows a schematic view of the ionizer:
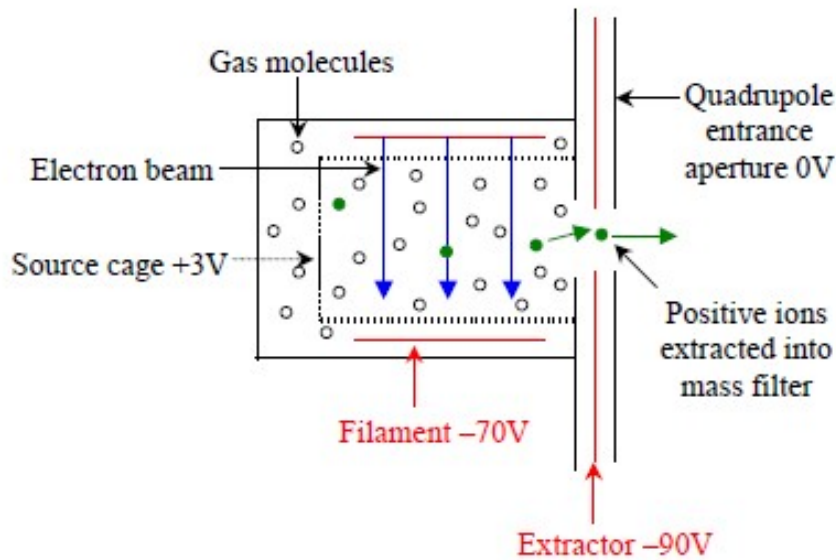
Figure 4.7: Scheme of ionizer [54]

- **Mass filter**: it differentiates the ions and selects species for the detection. The most common form of mass filter is the quadrupole, which consists of two pairs of parallel, equidistant metal rods (called poles) charged with equal but opposite potentials. Figure 4.8 illustrates the twin potentials applied on the poles.

  When the ions enter the quadrupole, the magnetic field that is created deflects them from their original trajectory and the extent of the deflection depends on the mass-to-charge ratio. All other species are neutralized by impact upon the rods of the quadrupole.
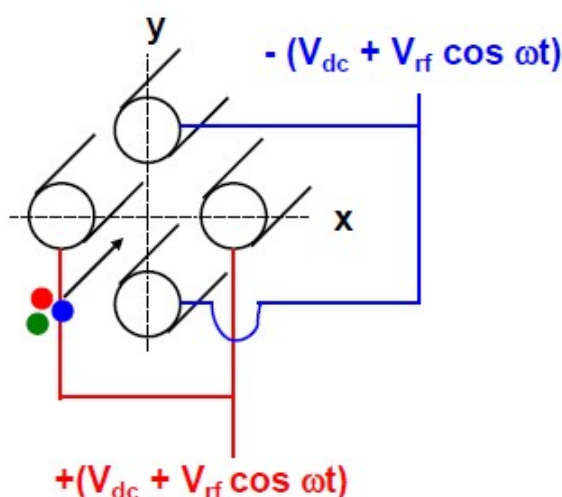
Figure 4.8: Scheme of mass filter [54]

- **Detector**: it is an instrument that receives the ions that have been deflected by the magnetic field. The ions generate a current which is measured by an amplifier.

  There are two types of detector:

  – **Faraday cup**: it is a conducting surface on which the ions coming from the quadrupole cause the generation of several "secondary" electrons, providing an amplification.

  The advantages of the Faraday cup are that it has a relatively low cost and it is indestructible but, on the other hand, it has a detection limit of 10^{-11} Torr of partial pressure of the species to be analysed.

– **Secondary Electron Multiplier (SEM)**: it is a surface designed to generate secondary electrons. The ions strike the surface generating 2 or 3 electrons which impact again the surface generating more electrons and so on, in a cascade effect. SEM has a better detection limit (it measures also at 10^{-13} – 10^{-14} Torr) and has a faster measurement than the Faraday cup, but it is much more expensive and it is consumed after a certain period of employment and it has to be replaced.

The information coming from the analysis of a gas sample can be presented as peaks of mass/charge. For instance, in Figure 4.9 are shown the peaks that appear when air is under analysis:
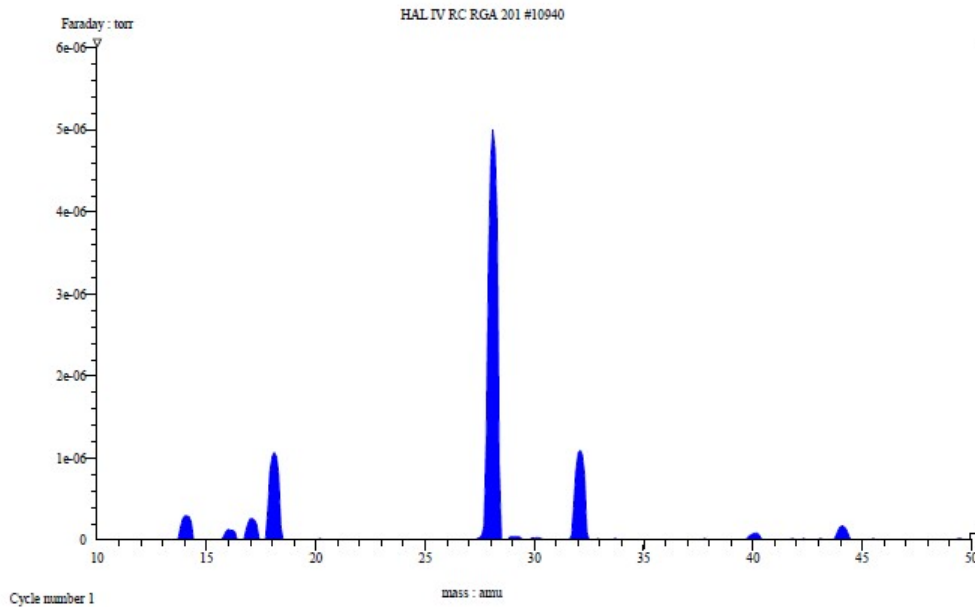
Figure 4.9: Peaks during air analysis [54]

There is another way of representation in which the variation of the species concentrations is shown as a function of time. These are the graphs that will be considered in the following paragraphs.

4.5.2   Background and calibration procedures

The calibration of the quadrupole mass spectrometer is a very delicate procedure and must follow specific steps.

In order to do this, a small circuit has been built, whose scheme and the relative legend are shown in Figure 4.10 and Table 4.8.
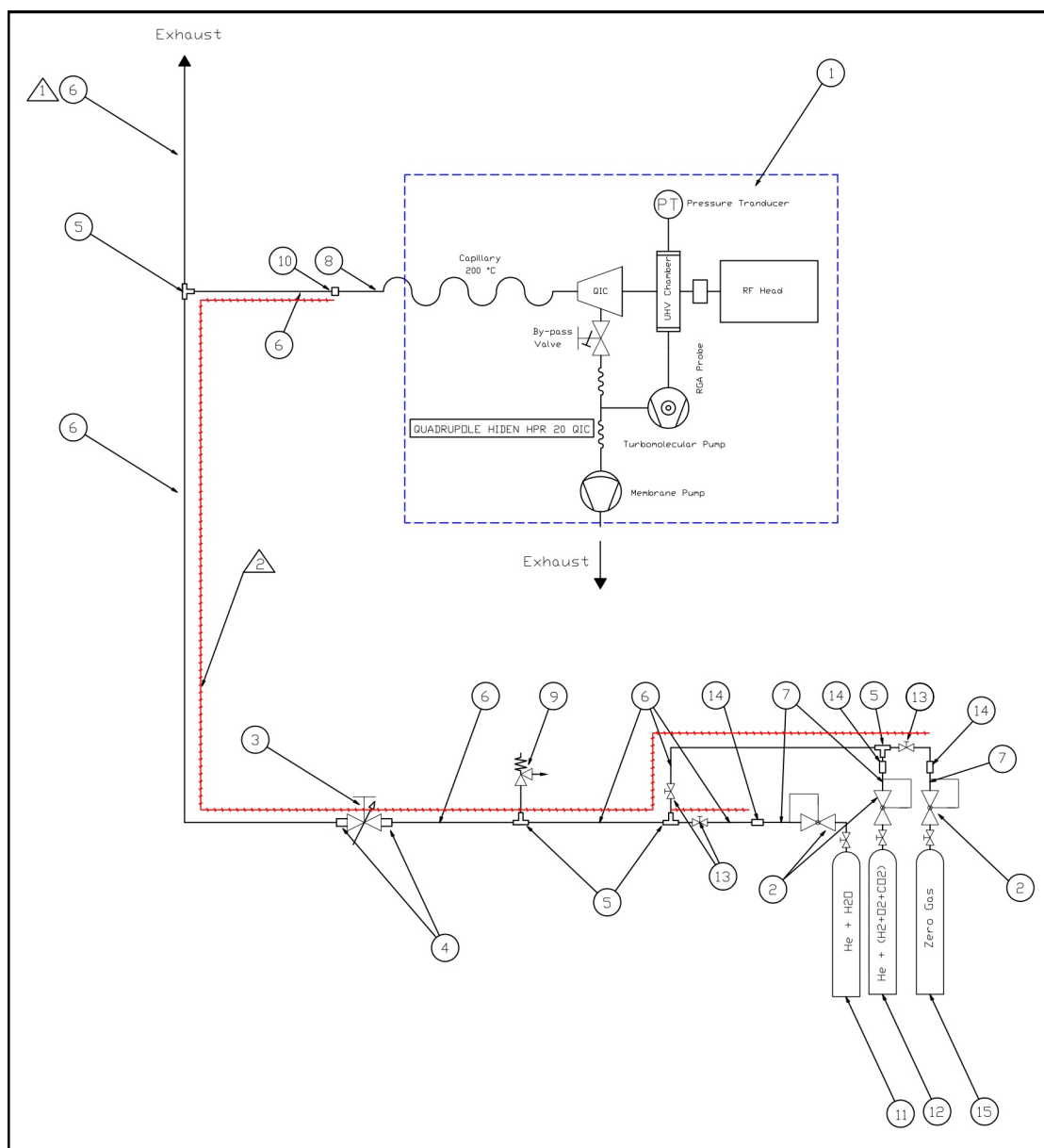

Figure 4.10: Scheme of the calibration circuit

Table 4.8: Legend

POS.	QTY	DESCRIPTION	MATER./SUPP.	TYPE
1	1	Quadrupole	Hiden	HPR 20 QIC
2	3	Pressure Reducer	Air Liquide	HBS 200-1-2
3	1	Flow Meter/Controller	Cole-Parmer	CP03218-07
4	2	Male Connector	HAM-LET	768L-SS-1/4x1/8
5	4	"T" Union	HAM-LET	764L-SS-1/4
6	-	Pipe	Swagelok	O.D. 1/4"
7	-	Pipe	Swagelok	O.D. 6 mm
8	-	Pipe	Swagelok	O.D. 1/16"
9	1	Exhaust Valve	HAM-LET	H-900-SS-L-1/4-SL-10
10	1	Reducer	HAM-LET	763L-SS-1/4x1/16
11	1	Cylinder	Air Liquide	GSPR: 14544/10
12	1	Cylinder	Air Liquide	GSPR: 14545/10
13	3	ON/OFF Valve	HAM-LET	H-6800-SS-L-1/4-P-S-S
14	3	Reducer	HAM-LET	763L-SS-6x1/4
15	1	Cylinder	SAPIO	HELIUM GRADE BIP

In Figure 4.11 it is possible to see the calibration circuit.

Figure 4.11: Calibration circuit

Background procedure

First of all, a background measurement must be made, using a zero-gas connected to the gas analysis system. The chosen gas for the background analysis must be a very high purity gas, and, for a more accurate analysis, it has to flow into the circuit for several hours before making the measurement.

For this purpose, a cylinder with helium grade BIP has been used and the list of its impurities is shown in Table 4.9:

Table 4.9: Impurities of Helium BIP

Parameter	Value
O_2	< 10 ppbv
N_2	< 5 ppmv
$CO + CO_2$	< 0.5 ppmv
Hydrocarbons (CH_4)	< 100 ppbv
H_2O	< 20 ppbv

Using QGA Professional Software, an automatic background measurement has been carried out. Figure 4.12 shows the starting window of the software:
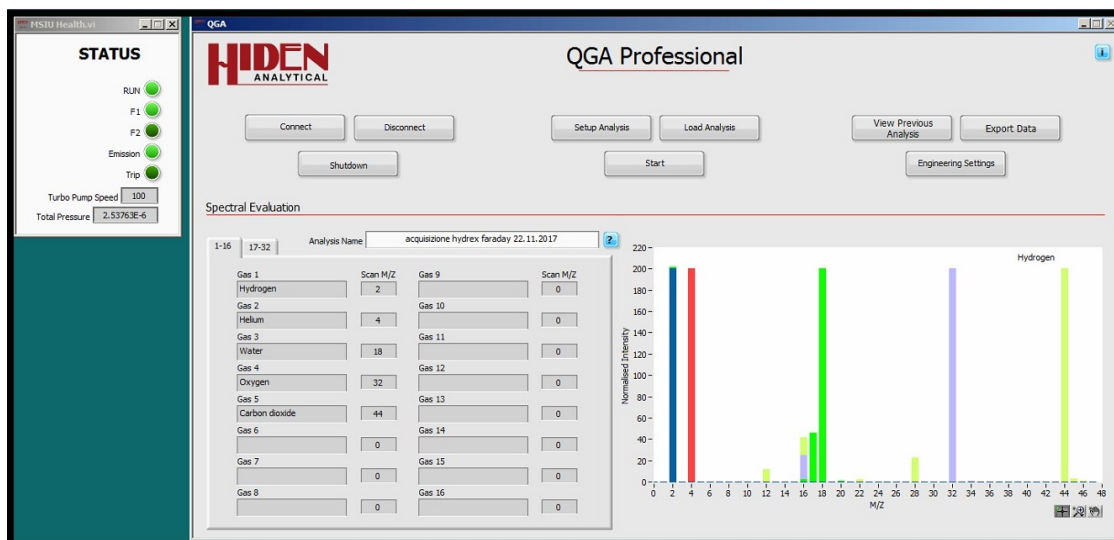
Figure 4.12: Starting window

Clicking on the "Setup analysis" button, it is possible to choose the species that are going to be studied and the type of detector to be used. In particular, Figure 4.13 shows that the instrument employed for the analysis is the Faraday cup and the species to be analysed are hydrogen, helium, water, oxygen and carbon dioxide. The reason why the Faraday cup has been selected as detector is that the concentrations of the chemical species inside the loop is unknown and the SEM detector could be damaged if the partial pressures are too high. On the other hand, using Faraday cup the detection limit is 10^{-11} Torr, which is higher than the one for the SEM (10^{-13} Torr).
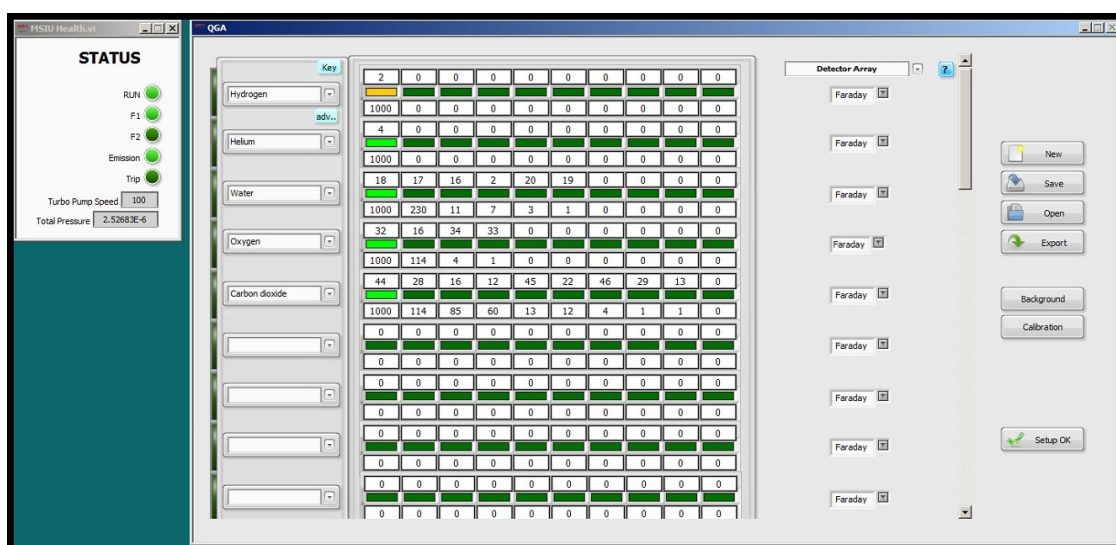
Figure 4.13: Setup analysis window

Clicking on the "Background" button, the Background Measurement window will be opened, as shown in Figure 4.14. At this step, the gases to be included in the background measurement must be selected, and will be highlighted. The carrier gas must not be selected.
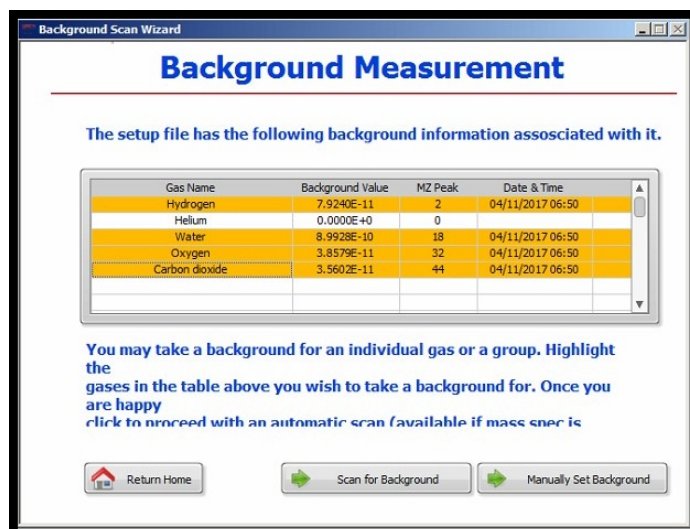
Figure 4.14: Background measurement window

The next step consists of selecting the background accuracy and it is done clicking the "Scan for Background" button. Referring to Figure 4.15, the background value is the mean of the selected number of values specified in the "Rolling Average" box. The RSD (Relative Standard Deviation) is an indication of the stability of the values. As shown in Figure 4.15, the scan can be stopped manually or continue until the specified % value indicated in the "RSD Target" box is reached. In any case the maximum number of scans is equal to 1000.
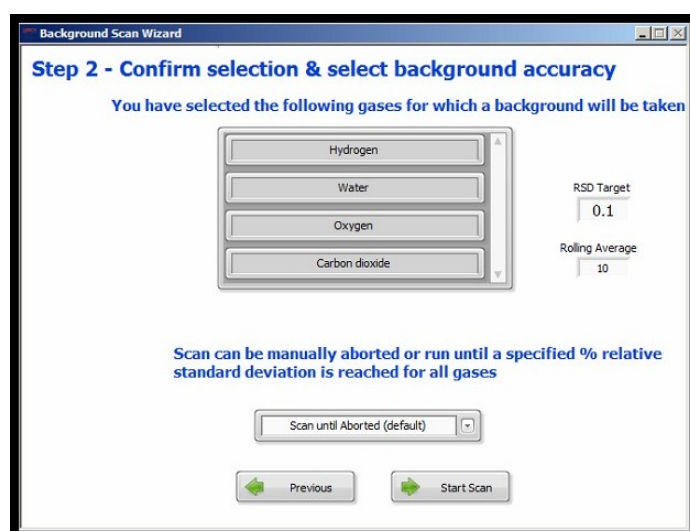
Figure 4.15: Background accuracy window

At this point, the scan can start. Clicking on the "Start Scan" button the Scan underway window will be opened, as shown in Figure 4.16:
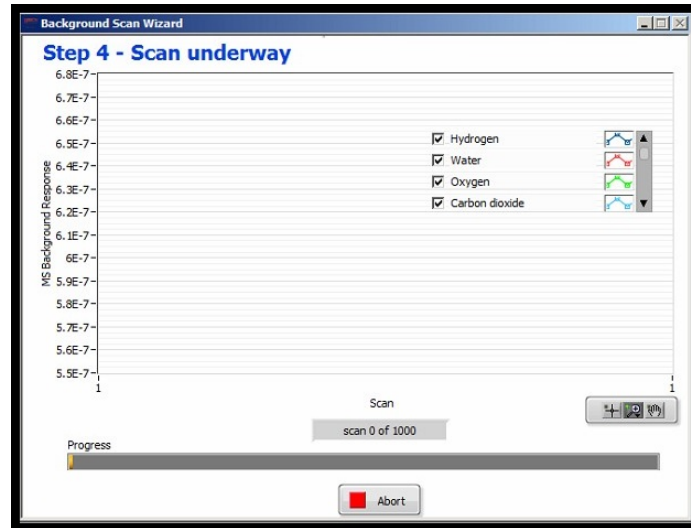
Figure 4.16: Scan underway window

As the scans proceed, more and more values will be registered and a broken line will form. Figure 4.17 shows the situation at 16 and 403 scans.

Figure 4.17: Scan progress

98

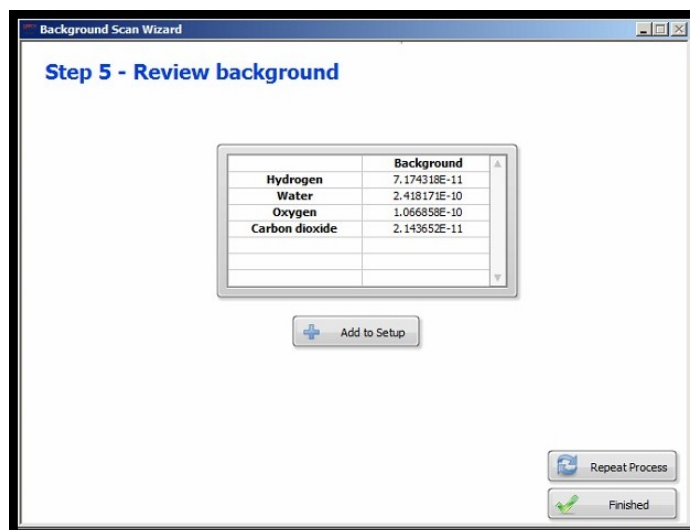When the values have reached the desired stability, the Review background window will be displayed (see Figure 4.18):

Figure 4.18: Review background window

Clicking the "Finished" button, the background procedure is complete and the relative values are inserted in the Setup analysis window, as can be seen in Figure 4.19:
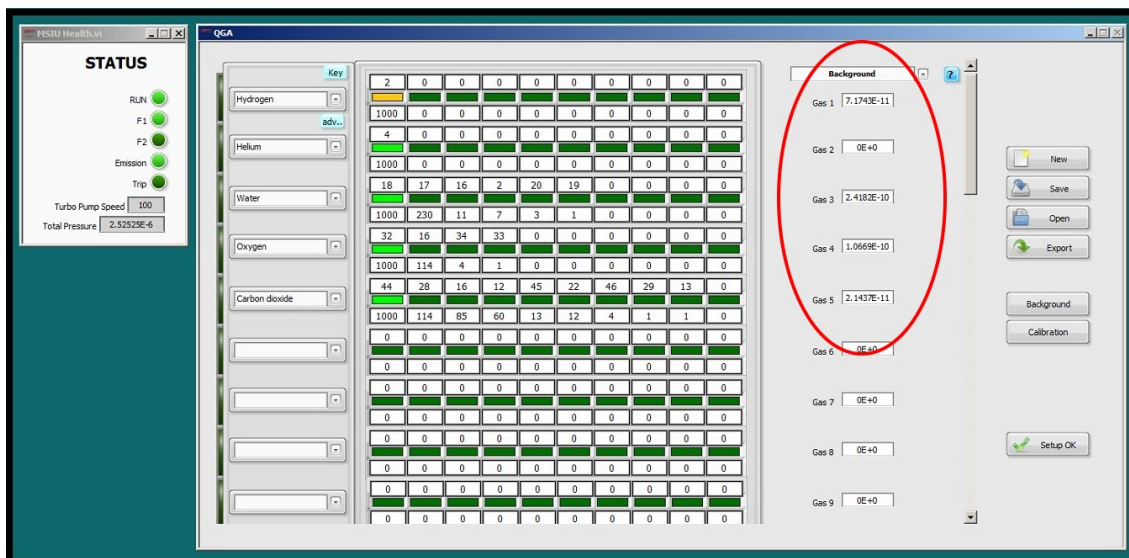

Figure 4.19: Insertion of background values

Calibration procedure

The calibration procedure can be performed when the background was completed. In this case, two different cylinders are employed: the mixture in the first cylinder contains approximately 300 ppmv of H_2O and helium for the remaining; the second cylinder contains approximately 1000 ppmv of H_2, 100 ppmv of O_2 and 10 ppmv of CO_2 and helium for the remaining. Both cylinders have a capacity of 10 litres and their composition is shown in Table 4.10:

Table 4.10: Composition of the cylinders used for calibration

	Cylinder 1	**Cylinder 2**
H_2O	[-]	299.85 [ppmv]
CO_2	9.928 [ppmv]	[-]
O_2	99.853 [ppmv]	[-]
H_2	1000.134 [ppmv]	[-]
He	Remaining	Remaining

The calibration procedure is quite similar to the background one but, in this case, RS (Relative Sensitivity) values must be calculated to allow a quantitative analysis of the gas mixture. Basically, what is done is to impose the known values of the concentrations related to the mixtures contained in the cylinders to the ones measured by the quadrupole. Then, the software compares the actual values with the measured values and computes the RS values.

The first step is to click on the "Calibration" button from the setup window (see Figure 4.13) and the subsequent window is shown in Figure 4.20:
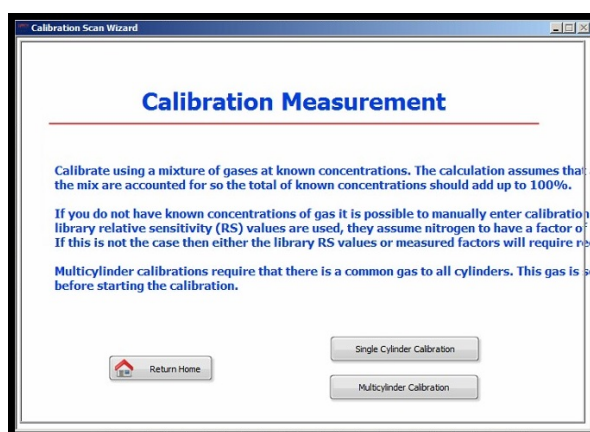

Figure 4.20: Calibration measurement window

There are two options: the first involves only one cylinder for the calibration and the other one more cylinders. In case of multi-cylinder calibration, the mixtures inside the cylinders must have a common gas. In this case the second option will be chosen. Figure 4.21 shows the selection of the common gas for the two cylinders, in this case Helium, and the selection of the gases included in the first cylinder.
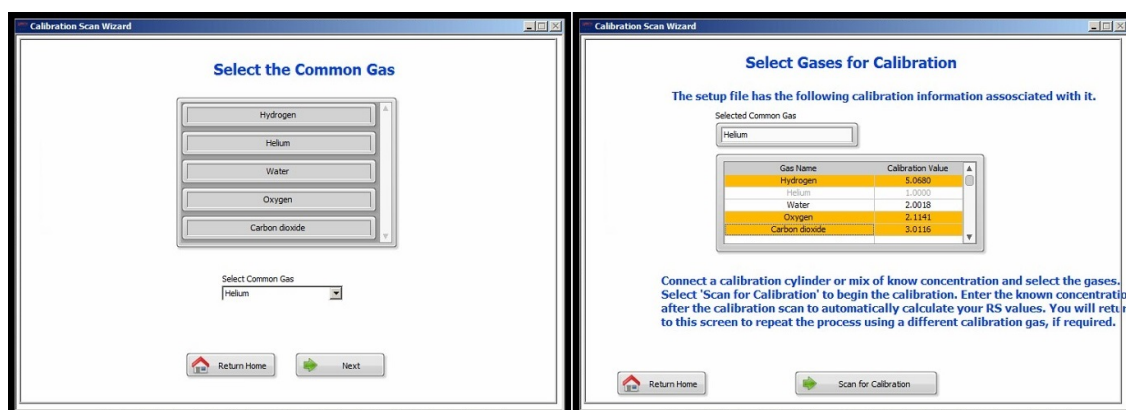

Figure 4.21: Gas selection

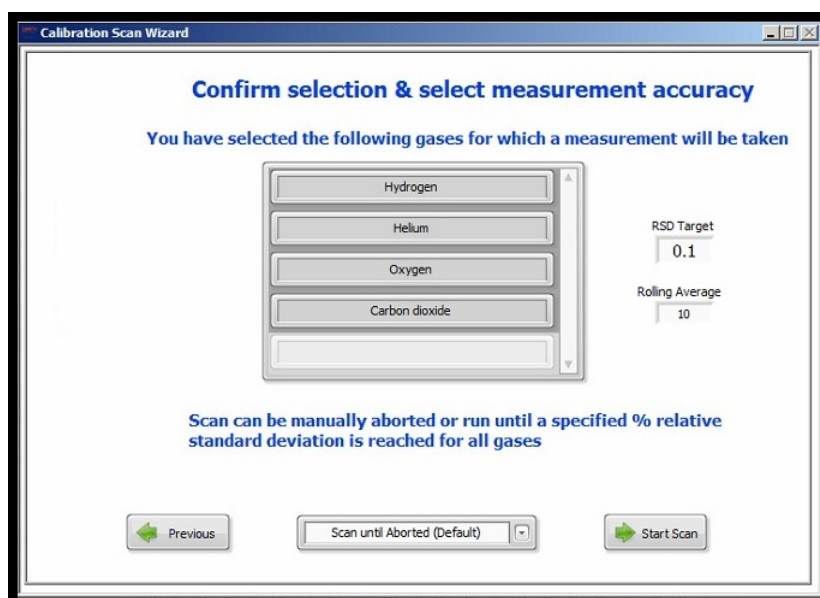Figure 4.22 is quite similar to Figure 4.15: setting up the measurement accuracy it is possible to start the scan.

Figure 4.22: Calibration accuracy window

The "Scan underway" window is opened (see Figure 4.23). Figure 4.24 shows the situation at the end of the process.
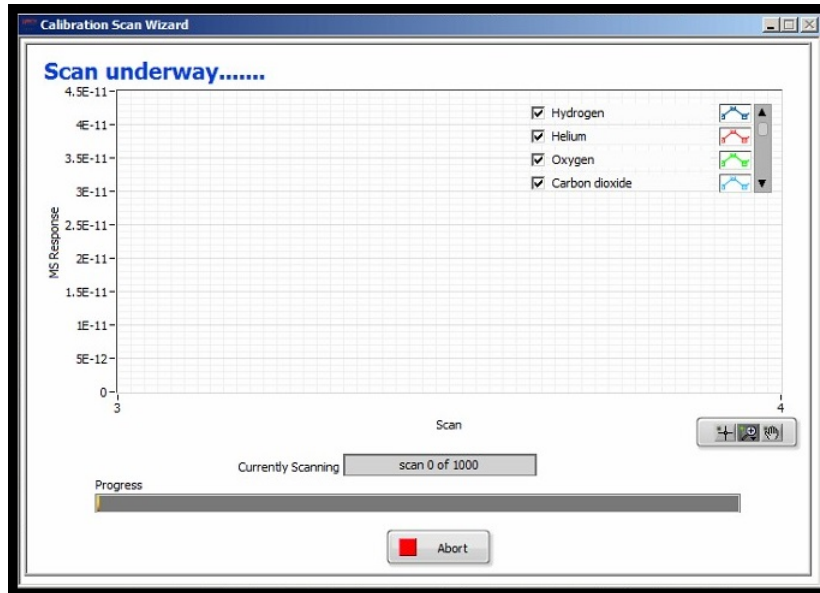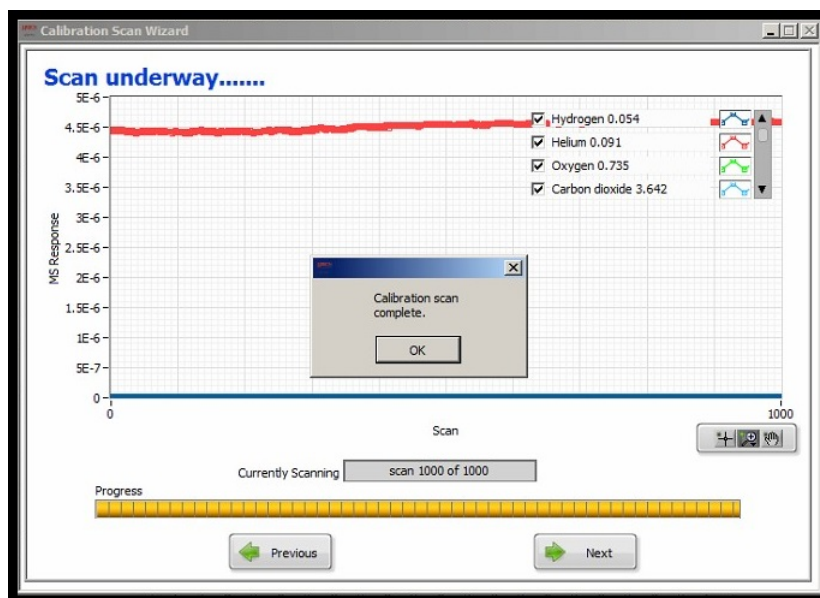

Figure 4.23: Scan underway window

Figure 4.24: Scan underway window: calibration complete

At this point, the actual values of the cylinder must be inserted, as shown in Figure 4.25 and the RS values will be calculated for the first cylinder.

Figure 4.25: Calculation of RS values (first cylinder)

After having added the values to setup, it is possible to proceed with the next cylinder, for which the procedure is exactly the same, as shown in Figure 4.26 and Figure 4.27.

Figure 4.26: Gas selection (second cylinder)
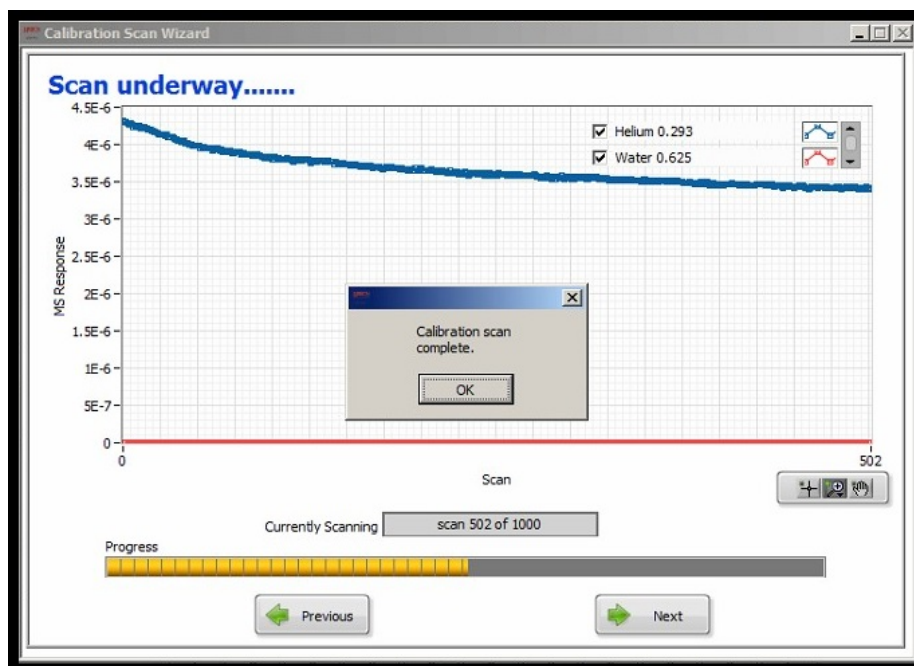
Figure 4.27: Scan underway window: calibration complete

Figure 4.28 shows the obtained RS values for the second cylinder.
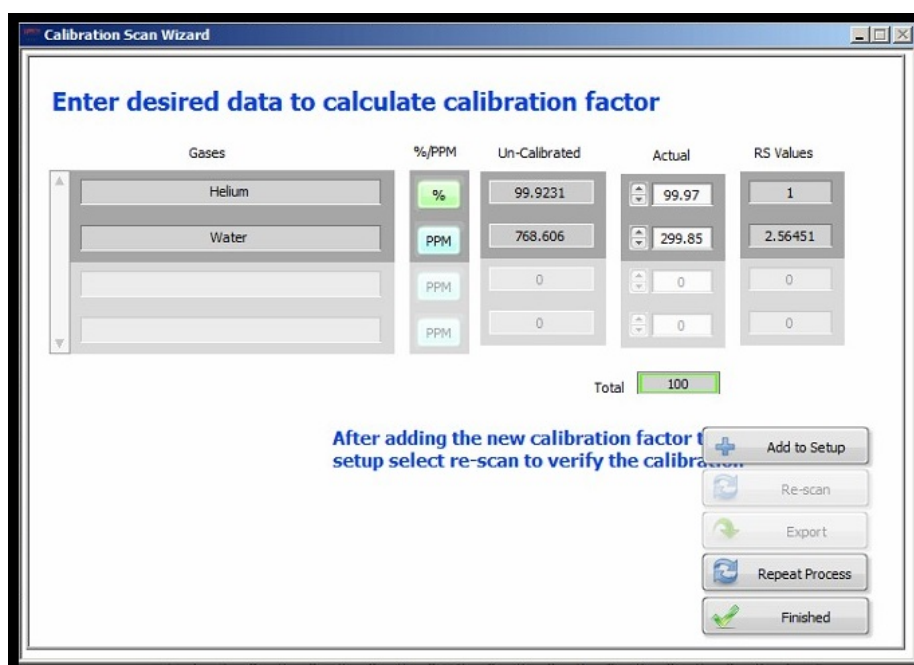
Figure 4.28: Calculation of RS values (second cylinder)

Figure 4.29 shows a summary of the RS values. Clicking on the "Calculate RS" button, the Mean RS values will be computed. Mean RS values are the calibration factors that will be added to the software setup, clicking on the "Add to setup" button. At this point the calibration procedure is complete.
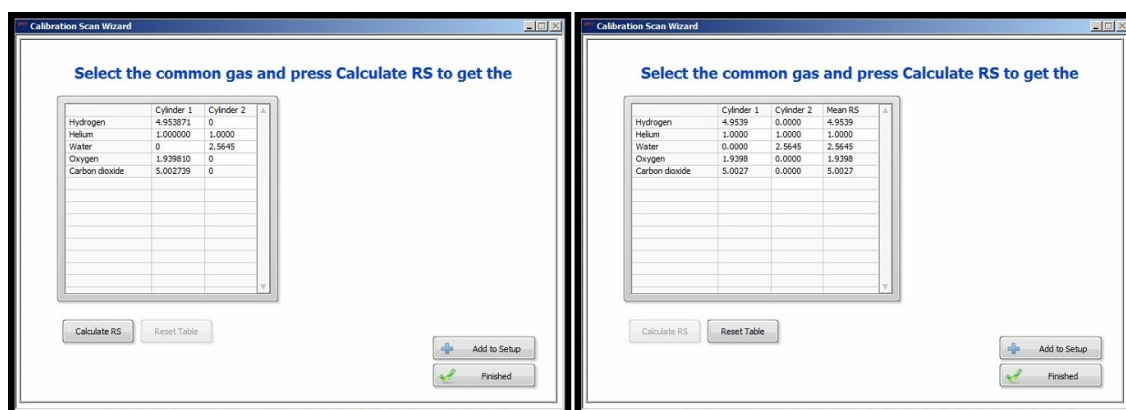
Figure 4.29: Calculation of Mean RS values

Figure 4.30 shows the "Setup analysis" window with the calibration factors just inserted.
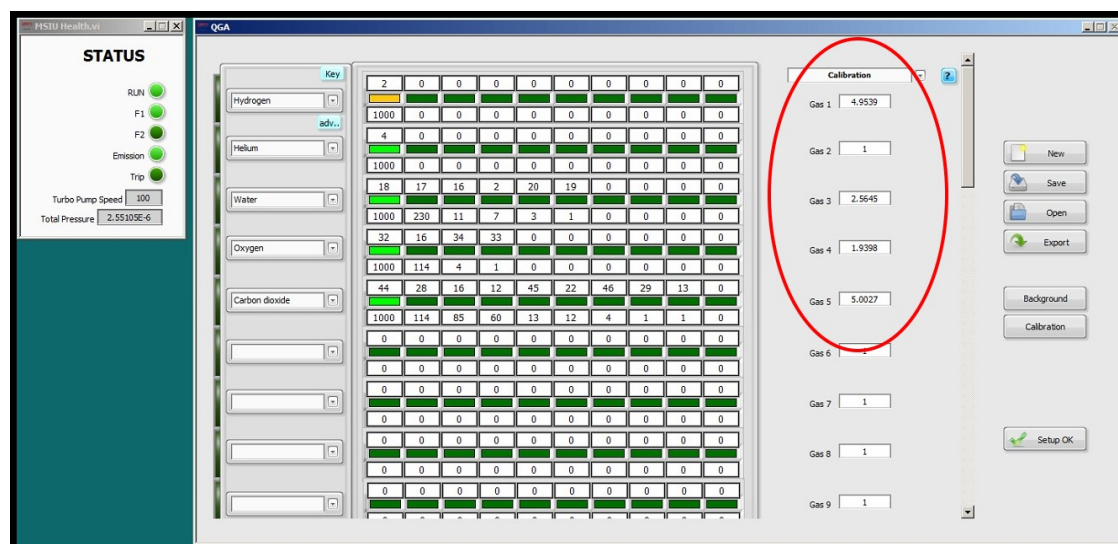
Figure 4.30: Insertion of calibration factors

4.5.3   Quadrupole interfacing with HYDREX

At the end of the calibration procedure, the quadrupole is ready to be installed on HYDREX. As said in paragraph 4.3.4, the gas to be analysed is taken from the main loop using lines LP18 and LP19.

The scope of the tests described in this paragraph is to verify the correct interfacing between the facility and the quadrupole. The purpose of these tests is not to obtain a precise evaluation of the composition of the gas contained inside the loop. In fact, a correct analysis should require an employment of the instrument immediately after the calibration procedure. In addition, it should be noticed that the instrument needs a lot of hours to reach the ideal conditions for the analysis. For these tests the Faraday cup has been used; considering the minimum pressure that the vacuum system of the instrument is able to reach, the detection limit for the concentrations has been estimated to be about 4 ppmv.

In adsorption phase, when PV05 valve is open, it is possible to analyse the gas that enters the PTSA, while when PV06 valve is open, it is possible to analyse the gas that exits the PTSA. In both cases, the gas coming from the loop goes through the pressure reducers PRV06 and PRV07, to decrease the pressure to the value required by the quadrupole (max 1 barg). The Mass Flow Controller MFC04 regulates the flow rate sent to quadrupole. The typical gas consumption of the instrument is about 1.2 [Nl/h] but the gas to be sent must have a value that is slightly higher. The excess of flow rate is discharged into the external environment.

In regeneration phase, opening PV05 valve it is possible to analyse the gas that exits the PTSA. In this case, the gas coming from the loop goes only through the pressure reducer PRV07, because in this phase the pressure of the streaming gas is lower than in adsorption phase.

Before starting the analysis, it is necessary to verify that the plant is in "basic conditions", which means that the loop must be full of non-contaminated helium and temperatures and pressure must be constant [51]. In order to eliminate air contaminations inside the facility, a vacuum procedure has been carried out in advance. According to the operative manual [51], the vacuum pump operates when the facility is in stand-by, that is without pressurized helium in the pipes and at room temperature. The vacuum pump is a mechanical rotating pump that allows to reach a vacuum grade of $10^0 \div 10^{-1}$ mbar. After, it is possible to proceed with the filling of the facility with helium. The gas has a purity grade 5.0 and the characteristics are shown in Table 4.11.

Table 4.11: Helium grade 5.0, impurities concentrations

Parameter	Value
Oxygen, O_2	1 [ppmv]
Nitrogen, N_2	5 [ppmv]
Carbon oxides, CO & CO_2	0.5 [ppmv]
Hydrocarbons, CH_4	0.5 [ppmv]
Water, H_2O	3 [ppmv]

Regeneration test

The first operation to be done on the facility is a regeneration procedure. In fact, the zeolites have adsorbed a certain quantity of water because they were initially in contact with air, so they need to be dried in order to perform a correct purification.

Referring to Figure 4.6, the flow of gas, coming from the external cylinders, follows the yellow line but the reducing bed is excluded, so then it follows the green line. Looking at Figure 4.2 (the synoptic), the heating cables under interest are CS03, CS05, CS11 CS14 and the cables on the quadrupole lines (CS09, CS10 and CS12) that are at a temperature which prevents water condensation on the piping walls. The heating cables related to the oxidizers (CS01, CS02, CS07 and CS08) are switched on but this part of the loop is not involved in this phase. The temperatures related to the above-mentioned heating cables are summarised in Table 4.12.

Table 4.12: Temperatures of Heating Cables

Heating Cable	Temperature
CS01, CS02, CS03, CS07, CS08	150 [℃]
CS05, CS11, CS14	250 [℃]
CS09, CS10	85 [℃]
CS12	70 [℃]

The gas has been let flowing, using the Mass Flow Controller MFC02, at 100 [Nl/h] for a suitable number of hours before starting the analysis on the quadrupole, in order to reach a sort of stability. The pressure of gas inside the loop has been set to approximately 1 barg. Then the quadrupole has been activated.

For what regards the data coming from the quadrupole, after a short transient, the concentrations of H_2, O_2 and CO_2 decreased while the water concentration increased until it reached the value of about 1750 ppm and then decreased, as can be seen in Figure 4.31.
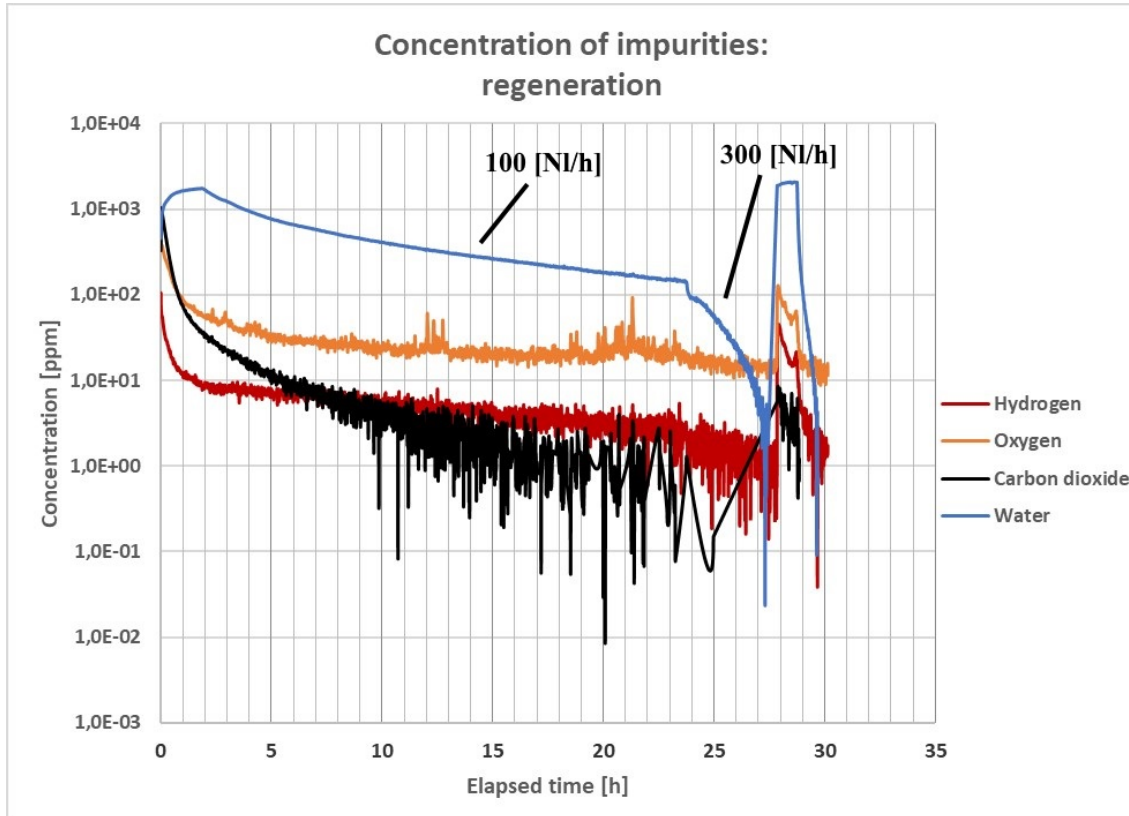
Figure 4.31: Quadrupole data during the regeneration test

What can be observed is that, after about 24 hours, there were about 140 ppm of water and 20 ppm of oxygen, while H_2 and CO_2 contents were practically disappeared. So, it was decided to increase the flow rate from 100 to 300 [Nl/h] and, consequently, a sudden decrease of the H_2O concentration was noticed and after about 4 hours from this operation, all impurities concentrations were close to zero, except for oxygen concentration, which remained practically constant.

Then, valve PV06 has been opened and valve PV05 has been closed: because of this, the water concentration went beyond 2000 ppmv but after few hours all concentrations, except for the oxygen, became again close to zero. This means that also the line LP19 was clean from water.

As already written, the scope of this tests is not to obtain a correct analysis of the gas. However, observing Figure 4.31, an attempt to explain the behaviour of the concentration curves, has been done.

The water detected in the loop is due to the humidity of the air that was in contact with the internal walls of the pipes before the filling procedure. A small quantity of water remains in the gas mixture also after the vacuum procedure. Moreover, it is known that a certain amount of water exists on the surfaces of piping materials such as stainless steel [55]; in particular, it can be classified into physically adsorbed water, chemically adsorbed water and structural water. The structural water consists of any chemically adsorbed water and some chemical groups containing hydrogen, for examples –OH bases, which are strongly connected with the surfaces. The physically adsorbed water can be removed with the flow of dry gas; the chemically adsorbed water can be reduced to negligible quantity with dry gas at temperature above 127 ℃. A small amount of chemically adsorbed water and structural water remains on the surfaces even after this operation.

Since the pressure inside the loop is, in any phase, above the atmospheric pressure and the helium coming from the cylinders contains oxygen at very low level, the O_2 content in the gas mixture should come from the exposition to air before vacuum procedure.

Regarding CO_2 content, as illustrated in the next paragraph, it should be originated inside the oxidizing beds, and then spread to the rest of the loop when all parts are communicating.

For what regards H_2, except for the very first period, it can be noticed that its content is very low, close to the detection limit. It must be also considered that the hydrogen measured by the quadrupole could come from cracking phenomena of water molecules that happen in the ionization chamber of the instrument.

It is possible to notice that the concentrations of CO_2, H_2 and O_2 initially decrease quickly with time due to the purging effect of the pure helium on the molecules inside the mixture. Then, the decrease is lower, probably due to the fact that the involved molecules show some interaction effect with the walls of the pipes. The behaviour of the H_2O is different: this could be due to the different mechanisms of interaction between water and pipes, as previously explained.

Purification test

Since the regeneration loop seemed to be clean from water, it was decided to measure the impurities concentration in the purification loop, initially excluding the PTSA line, to have the situation at the beginning of the test, avoiding its contamination.

Referring to the Figure 4.5 the purification is performed using a closed loop. The circulation of the gas is carried out by means of a compressor. In this case, the heating cables under interest are CS01, CS02, CS03, CS07, CS08 and the cables on the quadrupole lines (CS09, CS10 and CS12). The heating cables related to the PTSA (CS11, and CS14) are switched off because the zeolites work at room temperature in this phase. In normal operating conditions, the temperature related to the cables CS01, CS02, CS03, CS07, CS08 should be greater than 250 ℃, to allow the transformation of the hydrogen in water. Since this reaction is not required for this test, these temperatures have been set to a lower value, as can be seen in Figure 4.32. In the figure it is also shown the temperature of the heating cable CS10, as an example.
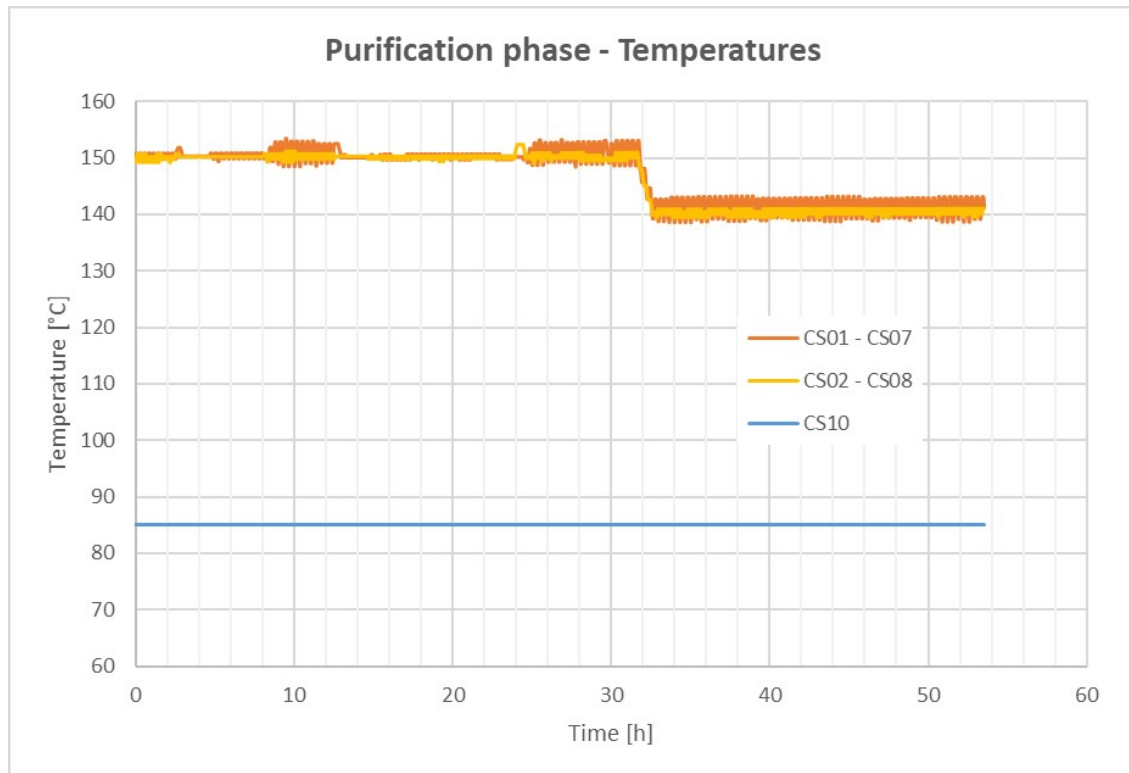

Figure 4.32: Temperatures during purification test

Two different flow rates are involved in this test: the first one, measured through the flow meter FM02, is the recirculation flow rate given by the compressor, while the second one, measured through the mass flow controller MFC02, is the flow rate used to reintegrate the gas consumption required by the quadrupole. Since the flow rate released from MFC02 is much higher than the quadrupole consumption, the pressure inside the loop increases over time up to a maximum value set on the Pressure Control Valve PCV01. When the pressure exceeds this value, the PCV01 opens and discharges the gas into external environment. These flow rates are shown in Figures 4.33 and 4.34. The main flow rate has been adjusted by means the regulation valve PV35. Initially the flow rate has been set to about 1.5 [Nm^3/h], adjusting the opening percentage of the valve PV35 at 52%. After few hours, further opening the valve, the flow rate has been set to 3.5 [Nm^3/h]. Subsequently, the compressor has been turned off for about 12 hours and then restarted. Almost for the entire period, a flow rate between 90 [Nl/h] and 100 [Nl/h] has been maintained through the mass flow controller MFC02.

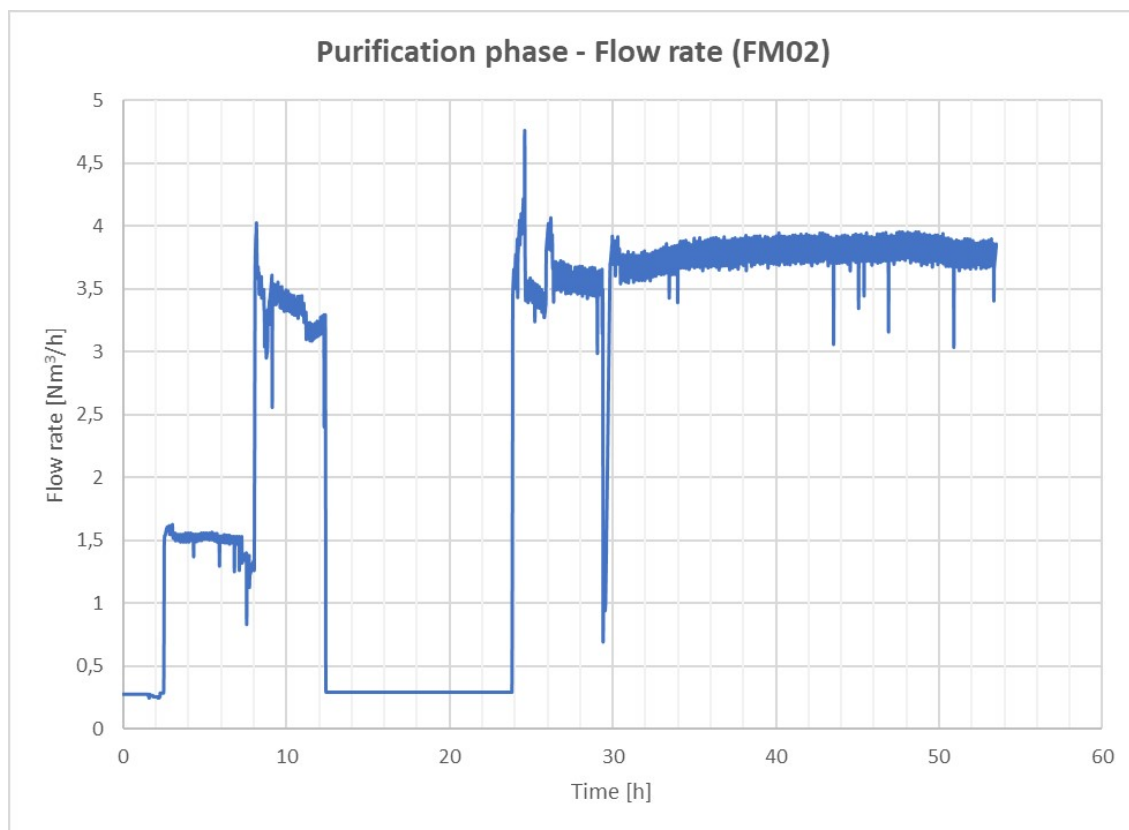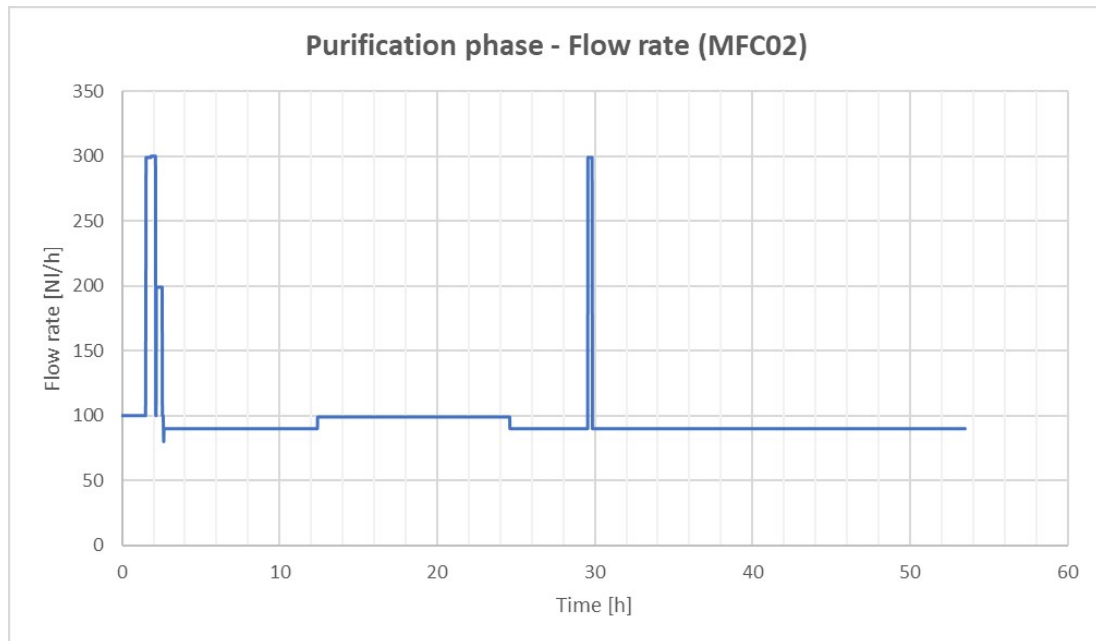Figure 4.33: Flow rate through the Flow Meter

Figure 4.34: Flow rate through the Mass Flow Controller

Figure 4.35 shows the pressures in different points of the loop. The acquisition system shows that at the beginning, the PTSA line was excluded (PT03, PT05), so it stayed at 1 barg, while the rest of the circuit has been pressurized between 9 ÷ 10 barg.
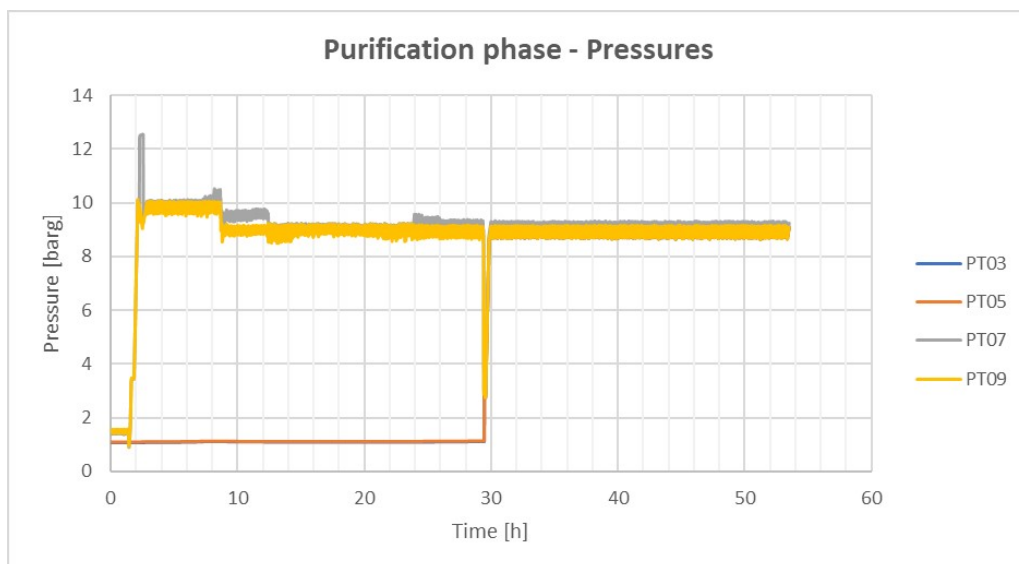

Figure 4.35: Pressures in purification mode

112

After about 30 hours, the pressure of the plant went to 1 barg to allow the PTSA line to be set up to 10 barg without a rapid compression. Figure 4.36 shows the impurity concentration trends.
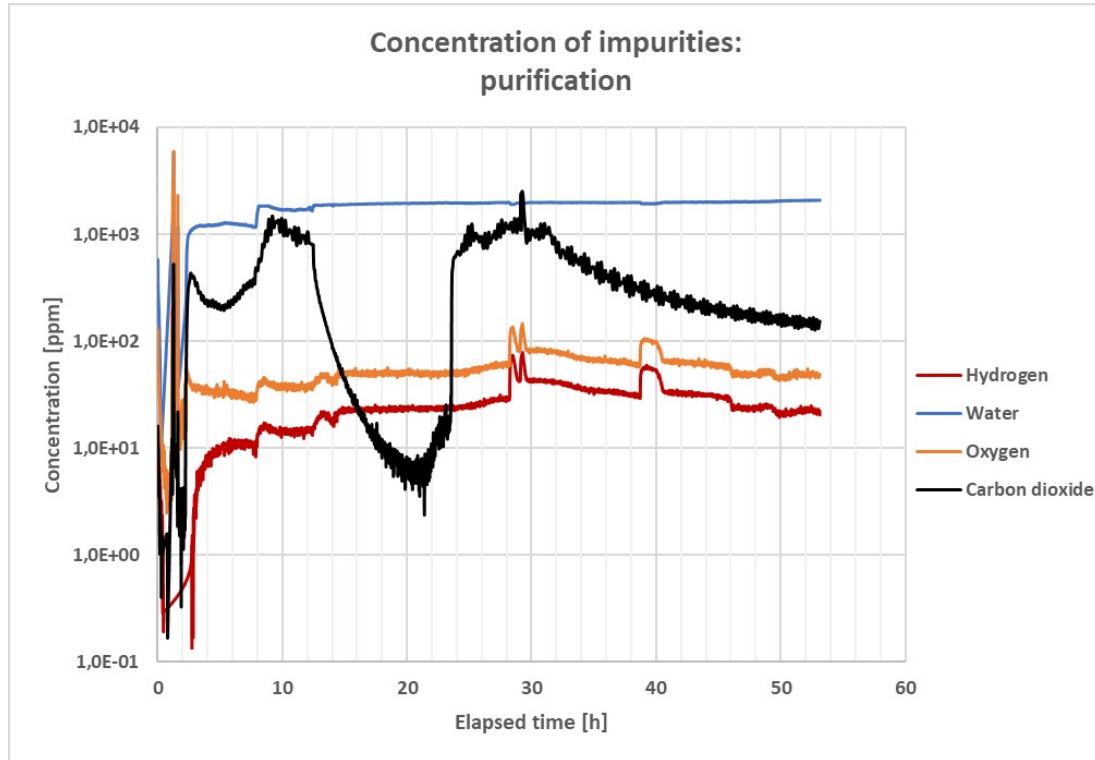
Figure 4.36: Quadrupole data during the purification test

After 30 hours from the start of the operation, the water content seemed to be stable at about 2000 ppmv, H_2 and O_2 were oscillating around constant values (20 and 50 ppmv, respectively), but with decreasing trend, while CO_2 was decreasing more quickly. Abrupt variations of concentrations are in general caused by changes in pressures and flow rates.

The reason for the decreasing concentrations is that a small amount of gas is sent to the quadrupole and PCV01, periodically, discharges a certain quantity of helium when the pressure exceeds the foreseen value. The consumed gas is replaced by fresh helium, coming from the cylinders.

Regarding to the CO_2 concentration, observing the behaviour of the curve, it can be noticed that the amount is higher than in the regeneration phase. With respect to the regeneration test, some parts of the loop are different and, in particular, in the purification test compressor and oxidizers are involved.

Because the process gas contamination by the compressor is almost impossible, it can be supposed that the impurity is related to the oxidizing material. Theoretically the oxidizing material can produce carbon dioxide according to the following reaction:

$$CO + CuO \longrightarrow CO_2 + Cu$$

Since the helium should contain CO and CO_2 at very low levels, it is not clear how CO_2 is generated; it is necessary to contact the oxidizing material producer to have a clarification.

On the other hand, it was expected that the regenerated zeolites should have adsorbed water, causing a decrease of water content. This fact did not happen. Some preliminary hypotheses could be made to explain this:

- the zeolites have not been regenerated due to channeling (too low pressure drop inside PTSA: it is necessary to increase the regeneration flow rate);

- the water content inside the loop is so high that the water adsorbed by PTSA is not remarkable;

- the aging of the zeolites (they have been installed for some years) caused their lack of efficiency.

Moreover, the water concentration seems to increase. The hypothesis is that, because of the presence of long parts of the loop not heated, the water adsorbed on the pipes is released much more slowly. This release could be greater than the water removed from the loop.

Conclusions

The main purpose of this thesis was the analysis of the Coolant Purification System to be used in the Test Blanket Systems destined to ITER reactor and the verification of its applicability for the purification of the cover gas of the Sodium-cooled fast Reactor ASTRID from tritium, including a preliminary design of a purification system based on the same technology. Some of the above-mentioned technologies require an experimental validation to assess the applicability to the TBM design; for this reason, in the Research Centre of ENEA Brasimone has been built the experimental facility, named HYDREX, to perform experimental tests to support the design. Part of the work has concerned the commissioning tests of the facility and the characterisation of the main equipment and components installed. The first tests are actually in progress, including the verification of the correct interfacing between quadrupole mass spectrometer and experimental plant.

After a brief introduction about the research activity on fusion and fission reactors (Chapter 1), the thesis goes more in detail for what regards the purification from tritium. In fact, Chapter 2 describes the main technologies that are used in fusion and fission systems, Coolant Purification System and cold traps respectively, giving particular attention to the functioning of the CPS since it is taken as reference for the design of the purification of the cover gas of the ASTRID reactor.

In Chapter 3, a preliminary design has been carried out. The chapter begins with the description of the systems that are supposed to be designed, proposing two types of solution: one with the regeneration of the adsorption column and one without regeneration. The theoretical aspect is enriched with the description of how a fixed bed is made and of the mathematical approach, in particular of the Ergun equation, for the evaluation of pressure drop in fixed beds. The chapter ends with the sizing of the two main components of the system, that are the oxidizing bed and the adsorption column. The calculations carried out in this chapter, demonstrate that the purification technologies foreseen in fusion applications can be used also in fission systems.

Chapter 4 dedicates attention to the activities done on the HYDREX facility, whose scope is to have an experimental confirmation of the design procedure of the Purification System employed in Chapter 3. This chapter begins with the description of the experimental facility, explaining the functioning, the main components and the operating procedures, that are adsorption and regeneration modes. Then, after a short description on the customise mass spectrometer installed in HYDREX, full attention is given to the calibration procedure of the Quadrupole Mass Spectrometer used for the analysis of the gas inside HYDREX facility, since this operation is a fundamental and very delicate step for the experimental campaign that is being carried on for this facility. So, background and calibration procedures are described, illustrating all passages in detail. Being the instrument ready to be used, the verification of its correct functioning, when interfaced to HYDREX, has been performed. Some preliminary analyses have been carried out and a regeneration test and a purification test have been proposed in the chapter.

What can be observed is that the quadrupole interfaces in a good way with the facility. In addition to the verification of the correct interfacing between the quadrupole and the facility, the preliminary tests resulted very useful because they allowed to highlight some issues, described in the chapter, that will need further studies.

Bibliography

[1] *Technology Roadmap Update for Generation IV Nuclear Energy Systems.* Generation IV International Forum, GIF, 2014, www.gen-4.org.

[2] *Fusion electricity. A roadmap to the realisation of fusion energy.* European Fusion Development Agreement, EFDA, 2012, www.efda.org.

[3] *A short history of magnetic fusion*, Association EURATOM-CEA, http://www-fusion-magnetique.cea.fr/gb/accueil/index.htm.

[4] *History of Fusion Energy Research*, Nuclear Fusion, Britannica Online Encyclopedia, https://www.britannica.com/science/nuclear-fusion/History-of-fusion-energy-research.

[5] *Tokamak principle*, https://www.euro-fusion.org/2011/09/tokamak-principle-2/.

[6] Yuhong Xu, *A general comparison between tokamak and stellarator plasmas.* Southwestern Institute of Physics, People's Republic of China, 2016.

[7] *JET: Europe's largest fusion device*, https://www.euro-fusion.org/jet/

[8] https://www.idom.com/project/reliability-studies-for-the-joint-european-torus-jet-experimental-reactor/

[9] *Nuclear Fusion Power*, http://www.world-nuclear.org/information-library/current-and-future-generation/nuclear-fusion-power.aspx

[10] Kaname Ikeda, *ITER on the road to fusion energy*, IAEA, 30 December 2009, Vienna.

[11] World Nuclear Association, *Fast neutron reactors*, http://www.world-nuclear.org/information-library/current-and-future-generation/fast-neutron-reactors.aspx

[12] Vitaly Sobolev, *Database of thermophysical properties of liquid metal coolants for GEN-IV*, Scientific Report, SCK·CEN-BLG-1069, November 2010 (rev. Dec. 2011).

[13] *Sodium-cooled Fast Reactor (SFR) Technology and Safety Overview.* Office of Nuclear Energy, U.S. Department of Energy, Washington DC, 2015.

[14] *Sodium-cooled Fast Reactor (SFR) Technology Overview.* Argonne National Laboratory, IAEA Education & Training Seminar on Fast Reactor Science and Technology, Mexico City, 2015.

[15] Idaho National Laboratory, *LFR* http://www4vip.inl.gov/research/lead-cooled-fast-reactor/

[16] Idaho National Laboratory, *GFR* http://www4vip.inl.gov/research/gas-cooled-fast-reactor/

[17] Manohar S. Sohal et al., *Engineering Database of Liquid Salt Thermophysical and Thermochemical Properties*, Idaho National Laboratory, June 2013.

[18] World Nuclear Association, *Molten Salt Reactors*, http://www.world-nuclear.org/information-library/current-and-future-generation/molten-salt-reactors.aspx.

[19] Idaho National Laboratory, *MSR* http://www4vip.inl.gov/research/molten-salt-reactor/.

[20] Gen IV International Forum Portal, *Supercritical-water-cooled reactors*, https://www.gen-4.org/gif/jcms/c_40679/technology-system-scwr.

[21] Idaho National Laboratory, *SCWR* http://www4vip.inl.gov/research/supercritical-water-cooled-reactor/.

[22] Idaho National Laboratory, *VHTR* http://www4vip.inl.gov/research/very-high-temperature-reactor/.

[23] I. Ricapito et al. *The ancillary systems of the European test blanket modules: Configuration and integration in ITER.* Fusion Engineering and Design 85 (2010) 1154-1161.

[24] A. Ciampichetti et al., *The coolant purification system of the European test blanket modules: Preliminary design.* Fusion Engineering and Design 85 (2010) 2033-2039.

[25] F. Franza et al., *Analisi del trasporto del trizio nei sistemi SFR*, NNFISS-LP3_020, 2011.

[26] M. Succi, C. Solcia, *Advanced technologies for semiconductors gas purification*, SAES Getters Technical Paper TP0214D.

[27] C.C. McPheeters, D.J. Raue et al., *Sodium Technology Annual Report*, July 1975 – June 1976, Chemical Engineering Division, Argonne National Laboratory.

[28] M.G. Hemanath et al., *Theoretical and experimental performance analysis for cold trap design.* Nuclear Engineering and Design 240 (2010), 2737-2744.

[29] Nuclear Regulatory Commission, https://www.nrc.gov/reading-rm/doc-collections/fact-sheets/tritium-radiation-fs.html.

[30] D. Basmadjian, *Little adsorption book. A Practical Guide for Engineers and Scientists*. Department of Chemical Engineering and Applied Chemistry, University of Toronto. CRC Press, 1997.

[31] S. Ergun, *Fluid flow through packed columns*. Chem. Eng. Prog. 48 (1952).

[32] SAES Pure gas, *Ambient Inline Purifier 902 Purification Media Specification*, www.saespuregas.com.

[33] BASF Puristar® R3-11G, Technical Information data sheet.

[34] Jong-Hwa Kim et al., *Adsorption equilibria of Water Vapor on Alumina, Zeolite 13X and a Zeolite X/Activated Carbon Composite*, J. Chem. Eng. Data (2003), 48, 137-141.

[35] Yu Wang et al., *Adsorption Equilibrium of Carbon Dioxide and Water Vapor on Zeolites 5A and 13X and Silica Gel: Pure Components*, J. Chem. Eng. Data (2009), 54, 2839-2844.

[36] UOP, *An Introduction to Zeolite Molecular Sieves*, Data Sheet.

[37] Grace Davison, *SYLOBEAD® - Adsorbents for Process Applications*, Data Sheet.

[38] GRACE Davison, *SYLOBEAD Adsorbents – The products*, Data Sheet.

[39] Private communication from CEA researchers.

[40] E-mail sent from CEA to ENEA on 17/10/2017.

[41] M. Haruta et al., *Catalytic combustion of Hydrogen. Its role in hydrogen utilization systems and screening of catalyst materials*. Int. J. Hydrogen Energy vol. 6 (1981).

[42] Jean-Paul Grouiller, *Plutonium recycling capabilities of ASTRID reactor*, CEA, Nuclear Energy Division Cadarache Centre, France 2017.

[43] SAES Pure Gas, *MicroTorr: Ambient Inline Purifiers*. SAES Group, 2016.

[44] Hougen & Watson, *Chemical Process Principles*. John Wiley & Sons.

[45] POROCEL Application Bulletin #3, *Fixed Bed Pressure Drop Calculations*.

[46] GPSA Engineering Databook, *Chapter 20*, 14th Edition.

[47] Grace Davison, *SYLOBEAD® MS 514 Adsorbent for Drying and Purification of Gases and Liquids*, Product Information.

[48] POROCEL, Application Bulletin #1C, *Fixed Bed Adsorber Design Guidelines*.

[49] Sandvik, *End caps, butt weld fittings*, www.materials.sandvik.

[50] National Institute of Standards and Technology, *NIST Chemistry WebBook*, US Department of Commerce.

[51] D. Diamanti, *Manuale operativo impianto HYDREX*, IT-I-T-327.

[52] A. Aiello et al., *Finalization of the conceptual design of the auxiliary circuits for the European test blanket systems*, Fusion Engineering and Design 96-97 (2015) 56-63.

[53] PremierBioSoft.com, http://www.premierbiosoft.com/tech_notes/mass-spectrometry.html.

[54] Hiden Analytical, *Quadrupole Mass Spectrometry Concepts. Mass Spectrometers for Residual Gas Analysis*, www.HidenAnalytical.com.

[55] M. Nishikawa et al., *Tritium trapping capacity on metal surface*, J. Nucl. Mat. (2000), 277, 99-105.